A PREDICTION METHOD FOR SPOILER PERFORMANCE

by

PETER A. TAM DOO
B.Sc., University of Manitoba, 1972

A THESIS SUBMITTED IN PARTIAL FULFILLMENT OF
THE REQUIREMENTS FOR THE DEGREE OF
DOCTOR OF PHILOSOPHY

in

THE FACULTY OF GRADUATE STUDIES
(Department of Mechanical Engineering)

We accept this thesis as conforming
to the required standard

THE UNIVERSITY OF BRITISH COLUMBIA
October, 1977

© Peter A. Tam Doo, 1977

In presenting this thesis in partial fulfilment of the requirements for an advanced degree at the University of British Columbia, I agree that the Library shall make it freely available for reference and study. I further agree that permission for extensive copying of this thesis for scholarly purposes may be granted by the Head of my Department or by his representatives. It is understood that copying or publication of this thesis for financial gain shall not be allowed without my written permission.

Department of Mechanical Engineering

The University of British Columbia
2075 Wesbrook Place
Vancouver, Canada
V6T 1W5

Date 28th October 1977

ABSTRACT

The prediction of the aerodynamic characteristics of a finite rectangular wing with part span spoilers is attempted using the lifting line theory of Prandtl. Required inputs to the theory are sectional values of lift coefficient, pitching moment coefficient, zero lift angle of attack, and aerodynamic center at selected points along the span. The value of these parameters for the spoilered wing sections is calculated by Brown's linearised thin airfoil theory for spoilers. This theory, in common with other sectional spoiler theories, requires as input the base pressure coefficient in the spoiler wake. The base pressure coefficient must be determined by experiment, since at the present time it cannot be predicted theoretically.

The effect of base venting on spoilered section characteristics is examined experimentally. It is found that for small base vents of around ten percent of spoiler height or less, the vented section characteristics are little different from the unvented. Thus for the purposes of preliminary design, the unvented section characteristics may be used with little loss of accuracy, if the spoiler vent is about ten percent of spoiler height or less.

The results of the finite wing theory are compared with experiment. Good agreement is found. The method is subject to the limitations of the lifting line theory, which limits its applicability to unswept wings of moderate to high aspect ratios operating at low subsonic speeds. The method is also subject to the additional limitations imposed by the sectional theories employed.

TABLE OF CONTENTS

LIST OF TABLES

LIST OF FIGURES

ACKNOWLEDGEMENTS

The author wishes to thank Dr. G.V. Parkinson for his guidance in the preparation of this thesis. His many suggestions during the course of this research were invaluable and much appreciated.

The author also wishes to thank the Mechanical Engineering Machine Shop for building the models and the Computing Center at the University of British Columbia for the use of their facilities.

This research was supported initially by the Defense Research Board under Grant Number 9551-13 and by the National Research Council under Grant Number A586.

LIST OF SYMBOLS

$a_x = \frac{\partial \phi}{\partial x} = \frac{\partial \psi}{\partial z}$	x component of acceleration
$a_z = \frac{\partial \phi}{\partial z} = - \frac{\partial \psi}{\partial x}$	z component of acceleration
$\bar{a}$	acceleration vector
A_n	Fourier coefficient
$AR = 2b^2/S$	aspect ratio of wing
b	wing semispan
b_s	spoiler span
b_t	coordinate along spoiler span measured with respect to inboard spoiler tip
c	wing chord
c_e	root semichord of elliptic disk
c_η	flap chord
C_{ds}	spoilered sectional drag coefficient
C_l	unspoilered sectional lift coefficient
C_{ls}	spoilered sectional lift coefficient
C_{mo}	unspoilered pitching moment coefficient about origin
C_{mos}	spoilered pitching moment coefficient about origin
C_{mac}	unspoilered pitching moment coefficient about the aerodynamic center
C_{macs}	spoilered pitching moment coefficient about the aerodynamic center
C_L	half wing lift coefficient
C_{MO}	half wing pitching moment coefficient about origin
C_{MAC}	half wing pitching moment coefficient about the aerodynamic center
C_{ps}	pressure coefficient for spoilered section

C_R	half wing rolling moment coefficient
C_{pb}	base pressure coefficient in spoiler wake
$\bar{C}_{pb}$	base pressure coefficient in spoiler wake averaged over incidence
$\bar{\bar{C}}_{pb}$	base pressure coefficient in spoiler wake averaged over incidence and spoiler span
$\bar{\bar{C}}^*_{pb}$	Value of $\bar{\bar{C}}_{pb}$ at the 0.7 chord position
d	height of spoiler base vent
E	semiperimeter of wing/semispan, Jones Edge Correction Factor
$F(Z)= \phi + i\psi$	complex acceleration potential
G	$\bar{\bar{C}}_{pb}/\bar{C}_{pb}$
G^*	value of G at the 0.7 chord position
h	spoiler height
k	chordwise coordinate of elliptic disk
k_e	chordwise coordinate of edge of elliptic disk
$K = -C_{pb}$	cavitation number
L'	sectional lift for unspoilered section
L'_s	sectional lift for spoilered section
ℓ	cavity length
m_o	unspoilered $dC_l/d\alpha$ (/rad.) for airfoil section
m_{os}	spoilered $dC_l/d\alpha$ (/rad.) for airfoil section
M_o	unspoilered sectional pitching moment about origin
M_{os}	spoilered sectional pitching moment about origin
M_{ac}	unspoilered sectional pitching moment about aerodynamic center
M_{acs}	spoilered sectional pitching moment about aerodynamic center

M_0	half wing pitching moment about origin
M_{AC}	half wing pitching moment about aerodynamic center
n	chordwise coordinate of flap hinge
P	pressure in flow field
P_c	pressure in spoiler wake
P_∞	free stream pressure
R	rolling moment of half wing
s	chordwise coordinate of spoiler base
S	half wing area
t	chordwise coordinate of spoiler tip
U	free stream velocity
u	non-dimensional perturbation velocity in x direction
w	non-dimensional perturbation velocity in z direction
w_i	downwash
x	chordwise coordinate
x_{ac}	chordwise coordinate for aerodynamic center of unspoilered section
x_{acs}	chordwise coordinate for aerodynamic center of spoilered section
X_{AC}	chordwise coordinate of wing aerodynamic center
y	spanwise coordinate
y_o	spanwise position at which the induced angle of attack is evaluated
y_1	spanwise coordinate of inboard spoiler tip
y_2	spanwise coordinate of outboard spoiler tip
z	coordinate perpendicular to xy plane

z'	complex transform plane
$Z = x + iz$	complex airfoil plane
α	geometric angle of attack for airfoil section
$\alpha_a = \alpha + \alpha_{lo}$	absolute angle of attack for unspoilered airfoil section
$\alpha_{as} = \alpha + \alpha_{los}$	absolute angle of attack for spoilered airfoil section
$\alpha_e = \alpha_a + \alpha_i$	effective angle of attack for airfoil section
α_i	induced angle of attack
α_{lo}	zero lift angle of attack for unspoilered section
α_{los}	zero lift angle of attack for spoilered section
α_{stall}	stall angle for wing or airfoil section
δ	spoiler erection angle
ζ, ν	complex transform planes
η	flap angle
θ	angular variable in ζ-plane
$\mu=\cos^{-1}(y/b)$	span variable for finite wing
μ_1	position of inner spoiler tip in terms of span variable μ
μ_2	position of outer spoiler tip in terms of span variable μ
ρ	air density
ϕ	acceleration potential
ϕ_e	velocity potential for elliptic disk
ψ	acceleration stream function
$\tau=\cos^{-1}(k/k_e)$	chordwise variable for elliptic disk
Γ	circulation

1. INTRODUCTION

Spoilers are versatile aerodynamic control surfaces which are used on many modern aircraft. They may best be described as small flaps that have been moved ahead of the trailing edge to the upper or lower wing surface. Spoilers may be deployed symmetrically to control lift and drag, or asymmetrically to produce roll and yaw. Since spoilers may be used together with full span flaps, their presence in V/STOL aircraft is becoming increasingly common.

The behavior of spoilers on wings is, however, difficult to predict because flow separates from the spoiler edges, and a turbulent wake is formed behind the spoiler. The standard potential flow methods of airfoil theory cannot therefore be used. They must be modified to account for the presence of the wake. Woods (1) was among the first to tackle the problem. He developed a linearised thin airfoil theory for spoilered wing sections. Barnes (2) later modified the theory to account for the presence of the boundary layer on the airfoil. Here at the University of British Columbia, work on spoiler theory was begun by Jandali and Brown in an effort to improve on the accuracy of prediction. Jandali developed an analytic thick airfoil theory for airfoil sections with normal spoilers (3). Brown developed a thin airfoil theory, and a numerical thick airfoil theory (4). All of the above theories apply for spoilered airfoils with wakes which do not reattach to the airfoil surface.

The present work extends the spoiler theory into three dimensions. Since low speed applications are of principal interest in Canada, and since the sectional theories developed by Jandali and Brown are applicable

to incompressible flow, it was decided that it would be appropiate to extend the theory into three dimensions by means of Prandtl's lifting line theory (5). The lifting line theory overpredicts the lift for smaller aspect ratios. Jones (6) has proposed a modification to the lifting line theory which corrects the overprediction and this is incorporated into the theory. The linearised thin airfoil theory of Brown is used to calculate the spoilered section parameters which are required as input to the lifting line theory. Other theories, such as those of Woods or Jandali, or Brown's numerical thick airfoil theory, may of course be used.

If the sectional parameters derived from two dimensional base pressure inputs to the spoiler theories are used in the lifting line theory, errors will result because the three dimensional base pressures differ from the corresponding two dimensional values. Flow around the vertical edges of the finite span spoiler reduces the negative base pressure and creates spanwise gradients of base pressure which are absent from two dimensional flows. Since spoilered section characteristics are a function of base pressure coefficients, it is clear that three dimensional base pressure coefficients must be used as input to the sectional theories in order to obtain sectional parameters appropiate to finite span flows.

All of the above mentioned spoiler theories are developed for unvented spoilers. While the possibility exists that some of the theories may be modified to take into account the effect of base vents, this course of action is not attempted in the present thesis. Instead the effect of base venting is examined experimentally. It is found that for small base vents of about ten percent spoiler height or less, the vented

spoiler behavior is little different from the unvented. Thus for the purposes of preliminary design, the unvented spoiler characteristics may be used for spoilers with base vents of about ten percent or less. The restriction to base vents of about ten percent or less is not a serious limitation, since in practice, most base vents are about this size.

2. THEORY

2.1.1 The Lifting Line Theory

The linearised lifting line theory as formulated by Prandtl, is applicable to unswept wings of moderate to large aspect ratio operating at low mach numbers. The wing is placed in a right handed orthogonal coordinate system as shown in Figure 1. The origin of the system is located at the aerodynamic center of the wing root section. The free stream velocity is in the positive x direction. The wing is modelled as a lifting line of bound vortices located on the y axis, covering the span of the wing, and a system of trailing vortices in the plane of the free stream velocity. The trailing vortices induce a downward velocity over the wing, called the downwash w_i, which alters the direction of the onset flow, and thus reduces the effective sectional angle of attack by an amount known as the induced angle of attack α_i. The sectional lift coefficient is therefore given by

$$C_l = m_o (\alpha_a + \alpha_i) = \frac{L'}{\frac{1}{2}\rho U^2 c} \qquad (1)$$

The sectional lift is still given by the Kutta-Joukowsky Law,

$$L' = \rho U \Gamma \qquad (2)$$

Substitution of equation (2) into equation (1) gives

$$C_l = \frac{2\Gamma}{Uc} = m_o \left(\alpha_a + \alpha_i \right) \tag{3}$$

In this equation, only the circulation is unknown, since the induced angle of attack may be expressed in terms of the circulation by the Biot-Savart Law. Thus

$$\alpha_i = \frac{w_i}{U} = \frac{1}{4\pi} \int_{-b}^{b} \frac{d\Gamma/dy}{y - y_o} \, dy \tag{4}$$

Glauert (7) has shown that the circulation of a finite wing may be expressed in terms of the Fourier series

$$\Gamma = 4bU \sum_{n=1}^{\infty} A_n \, \mathrm{Sin}\, n\mu \tag{5}$$

where U is the free stream velocity, b the wing semi-span, and μ is defined in terms of the spanwise coordinate by

$$y = b \, \mathrm{Cos}\, \mu \tag{6}$$

Substitution of equations (5) and (4) into (3) leads to the fundamental equation for the unknown coefficients A_n

$$\sum_{n=1}^{\infty} A_n \, \mathrm{Sin}\, n\mu \left[\frac{8b}{m_o c} \mathrm{Sin}\mu + n \right] = \alpha_a \mathrm{Sin}\mu \tag{7}$$

where c, m_o and α_a are the sectional chord, lift curve slope and absolute angle of attack. The parameters c, m_o and α_a may vary along the span, depending on whether or not the wing has section changes, taper and twist. The equation must be satisfied for all points between 0 and π for μ.

Solution for the unknown A_n's is achieved by considering a finite number of terms of the Fourier series, say m terms. By choosing the number of span variables μ, equal to the number of terms in the truncated Fourier series, a system of m equations in m unknowns is obtained, and hence a solution for the unknown A_n's. Since only m terms of the Fourier series are considered, equation (7) is satisfied for only m points along the span. Wieselsberger (8) has shown that it is necessary to include the wing tips in calculations for flapped wings. Since equation (7) is degenerate at the tips where μ is equal to 0 or π, L'Hospital's rule must be applied to obtain the result

$$\alpha_a(0) = \sum_{n=1}^{\infty} n^2 A_n$$

$$\alpha_a(\pi) = \sum_{n=1}^{\infty} n^2 A_n (-1)^{n+1} \qquad (8)$$

Once the solution for the unknown Fourier coefficients is found, the lift L, rolling moment R, and the pitching moment about the origin, M_0 may be computed. Since

$$dL = L'dy = \rho U \Gamma(y)\, dy$$

$$dM_0 = (-L' x_{ac} + M_{ac}) dy \tag{9}$$

$$dR = L'y\, dy$$

L,R, and M_0 are obtained by integrating across the span. The pitching moment about the origin M_0 is related to the pitching moment about the aerodynamic center M_{AC} by

$$M_0 = -Lx_{AC} + M_{AC} \tag{10}$$

Since the results are to be compared with reflection plane experiments, the integrations are made over the semi-span. The results may be expressed in coefficient form by means of the formulae

$$C_L = \frac{L}{\frac{1}{2}\rho U^2 S}$$

$$C_{MAC} = \frac{M_{AC}}{\frac{1}{2}\rho U^2 Sc} \tag{11}$$

$$C_R = \frac{R}{\frac{1}{2}\rho U^2 Sb}$$

where S is the planform area of the half wing. When equations (9) are integrated and substituted into equations (11), the following results are obtained:

$$C_L = \frac{2\pi b^2}{S} A_1 \tag{12}$$

$$C_R = \frac{8b^2}{S} \sum_{i=1}^{m} A_{(2i-1)} \frac{(-1)^i}{(2i-3)(2i+1)} \tag{13}$$

$$C_{MO} = \frac{b}{S^2} \int_o^b c^2 C_{mac}\, dy - \frac{8b^3}{S^2} \cos \alpha_r$$

$$\int_o^{\pi/2} x_{ac} \sum_{i=1}^{m} A_{(2i-1)} \sin(2i-1)\mu \sin\mu \, d\mu \tag{14}$$

In equation (14), α_r is the angle of attack of the wing root section.

2.1.2 The Jones Edge Correction Factor

Jones (6) has proposed a correction for the lifting line theory, which is known to overpredict lift for the smaller aspect ratios. In wing section theory the Kutta condition, which determines circulation and hence lift, depends on the edge velocity induced by the relative normal velocity of the section. Jones has shown that the velocity potential on the surface of an elliptic disk, lying in the xy plane with its center at the origin of the coordinate system, and moving with unit velocity in z direction, is given by

$$\phi_e = \frac{k_e}{E} \sin \tau$$

where τ is the chordwise variable given by $\tau = \cos^{-1}(k/k_e)$, E is the semi-perimeter of the disk divided by the semi-span, k is the chordwise coordinate, and k_e the chordwise coordinate of the edge of the elliptic disk, the value of which is given by $k_e = c_e(1 - y^2/b^2)$. Here y is the spanwise coordinate, b the length of the semi-major axis (semi-span) and c_e the length of the semi-minor axis (root semi-chord), of the elliptic disk.

For an infinite disk, E = 1. Thus the ratios of the edge velocities for the infinite and finite elliptic disks is 1/E. The factor E is called the Jones Edge Correction Factor. It is an exact correction for elliptic wings, but is approximate for other planforms. From this correction it can be seen that the sectional values of lift and circulation must be reduced by a factor of 1/E in three dimensional flows. The various equations in Section 2.2.1 must be modified accordingly. In particular equation (7) must be rewritten as,

$$\sum_{n=1}^{\infty} A_n \, \mathrm{Sin}\, n\mu \, [\frac{8bE}{m_o c} \mathrm{Sin}\mu + n] = \alpha_a \, \mathrm{Sin}\mu \qquad (7a)$$

2.2 Application to Wings with Spoilers

Experimental and theoretical investigations of two dimensional airfoils with spoilers (2), have shown that the effect of the spoiler on the sectional characteristics is to alter the lift curve slope m_o, the zero lift angle of attack α_{lo}, the aerodynamic center x_{ac}, and the pitching moment about the aerodynamic center, M_{ac} (The absolute angle of attack α_a is related to the geometric angle of attack by ($\alpha_a = \alpha - \alpha_{lo}$)). Let m_{os} and α_{los} be the lift curve slope and zero lift angle of attack of the spoilered sections. Then in applying equation (7a) to a wing with a part span spoiler, α_{as}, the absolute angle of attack of the spoilered section ($\alpha_{as} = \alpha - \alpha_{los}$), and m_{os} must replace α_a and m_o over the spoilered wing sections. This results in discontinuities in the lift curve slope and angle of attack distributions across the wing. For an infinite Fourier series, the positions of the discontinuities are exactly fixed, since all values of the span variable μ are covered by the series. For a finite Fourier series however, the values of the lift curve slope and angle of attack must change from one value to another over two adjacent values of μ. This may be considered to be a gradual change in sectional lift curve slope and angle of attack over a finite range of μ, and is an approximation of the real situation. The positions of each discontinuity may be made to lie midway between two adjacent values of μ.

Once equation (7a) is solved, the various aerodynamic coefficients may be found by applying equations (12) to (14). For an untwisted rectangular wing of constant section with part span spoilers, equation (14) may be further simplified. Let C_{macs} and x_{acs} be the pitching moment coefficient about the aerodynamic center, and the aerodynamic

center of the spoilered sections. C_{mac}, the pitching moment coefficient about the aerodynamic center of the unspoilered sections, is constant since the wing is of constant section. Also, $x_{ac} = 0$ for a rectangular wing over the unspoilered sections. Hence equation (14) reduces to

$$C_{MO} = C_{mac} \left[1 - \frac{b_s}{b} \right] + \frac{1}{b} \int_{y_1}^{y_2} C_{macs}\, dy - \frac{8b}{c} \cos \alpha_r$$

$$\sum_{i=1}^{m} A_{2i-1} \int_{\mu_1}^{\mu_2} \frac{x_{acs}}{c} \sin (2i-1)\mu \sin\mu \, d\mu \qquad (15)$$

where b_s is the spoiler span, y_1 and y_2 are the spanwise positions of the inner and outer spoiler tips. Similarly μ_1 and μ_2 are the positions of the inner and outer spoiler tips in terms of the span variable μ. C_{MAC} may be obtained from C_{MO} by applying equation (10).

The spoilered section parameters m_{os}, α_{los}, C_{macs}, and x_{acs} may be calculated using any of the previously mentioned theories for spoilers. In the present work, Brown's linearised thin airfoil theory for spoilers (2) is used. Brown has developed the theory to predict lift only. Bernier (9) has extended the theory to include the prediction of the pitching moment coefficient.

2.3 Brown's Thin Airfoil Theory for Spoilers

The airfoil section of chord c, is positioned in the physical plane as shown in Figure 2, with its leading edge at the origin. The free stream velocity U, is in the positive x direction, and the airfoil is inclined at a small angle α to the free stream. The spoiler, inclined at an angle δ to the chord, is of height h. Its base is located at a distance s from the leading edge. The airfoil may also have a flap of chord c_η deflected at an angle η to the chord. The wake behind the spoiler is modelled as a constant pressure cavity of finite length. The pressure in the cavity may be defined in terms of the base pressure coefficient, which is given by

$$C_{pb} = \frac{P_c - P_\infty}{\frac{1}{2}\rho U^2}$$

where P_c is the pressure in the spoiler wake, or in terms of the Cavitation Number, K given by

$$K = \frac{P_\infty - P_c}{\frac{1}{2}\rho U^2} = - C_{pb}$$

The airfoil-cavity combination is of total length ℓ.

In the linearised physical plane as shown in Figure 3, the wetted airfoil surface and cavity boundary occupies a slit on the positive x axis. The field in the linearised physical plane is mapped conformally onto the upper half ζ-plane external to a unit semicircle centered at

the origin by a series of transformations. The wetted airfoil surface itself is mapped onto the unit semicircle, while the cavity boundaries occupy the real axis external to the unit semicircle.

The flow model adopted is similar to that of Parkin (10), who has extended the complex acceleration potential method of Biot (11) to solve the foil-cavity problem. As the theory is linearised, the various geometric parameters of the airfoil may be considered separately and superimposed to give the complete solution. Complex acceleration potentials satisfying the boundary conditions imposed by the geometric parameters of the airfoil are found in the ζ-plane and superposed to give the complete solution for the airfoil with spoiler. The solution in the Z-plane is found by matching corresponding points in the Z and ζ-planes. The airfoil coefficients may be obtained by applying the Blasius Equations

$$C_{ds} - iC_{ls} = \frac{2i}{c}\oint F(Z)\, dZ$$

$$C_{mos} = \frac{2}{c^2}\, RL \oint ZF(Z)\, dZ \qquad (16)$$

The aerodynamic center and the pitching moment coefficient about the aerodynamic center are found using

$$C_{mos} = \frac{-x_{acs}}{c}\, C_l + C_{macs}$$

$$\frac{dC_{mos}}{dC_l} = \frac{-x_{acs}}{c} \qquad (17)$$

2.3.1 The Acceleration Potential

Newton's second law for an incompressible fluid element

$$-\nabla \frac{P}{\rho} = \bar{a}$$

suggests the existence of an acceleration potential ϕ, which has the property

$$\nabla\phi = \bar{a} = -\nabla \frac{P}{\rho}$$

Biot (9) has shown that the acceleration potential function is harmonic, so that a conjugate function ψ, the acceleration stream function exists as well as the complex acceleration potential

$$F(Z) = \phi + i\psi$$

For a small perturbation to the free stream velocity U, the Euler and Cauchy-Riemann equations are related to ϕ and ψ by the linear first order differential equations,

$$\frac{\partial u}{\partial t} + U \frac{\partial u}{\partial x} = U \frac{\partial \phi}{\partial x}$$

$$\frac{\partial w}{\partial t} + U \frac{\partial w}{\partial x} = -U \frac{\partial \psi}{\partial x} \qquad (18)$$

where u, w, ϕ and ψ are non-dimensional but not U, x, z, or t. For steady flows, equations (18) may be integrated to give

$$u = \phi + K/2$$

$$w = -\psi \tag{19}$$

where K is the cavitation number. The constants of integration are determined by choosing the constant value of ϕ to be equal to zero on the cavity boundaries, and by the conditions at infinity. The linearised pressure coefficient is given by

$$C_p = -2u = -2\phi - K \tag{20}$$

2.3.2 Conformal Transformations

The airfoil in the linearised physical Z-plane is shown in Figure 3. The spoiler base and tip are at x = s and x = t respectively. The flap hinge point is at x = n, the trailing edge at x = c, and the cavity termination is at x = ℓ.

The first transformation

$$z' = \frac{Z}{\ell - Z}$$

maps the cavity termination to infinity, and the point at infinity to -1.

The second transformation

$$\nu = a\,(z')^{\frac{1}{2}} \qquad \text{where} \quad a = \left(\frac{\ell - c}{c}\right)^{\frac{1}{2}}$$

maps the entire z' plane onto the upper half of the ν-plane. The airfoil lies between $-1 \leq \nu \leq b$ on the real axis. The upper and lower boundaries of the cavity lie on the real axis between $b \leq \nu \leq \infty$, and $-\infty \leq \nu \leq -1$ respectively. The final transformation

$$\nu = \frac{b+1}{4}\left(\zeta + \frac{1}{\zeta}\right) - \frac{1-b}{2} \qquad \text{where} \quad b = a\left(\frac{t}{\ell - t}\right)^{\frac{1}{2}}$$

is a Joukowsky transformation which maps the wetted airfoil surface onto a unit semicircle centered at the origin. The cavity boundaries remain on the real axis, external to the unit semicircle. By combining the transformations, the equation

$$Z = f(\zeta) = \frac{\ell a^{-2}\left[\frac{1}{4}(b+1)(\zeta+\zeta^{-1}) - \frac{1}{2}(1-b)\right]^2}{1 + a^{-2}\left[\frac{1}{4}(b+1)(\zeta+\zeta^{-1}) - \frac{1}{2}(1-b)\right]^2}$$

is obtained. Major points of interest in the ζ-plane are:

a) the airfoil nose

$$\theta_o = \mathrm{Cos}^{-1}\left(\frac{1 - b}{1 + b}\right) ;$$

b) the spoiler base

$$\theta_1 = \text{Cos}^{-1}\left[\frac{2}{1+b}\left\{a\left(\frac{s}{\ell-s}\right)^{\frac{1}{2}} + \frac{1-b}{2}\right\}\right] ;$$

c) the flap hinge point

$$\theta_2 = \text{Cos}^{-1}\left[\frac{2}{1+b}\left\{\frac{1-b}{2} - a\left(\frac{c - c_\eta}{\ell-c-c_\eta}\right)^{\frac{1}{2}}\right\}\right] ;$$

d) the point at infinity

$$\zeta_i = \frac{2}{1+b}\left[ia + \frac{1-b}{2}\right] + \left[\left(\frac{2}{1+b}\right)^2\left\{ia + \frac{1-b}{2}\right\}^2 - 1\right]^{\frac{1}{2}} .$$

2.3.3 Boundary Conditions

The boundary conditions for the problem are:

(i) $\phi = 0$ on the cavity boundaries;

(ii) the Kutta condition, ϕ is continuous at the spoiler tip and the airfoil trailing edge;

(iii) the airfoil surface normal boundary condition

$$w = -\psi = \frac{dy}{dx} ;$$

(iv) the boundary condition at infinity

$$F(Z) = -K/2 ;$$

(v) the body-cavity system to be the equivalent of a single closed

body. In potential flow, this equivalent body must have zero drag. Equation (16) gives

$$\mathrm{Im} \oint F(Z)dZ = 0$$

2.3.4 Flow Model

Complex acceleration potential functions are found in the ζ-plane to satisfy the boundary conditions enumerated in Section 2.3.3. Separate functions for incidence, camber, thickness, spoiler and flap, are found and superimposed to give the complete solution for the airfoil. The complex acceleration potential functions in the various planes are invariant at corresponding points. The accelerations differ only by the derivatives of the mapping functions. Thus

$$\frac{dF}{d\zeta} = \frac{dF}{dZ} \frac{dZ}{d\zeta}$$

The functions given below satisfy the boundary conditions (i) to (iii). The significance of the various terms in each function is explained in Reference (2).

Incidence function

$$F_{in}(\zeta) = iC_o \left[\frac{1}{\zeta e^{i\theta_0} - 1} + \frac{1}{\zeta e^{-i\theta_0} - 1} \right] + iB_o \left(\zeta - \frac{1}{\zeta} \right) + iD_o \qquad (22)$$

Camber function

$$F_c(\zeta) = -i \sum_{n=1}^{\infty} \frac{M_n}{\zeta^n} \tag{23}$$

Thickness function

$$F_t(\zeta) = \frac{i\zeta}{(\zeta - e^{i\theta_0})(\zeta - e^{-i\theta_0})} \sum_{n=0}^{\infty} \frac{N_n}{\zeta^n} \tag{24}$$

Spoiler function

$$F_s(\zeta) = \frac{\mathrm{Sin}\delta}{\pi} \left[\frac{i\theta_1}{\zeta e^{i\theta_0} - 1} + \frac{i\theta_1}{\zeta e^{-i\theta_0} - 1} + \ln \left(\frac{\zeta - e^{i\theta_1}}{\zeta - e^{-i\theta_1}} \right) \right] \tag{25}$$

Flap function

$$F_f(\zeta) = \frac{\eta}{\pi} \left[\frac{i(\theta_2 - \pi)}{\zeta e^{i\theta_0} - 1} + \frac{i(\theta_2 - \pi)}{\zeta e^{-i\theta_0} - 1} + \ln \left(\frac{\zeta - e^{i\theta_2}}{\zeta - e^{-i\theta_2}} \right) \right] \tag{26}$$

In these equations D_o, M_n, and N_n are real constants whose values are given by :

$$D_o = \alpha - \frac{1}{\pi} \int_0^{\pi} \frac{dy_c}{dx} d\theta + C_o \; ;$$

$$M_n = \frac{2}{\pi} \int_0^{\pi} \frac{dy_c}{dx} \mathrm{Cos}\, n\theta \, d\theta \; ;$$

$$N_o = \frac{2}{\pi} \int_0^{\pi} \frac{dy_t}{dx} (\mathrm{Cos}\theta_o - \mathrm{Cos}\theta) \, d\theta \; ;$$

$$N_n = \frac{4}{\pi} \int_0^{\pi} \frac{dy_t}{dx} \left(\cos\theta_0 - \cos\theta \right) \cos n\theta \, d\theta \quad ; \qquad n \geq 1 \quad ;$$

where y_c and y_t are functions representing the camber and thickness of the airfoil. B_o and C_o are real constants whose values are determined by boundary condition (iv),

$$F_{in}(\zeta_i)+F_c(\zeta_i)+F_t(\zeta_i)+F_s(\zeta_i)+F_f(\zeta_i) = -\tfrac{1}{2}K \ , \tag{27}$$

where ζ_i is the point at infinity. The unknown constants are contained in $F_{in}(\zeta_i)$. The real and imaginary parts of equation (27) give two simultaneous equations, which are solved to give

$$B_o = \frac{Rl\lambda_1[ImE - (\alpha - \tfrac{1}{2}M_o)] - Im\lambda_1 RlE + \tfrac{1}{2}KIm\lambda_1}{Rl\lambda_1 Im\lambda_2 - Im\lambda_1 Rl\lambda_2} \quad ;$$

$$C_o = \frac{Rl\ E - B_o Rl\lambda_2 - \tfrac{1}{2}K}{Rl\lambda_1} \quad ; \tag{28}$$

where

$$\lambda_1 = i \left[\frac{1}{\zeta_i e^{i\theta_0} - 1} + \frac{1}{\zeta_i e^{-i\theta_0} - 1} + 1 \right] ,$$

$$\lambda_2 = i \left(\zeta_i - \frac{1}{\zeta_i} \right) ,$$

$$E = - F_c(\zeta_i) - F_t(\zeta_i) - F_s(\zeta_i) - F_f(\zeta_i) \ .$$

The remaining unknowns are the cavity length ℓ, and the cavitation number K. The cavitation number cannot be predicted theoretically at the

present time. K and ℓ are related through boundary condition (v). Thus only K is required as input to the theory. By choosing a contour such that $|Z| >> \ell$, Z may be expressed as a Laurent series expansion, and the closure condition becomes,

$$\text{Rl [coefficient } Z^{-1} \text{] = 0 .}$$

The solution of this equation in terms of K and ℓ is equation (29), which is given in the appendix. An iterative technique must be used to solve this equation, because θ_0, θ_1, and θ_2 are complex functions of ℓ.

The solution to the problem may now be completed by determining the pressure, lift, and pitching moment coefficients. The pressure coefficient is obtained from equation (20). By adding the real parts of equations (22) to (26), which are the acceleration potentials and substituting into equation (20), the pressure coefficient in the ζ-plane is obtained. Points on the airfoil may be related to corresponding points on the circle by equation (21). Thus

$$x = \frac{\ell a^{-2}[\frac{1}{2}(b+1)\cos\theta - \frac{1}{2}(1-b)]^2}{1 + a^{-2}[\frac{1}{2}(b+1)\cos\theta - \frac{1}{2}(1-b)]^2} \quad .$$

The lift and pitching moment coefficients are obtained from equations (16) and the Laurent series expansion of ζ. The equations for pressure, lift, and pitching moment coefficient are given in the appendix.

2.3.5 Base Vented Spoilers

In some applications, base vented spoilers are used. Typically the base vent is about 10% of spoiler height. Although the possibility exists that Jandali's thick airfoil theory or Brown's numerical thick airfoil theory may be modified to include the effects of base venting, this course of action is not attempted in the present work. Instead the effects of base venting are examined experimentally. A two dimensional Joukowsky airfoil of 11% thickness and 2.4% camber is tested with a series of base vented spoilers of height equal to 10% of chord. The base vents on the spoilers ranged in size from 10 to 50% of spoiler height.

The results of the base venting experiments are presented in Figures 11 to 13. These figures show that for base vents of about 10% of spoiler height or less, the vented spoiler characteristics are quite close to the unvented. Thus it may be concluded that for base vents of about 10% of spoiler height or less, the unvented spoilered section characteristics are close enough to the vented to be used for preliminary design purposes.

2.4 Experimental Two Dimensional Base Pressures

Brown's theory, in common with the other spoiler theories mentioned previously, requires as input, the base pressure coefficient behind the spoiler. At the present time, the base pressure coefficient cannot be predicted theoretically, so experimentally determined values must be used. Figure 39 shows the results of an experiment designed to find the base pressure coefficient behind a two dimensional airfoil of NACA 0015 section fitted with a normal unvented spoiler of height equal to 9.7% of chord. The spoiler is fitted to the airfoil at positions ranging from 0.48 to 0.77 chord. Figure 40 presents a similar result for a 12.9% thick Clark Y airfoil with a 10% unvented normal spoiler. The spoiler position along the chord ranged between 0.5 and 0.7 chord.

If the experimental values of base pressure coefficient shown in the above mentioned figures are used directly in the theory, then a non-linear lift curve, inappropiate to a linear theory is obtained. To overcome this, Brown linearised the base pressure distribution. In the present work, an average value of base pressure coefficient, denoted by $\bar{C}_{pb}$, is used for the following reasons:

(i) Since the base pressure coefficient varies in a highly non-linear manner with angle of attack for most airfoils, the use of linearised values is no more appropriate than the use of an averaged value. Predictions using both inputs are shown in Figures 15 and 16. It may be seen that good results may be obtained using either input.

(ii) In taking three dimensional base pressure measurements behind finite span spoilers mounted on finite span wings, the downwash induced by the trailing vorticity reduces the effective angle of attack, so that $\alpha_e = \alpha_a + \alpha_i$, where α_i is the induced angle of attack. In general α_i

will vary along the span and is not easy to measure. Thus it will be hard to linearise the three dimensional base pressures because of the difficulty associated with finding the effective angle of attack at which each spoilered section is operating.

The base pressure coefficient $\bar{C}_{pb}$ is averaged over the incidence range given by $0 \leq \alpha \leq \alpha_{stall}$, where α is the angle of attack of the spoilered section, measured with respect to the zero lift angle of the unspoilered section. The rationale behind this choice of angles is that in practice, the spoilers will only be used when the basic wing is generating positive lift and operating below stall. Values of $\bar{C}_{pb}$ for both the Clark Y and NACA 0015 airfoil sections is given in Table I.

AIRFOIL	s/c	$-\bar{C}_{pb}$	AIRFOIL	s/c	$-\bar{C}_{pb}$
NACA 0015	0.48	0.552	CLARK Y	0.50	0.624
with 9.7%	0.58	0.559	with 10%	0.60	0.612
spoilers	0.68	0.562	spoilers	0.70	0.610
	0.77	0.551	(12.9% thick)		

Table I. Values of $\bar{C}_{pb}$ for Two Dimensional Clark Y and NACA 0015 Airfoils with Normal Unvented Spoilers.

Typical comparisons between theory and experiment are shown in Figures 15 and 16. The prediction of lift is good. The prediction of pitching moment is however less accurate, because Brown's theoretical model predicts a singularity at the spoiler base. This singularity, which is characteristic of linearised thin airfoil theories, causes a positive increase in the pitching moment prediction. A more accurate result for pitching moment

would be obtained by using thick airfoil theories for spoilered airfoils, such as those of Jandali and Brown (3,4). In these theories, a stagnation point would replace the singularity at the spoiler base. However, even if thick airfoil theories are used, there would still be errors in the pitching moment prediction, because in real flows a separation bubble would be formed in the region immediately in front of the spoiler, and the stagnation pressure would not be achieved.

2.5 Experimental Finite Span Base Pressures

Although Brown's theory is in good agreement with experiments, sectional parameters obtained from two dimensional base pressure inputs are inappropiate for use with finite span spoilers, which have wakes that are significantly different from two dimensional spoilers. Flow around the vertical edges of a finite span spoiler creates spanwise gradients of base pressure which are absent from two dimensional spoiler flows. Base pressure coefficients for finite span spoilers may be larger or smaller than the corresponding two dimensional value, depending on the length to height ratio of the spoiler, and on position along the spoiler span. Since spoilered section parameters are dependent on base pressure, it is clear that their values in three dimensional flows will differ from the two dimensional case. In this context, it should also be noted that the use of spoilered section parameters derived from two dimensional experiments will also be inappropriate. Such experimental values must be modified to account for the difference in base pressure between two and three dimensional flows. This is considered in Section 2.6.

Figures 41 to 43 show the results of tests designed to find the base pressures behind finite span unvented spoilers mounted normal to the wing surface. Rectangular half wings of NACA 0015 section and of equivalent aspect ratios ranging from 3.87 to 7.73 are tested in the reflection plane configuration. Spoiler spans of 20, 30, 40, and 50% of wing semispan, and of height equal to 9.7% of chord are mounted on the wings at positions varying from 0.48 to 0.77 chord. The inboard tips of the spoilers are always fixed at midspan. The height and chordwise location of the spoilers are the same as for the two dimensional tests mentioned in Section 2.4.

Figure 41 shows the effect of varying the chordwise location of the spoiler with the aspect ratio and spoiler span held constant. Figure 42 shows the variation of the base pressure coefficient as a function of spoiler span, with aspect ratio and spoiler position along the chord held constant. Figure 43 shows the variation of base pressure coefficient as a function of aspect ratio, with spoiler location along the chord and spoiler percent of span held constant. The figures give some idea about the complexity of the variation of base pressures along the spoiler span when changes are made to wing aspect ratio, spoiler span, and spoiler position along the chord.

For finite span wings with part span spoilers, the lifting line equation (7a) is solved for a finite number of terms, m by choosing m values of the span variable μ, and forming a system of m equations in m unknowns. Some of the m points will fall on the spoilered sections of the wing. The base pressure coefficients at these points are used as inputs to the two dimensional theory to obtain the spoilered section parameters α_{los}, m_{os}, x_{acs}, and C_{macs} which are required as inputs to equation (7a). Since base pressure varies across the spoiler span, the spoilered section characteristics will also vary. The solution of equation (7a) together with equations (12) to (15), give the aerodynamic coefficients of the spoilered wing. Such theoretical predictions are compared with experiments in Figures 17 to 24. Agreement between theory and experiment is seen to be good.

2.6 Empirical Relationships for Base Pressures

The theory as developed to this point requires as input the $\bar{C}_{pb}$ distribution across the spoiler span. This information must at present be obtained from wind tunnel tests, since no prediction methods are available. This is a serious defect, since one of the theory's purposes is to provide performance predictions for a variety of wing-spoiler combinations without incurring the cost and time penalties associated with the wind tunnel testing of every configuration. From the theoretical predictions, the designer may select the wing-spoiler combination most suited to his needs. This advantage is lost if base pressure distributions have to be measured experimentally for each configuration before the theory can be applied. Furthermore, it would be a relatively simple task to take lift and moment measurements together with the base pressures. Experimental values of lift and moment coefficients, more accurate than the theoretical predictions may then be calculated, thus rendering the theory superfluous. The theory would be little more than an interesting academic exercise. To be of utility, some method must be devised to predict the three dimensional base pressures behind the spoiler, either from experimental measurements or from theory. In the following sections, an attempt to predict the three dimensional base pressures is made, based on empirical measurements. The method does not eliminate experimental determinations of base pressure coefficients entirely, but rather reduces substantially, the amount of experimentation.

2.6.1 $\bar{C}_{pb}$ Averaged Across Span

Figures 47 to 49 show values of $\bar{C}_{pb}$ averaged across the spoiler span,

which will henceforth be denoted by $\bar{\bar{C}}_{pb}$, plotted as a function of non-dimensional spoiler span b_s/h. The quantity b_s/h may be considered to be the spoiler aspect ratio. The wing-spoiler combinations are the same as those mentioned in section 2.5. The Figures show that for each chordwise location of the spoilers, the value of $\bar{\bar{C}}_{pb}$ remains nearly constant with respect to spoiler aspect ratio, over the measured range $4 \leq b_s/h \leq 20$. This may appear to be a surprising result, since it may be expected that as the spoiler aspect ratio is increased, the flow would become increasingly two dimensional, and that the value of $\bar{\bar{C}}_{pb}$ would approach the sectional value $\bar{C}_{pb}$. Hoerner (12) presents a similar result for flat plates normal to the flow, which is a somewhat similar flow to that of a spoiler mounted on a wing. By combining the results from several sources, he showed that for $1 \leq b/h \leq 10$, where b/h is the width to height ratio of the plate, the drag coefficient is nearly constant. For values of b/h greater than 10, the drag coefficient rises slowly towards the two dimensional value. However, the two dimensional drag coefficient is not approached until b/h is about 50 or more. Thus it would appear that two dimensionality in flow is not approached until very high aspect ratios are reached. Since the drag of a flat plate normal to the flow is mostly pressure drag, a constant value of drag implies that the average pressure over the front and rear of the plate, and hence the base pressure, is also constant.

It may immediately be seen that the use of $\bar{\bar{C}}_{pb}$ as input to the sectional theory, has the advantage that if one spoiler of aspect ratio between 4 and 20 is tested on a finite wing, then the value of $\bar{\bar{C}}_{pb}$ so obtained will be valid for all spoilers of the same height and angle of

deflection δ, mounted on wings of the same section and at the same chordwise position, within the spoiler aspect ratio range of $4 \leq b_s/h \leq 20$. The amount of experimentation is thus reduced to a single determination of $\bar{\bar{C}}_{pb}$ for each wing section, chordwise spoiler position, spoiler height, and spoiler inclination. It should be noted that the spoiler aspect ratio range of $4 \leq b_s/h \leq 20$ is quite wide, and will likely cover all spoiler lengths that may be used.

A summary of the two and three dimensional base pressure coefficient measurements is given in Table II. The values of $\bar{\bar{C}}_{pb}$ shown, are averages for all spoiler lengths at the given chordwise location. G is defined as the ratio $\bar{\bar{C}}_{pb}/\bar{C}_{pb}$.

AIRFOIL	s/c	$-\bar{C}_{pb}$	$-\bar{\bar{C}}_{pb}$	G
NACA 0015 with	0.48	0.552	0.495	0.896
9.7% unvented	0.58	0.559	0.473	0.846
normal	0.68	0.562	0.470	0.836
spoiler	0.77	0.551	0.448	0.825
12.9% Clark Y	0.50	0.624	0.547	0.876
with 10% normal	0.60	0.612	0.519	0.848
unvented spoiler	0.70	0.610	0.512	0.839

Table II. Base Pressure Coefficients for Spoilered NACA 0015 & 12.9% Clark Y Airfoils

Although Table II shows that the values of $\bar{\bar{C}}_{pb}$ are quite different for the two airfoils, a plot of $\bar{\bar{C}}_{pb} / \bar{\bar{C}}^*_{pb}$ against s/c (Figure 50), where $\bar{\bar{C}}^*_{pb}$ is the value of $\bar{\bar{C}}_{pb}$ at the 0.7 chord position reveals that the variation of $\bar{\bar{C}}_{pb} / \bar{\bar{C}}^*_{pb}$ with spoiler position along the chord is almost the same for both airfoils. Also a plot of G/G* against s/c (Figure 50) where G* is the value of G at the 0.7 chord position, yields a similar result. The curves in Figure 50 show that there is a small decrease in $\bar{\bar{C}}_{pb}$ as spoiler position along the chord is moved toward the trailing edge. This decrease may be approximated by the linear relation

$$\bar{\bar{C}}_{pb} = \bar{\bar{C}}^*_{pb} \quad [\ 1.0 \quad - 0.445(s/c - 0.7)\ ] \tag{32}$$

Thus $\bar{\bar{C}}_{pb}$ need only be measured at s/c=0.7 for a given airfoil section. For any other chordwise location of the spoiler between $0.5 \leq s/c \leq 0.8$ equation (32) may be used to find $\bar{\bar{C}}_{pb}$. If the two dimensional base pressure coefficient is known at the 0.7 chord position, then the relationship,

$$\bar{\bar{C}}_{pb} = 0.830\ \bar{C}^*_{pb}\ [\ 1.0 \quad - 0.255\ (s/c - 0.7)\ ] \tag{33}$$

may be used. $\bar{C}^*_{pb}$ is the value of $\bar{C}_{pb}$ at the 0.7 chord position. Equations (32) and (33) are valid for both the Clark Y and NACA 0015 airfoils, fitted with 10% spoilers. Use of these equations is suggested for other airfoils, spoiler heights and inclinations, as it is unlikely that the variations will be too different from the above.

In Table III, the sectional characteristics in three dimensional flows of the NACA 0015 section fitted with 9.7% unvented normal spoilers, as predicted by Brown's theory, is given. The values of $\bar{\bar{C}}_{pb}$ used as input are obtained by using equation (32) together with the value of $\bar{\bar{C}}^*_{pb}$ from Table II.

s/c	$\bar{\bar{C}}_{pb}$	m_{os}	α_{los}	C_{macs}	x_{acs}/c
0.48	0.497	4.595	0.2116	0.0786	-0.0378
0.58	0.482	5.033	0.2049	0.1161	-0.0252
0.68	0.467	5.448	0.1997	0.1569	-0.0120
0.77	0.451	5.827	0.1960	0.1977	0.0010

Table III. Sectional Characteristics of a NACA 0015 Airfoil Fitted with 9.7% Unvented, Normal Spoilers

2.6.2 Variation of Sectional Properties with Base Pressure

In the previous section, it is shown that the use of $\bar{\bar{C}}_{pb}$, the base pressure coefficient averaged across span and incidence, as input to the theory, has the advantage of reducing by a large amount, the experimental determination of base pressurures. However the use of such an average will only be valid if the sectional characteristics vary linearly with the base pressure. Although the theory is linear, it must not be expected that the variation of sectional properties with base pressure will also be linear. In the satisfaction of boundary condition (v) in Section 2.3.3, a non-linear relationship between K, the cavitation number, (and hence $\bar{C}_{pb}$) and

ℓ, the cavity length is established through equation (29). The angles θ_0, θ_1, and θ_2, which appear in the complex acceleration potential functions in Section 2.3.4 are related to ℓ through the conformal transformations. Hence the solution to the problem is dependent on ℓ, which varies in a non-linear manner with the base pressure coefficient.

Figures 4 to 6 show the variation of sectional properties with base pressure coefficient, for a NACA 0015 airfoil section fitted with a normal unvented spoiler of height equal to 9.7% of chord. The spoiler is mounted at chordwise locations ranging from 0.48 to 0.77 chord. These figures show that the sensitivity of section characteristics to changes in base pressure coefficient is decreased as the spoiler position along the chord is moved towards the trailing edge. Also, the variation of section characteristics is only very slightly non-linear. Thus the use of $\bar{\bar{C}}_{pb}$ is justified.

In the prediction of rolling moment, an additional complication arises. Since the rolling moment about the origin is given by,

$$R = \int_0^b y \, dL'$$

where y is the spanwise coordinate, the sectional lift near the wing tips will contribute more to the rolling moment because of the weighting factor y. For example, if the $\bar{C}_{pb}$ distribution across the span is such that the spoilered section lift L'_s increases as y increases, then the prediction of rolling moment using $\bar{\bar{C}}_{pb}$ will be low. Conversely, if the $\bar{C}_{pb}$ distribution is such that L'_s decreases as y increases, then the reverse will be true.

this effect is minimised if the lift distribution across the spoilered section is symmetrical about the midspan of the spoiler. Fortunately this is approximately true, as Figures 41 to 46 show. In these figures the $\bar{C}_{pb}$ distribution across the spoiler span is approximately symmetrical. Since the sectional lift varies in a nearly linear manner with $\bar{C}_{pb}$, this means that the sectional lift distribution across the span is also approximately symmetric. A second factor which tends to minimise this effect is the insensitivity of the lift to changes in the base pressure coefficient.

2.6.3 Use of Experimental Two Dimensional Spoilered Section Parameters in Finite Wing Theory

The theory as developed to this point is capable of predicting the aerodynamic coefficients of a finite wing with spoiler, using only $\bar{\bar{C}}_{pb}$ as an empirical input. Experimental spoilered section characteristics, if available, may of course, also be used. It has already been shown, that the use of sectional characteristics derived from two dimensional tests in three dimensional theory is inappropriate because of differences in base pressures between two and three dimensional flows. Experimental two dimensional section characteristics must be modified to account for the difference in base pressures before they can be used in three dimensional theory.

In section 2.6.1, it is shown that if the two dimensional base pressure averaged over incidence, $\bar{C}_{pb}$, is known for a spoiler mounted at the 0.7 chord position, then the value of $\bar{\bar{C}}_{pb}$ may be obtained by using equation (33). Theoretical predictions may then be made using $\bar{C}_{pb}$ and

$\bar{\bar{C}}_{pb}$ as inputs. The difference in sectional characteristics due to the difference in base pressure coefficients may be calculated. The differences may then be deducted from the experimental two dimensional sectional parameters to obtain values appropriate for three dimensional flows.

3. EXPERIMENTS

The experimental part of this thesis consists of three series of experiments. In the first, the effect of base venting on spoilered section characteristics is examined. In the second the forces and moments generated by finite wings with part span spoilers are measured, and aerodynamic coefficients calculated. In the third, the base pressure distribution behind spoilers mounted on two and three dimensional wings is measured.

3.1.1 Base Venting Experiments

The purpose of these experiments was to determine the effect of base venting on section characteristics. A Joukowsky airfoil of 11% thickness, 2.4% camber and 12.08 inch chord was used. The airfoil was constructed mainly of wood, with an aluminium center section containing 37 pressure taps of which 24 were on the upper surface. Since the Joukowsky profile was structurally weak near the cusped trailing edge, the upper surface in this region was modified to give an approximately constant thickness of 1/8 inch. The modified profile is shown in Figure 7. The airfoil was fitted with end plates on which spoilers could be mounted at the 0.5, 0.6, 0.7, 0.8 and 0.9 chord positions, normal to the airfoil surface. This airfoil was used by Jandali to verify his spoiler theory, and a full description of it is given in reference (3). A set of 5 spoilers of height equal to 10% of chord, with base vents of 10,20,30,40 and 50 % of spoiler height were made for the airfoil.

The tests were conducted in the small low speed aeronautical wind tunnel in the Department of Mechanical Engineering at the University of

British Columbia. It has a test section of 27 inch height and 36 inch width. The tunnel has good flow uniformity and a turbulence level of less than 0.1 percent over its speed range. The airfoil was mounted vertically and spanned the test section, with small clearances at the roof and floor. The airfoil was attached to a six component pyramidal balance located under the tunnel, at the quarter chord position. Force and moment measurements were taken with the spoilers attached at the 0.5, 0.6, 0.7 and 0.8 chord positions, over a full angle of attack range. Pressure measurements were also taken at some angles of attack using a multi-tube manometer. Test Reynolds number was $4.4\ (10)^5$.

3.2 Finite Wing Experiments

For the finite wing experiments, half wing models were used in order to obtain a good range of aspect ratios, with as large a chord and Reynolds number as possible. Rectangular wings of NACA 0015 section were mounted vertically at the quarter chord position, in the same tunnel-balance system mentioned in Section 3.1. The wings were machined from solid aluminium in spanwise sections of 0.5 and 2.0 inches. The chord was 5.17 inches. By combining appropriate numbers of each of the two sizes of spanwise sections, half wing models of equivalent full aspect ratios of 3.87, 4.83, 5.80, 6.77, and 7.73 were assembled. Holes were drilled and tapped on the upper surface of the wing, so that spoilers of 20, 30, 40 and 50 % of half span, could be mounted at the 0.48, 0.58, 0.68 and 0.77 chord positions. The unvented spoilers, of height equal to 9.7% of chord were mounted on the wings so that in all cases, the inboard tip of the spoiler was positioned at midspan. Force and moment measurements were made for all possible

configurations over a full range of angle of attack.

In addition, two dimensional tests were made to obtain the spoilered section characteristics. A two dimensional wing was made by assembling the 5.17 inch chord sections into a wing spanning the test section of the wind tunnel vertically, with small clearances at the roof and floor. Full span 9.7% normal unvented spoilers were mounted on the wing at the 0.48, 0.58, 0.68 and 0.77 chord positions. Force and moment measurements were made. The two dimensional tests were made in order to obtain comparisons between experiment and the predictions of the Brown theory. Test Reynolds number was $3\ (10)^5$. The NACA 0015 section is shown in Figure 8.

3.3 Base Pressure Measurements.

Measurements of the base pressures behind the spoilers fitted to the two and three dimensional wings tested in Section 3.2 were taken in this series of experiments. This information was required as input to the sectional theory. An additional set of base pressures was taken using 12.9% thick Clark Y wings of 5.9 inch chord. The wings were made of wood in spanwise sections of 3, 6, and 12 inches, which were assembled to give a two dimensional model spanning the test section, and rectangular half wings with equivalent aspect ratios of 4.07, 6.10, and 7.12. In all tests with the Clark Y wing, 10% unvented, normal spoilers were used. They were taped to the surface of the wings at the 0.5, 0.6 and 0.7 chord positions. For the two dimensional tests, the spoilers were full span. For the finite wing tests, the spoilers were of length equal to 20, 30, 40, and 50% of the half wing span. They were mounted on the wings so that the inner tip of the spoilers were always fixed at midspan, as was the case

for the NACA 0015 wings. The Clark Y section is shown in Figure 9.

For the two dimensional tests, a single pressure tap, located at midspan, halfway between the spoiler base and the trailing edge, was used. For the three dimensional tests, ten taps, equally spaced in the spanwise direction, starting at a point 5% of spoiler span away from the inner spoiler tip and moving towards the outer spoiler tip was used. The location of all ten taps in the chordwise direction was halfway between the spoiler base and the trailing edge. The base pressures were measured using the system shown in Figure 10. Whenever a set of base pressures was to be measured, the external start switch was depressed. This activated the PDP-11 computer, which instructed the scanivalve to begin scanning the tunnel dynamic pressure taps, and the pressure taps behind the spoiler. The pressures at each tap were sequentially transmitted by the scanivalve to the barocel, which converted the pressures into voltages. The analog to digital converter then digitalised the voltages and transmitted them to the computer memory for storage. After all the pressure taps had been scanned, the base pressure coefficients were computed and printed on a typewriter. Test Reynolds Number was $3\ (10)^5$.

3.4 Wind Tunnel Wall Corrections

For the Joukowski airfoil, the wind tunnel wall correction technique employed was the same as that of Jandali (3), who used the corrections established by Pope and Harper (13). The non-dimensional wake blockage term was however, modified to $\frac{1}{4}(c/H)C_d$, instead of $\frac{1}{2}(c/H)C_d$, as Jandali found that measurements for airfoils of varying chord lengths collapsed better using the modified term. For pressure coefficients, Jandali used

the equation,

$$\frac{1 - C_p}{1 - C_{pu}} = \frac{C_l}{C_{lu}} \tag{34}$$

where C_p and C_l are the true pressure and lift coefficients at a given angle of attack, and C_{pu} and C_{lu} are the uncorrected pressure and lift coefficients.

The data for the Clark Y and NACA 0015 airfoils were not corrected for wind tunnel wall effects because of the small size of the wings in relation to the tunnel dimensions ($c/H < 0.2$, $S/C < 0.2$). The corrections to the various coefficients were less than 3% and were therefore ignored.

4. RESULTS AND COMPARISONS

4.1 Base Venting Experiments

A sample of the results of experiments using the two dimensional Joukowsky airfoil fitted with 10% normal spoilers with base vents of various sizes is presented in Figures 11 to 13. It may be seen from these figures that the effect of increasing the size of the base vent is to increase lift. For the larger base vents, this effect is substantial at the lower angles of attack. At higher incidence, the curves converge towards the unvented result. For small base vents of around 10% of spoiler height or less however, the increase in lift over the unvented spoiler is small at all angles of attack. The same result is true for the pitching moment about the aerodynamic center. Thus for base vents of about 10% spoiler height or less, the unvented spoiler characteristics are sufficiently close to the vented to be used for preliminary design purposes.

4.2.1 Two Dimensional NACA 0015 Airfoil Experiments

Figure 14 shows the unspoilered NACA 0015 section characteristics. The lift curve shows some non-linearity at the higher angles of attack and the lift curve slope is significantly lower than the theoretical. These effects are due to the low Reynolds number [$3(10)^5$] at which the the tests were conducted. For the theoretical finite wing predictions therefore, linearised experimental values of the section parameters m_o, α_{lo}, and C_{mac} are used.

Figures 15 and 16 are comparisons between experimental and theoretical section characteristics of the NACA 0015 airfoil, with 9.7% unvented normal spoilers mounted at the 0.48 and 0.68 chord positions. Two theoretical curves are shown. The broken lines represent the prediction using a base pressure coefficient linearised with respect to incidence, and the unbroken lines represent the prediction using $\bar{C}_{pb}$, the base pressure coefficient averaged over incidence. The use of these inputs is discussed in Section 2.4. Both inputs give good predictions for lift. The prediction for pitching moment is less accurate than for lift. The reasons for this are already discussed in Section 2.4

4.2.2 Rectangular Wings of NACA 0015 Section Fitted with Part Span Spoilers

Figures 17 to 20 show experimental and theoretical lift and pitching moment comparisons for rectangular half wings of equivalent aspect ratio equal to 7.73, fitted with part span spoilers. The unvented 9.7% normal spoilers are fitted to the wings at the 0.48 chord position. Their spans are equal to 20, 30, 40 and 50% of semi-span. The spoilers are mounted so that the inboard tip of the spoilers are always at mid-span. Figures 21 to 24 are the corresponding rolling moment coefficients for the above mentioned half wings. Since the tests are made with half wing models, the wing rolling moment is defined as

$$C_R = \frac{RM}{\frac{1}{2}\rho U^2 Sb}$$

rather than the more usual definition of

$$C_R = \frac{RM}{\frac{1}{2}\rho U^2 S(2b)}$$

as the former definition is more appropriate to half wing tests. In Figures 17 to 24, two theoretical curves are shown. The broken lines represent the prediction using $\bar{C}_{pb}$, the base pressure coefficient averaged over incidence but varying across the spoiler span. The solid lines represent the prediction using $\bar{\bar{C}}_{pb}$, the base pressure coefficient averaged over both incidence and spoiler span. $\bar{\bar{C}}_{pb}$ is obtained from equation (32), with the value of $\bar{\bar{C}}^*_{pb}$ coming from Table 2. The use of these two inputs is discussed in Sections 2.5 and 2.6, where the advantages of using $\bar{\bar{C}}_{pb}$ are discussed. The predictions given by both inputs are seen to be very close. This confirms that the use of $\bar{\bar{C}}_{pb}$ as predicted by equation (32) is sufficiently accurate for preliminary design purposes.

Figures 25 to 32 are similar to Figures 17 to 24, except that the equivalent aspect ratio is 3.87, and the spoilers are mounted at the 0.68 chord position. Only one theoretical prediction is shown, that using $\bar{\bar{C}}_{pb}$ as the input to the sectional theory. In all of the above mentioned cases, the prediction of lift and roll for the finite rectangular wings is seen to be good. The prediction of pitching moment is less accurate. This is to be expected, since the sectional theory's prediction of pitching moment is less accurate than for lift. Any inaccuracies in the prediction of sectional characteristics, will of course be carried over into the three dimensional theory.

Figure 33 compares the predicted and measured variation with respect to relative spoiler span b_s/h, of the effective moment arm of the incremental

lift caused by spoiler erection. The figure refers to wing spoiler combinations which are the same as for Figures 17 to 24. The data is presented in the form $\Delta C_R/\Delta C_L$, plotted against b_s/b. Figure 34 is similar to Figure 33, except that the wing-spoiler combinations are the same as for Figures 25 to 32. The dashed lines in the two figures represent the variation that would occur if the incremental lift acted at the midspan of the spoiler. The experimental values are averages over the incidence range of -4° to just below stall. The agreement between theory and experiment is seen to be good.

An insight into the reason for the inward shift of the effective moment arm of the incremental lift may be obtained by examining Figures 35 and 36, which show the spanwise distribution of the non-dimensionalised circulation $\Gamma/4bU$. The curves show clearly that the effect of the spoiler is not confined to the spoilered portions of the wing. There is also a loss of circulation and hence lift, over the unspoilered sections of the wings. The loss of lift over the unspoilered sections of the wings is larger inboard of the spoiler. Hence the center of incremental lift is shifted inwards, towards the wing root.

Figure 37 shows the spanwise distribution of the dimensionless circulation $\Gamma/4bU$ for rectangular wings of NACA 0015 section and of aspect ratio 7.73, fitted with symmetrically and asymmetrically deployed normal, 9.7% unvented spoilers of span equal to 40% of semi-span. The spoilers are mounted at the 0.48 chord position, with the inboard tips of the spoilers positioned midway between the wing root and tip. The lower curve is for symmetrically deployed spoilers (spoilers up on both half wings). The middle curve is for asymmetric deployment (spoiler up on one half wing

but retracted on the other). The upper curve is for the unspoilered wing. Figure 38 is similar to Figure 37 except that the aspect ratio is 3.87, and the spoilers are mounted at the 0.68 chord position. The two figures show that the curves for symmetric and asymmetric spoiler deployment are in close agreement. This implies that while the half wing tests strictly correspond to cases of symmetric spoiler deployment for complete wings, they may be used to model cases of asymmetric deployment as well.

4.3.1 Two Dimensional Base Pressure Experiments

Figure 39 shows the variation of base pressure with incidence for a two dimensional airfoil of NACA 0015 section fitted with a 9.7% unvented normal spoiler. The position of the spoiler is varied from 0.48 to 0.77 chord. Figure 40 is similar to Figure 39, except that the section is a 12.9% thick Clark Y, the spoilers are 10%, and the position of the spoiler is varied between 0.5 and 0.7 chord. A comparison of the curves for the NACA section shows that a rearward shift in spoiler position along the chord results in an earlier peak in the base pressure distribution. However, the average value of the base pressure coefficient $\bar{C}_{pb}$, as defined in Section 2.4, does not appear to vary by a large amount. The same trends are apparent for the 12.9% thick Clark Y section. Although the spoilers for both airfoils are similar in geometry and height, the base pressure distributions are quite different. However, the values of $\bar{C}_{pb}$ are not too far apart.

4.3.2 Three Dimensional Base Pressure Experiments

Figures 41 to 43 show the spanwise distribution of $\bar{C}_{pb}$, the base pressure distribution averaged over incidence, for part span spoilers

mounted on rectangular wings of NACA 0015 section. The wing-spoiler configurations are the same as in Section 3.3. In the figures b_t is the spanwise coordinate, measured with respect to the inner spoiler tip, and moving outwards, toward the outer spoiler tip. Figure 41 shows the effect of varying the chordwise position of the spoiler with aspect ratio and spoiler span held constant. Figure 42 shows the variation of $\bar{C}_{pb}$ as a function of spoiler span, with aspect ratio and spoiler position along the chord held constant. Figure 43 shows the variation of $\bar{C}_{pb}$ as a function of aspect ratio, with spoiler percent of span and chordwise spoiler position held constant. Figures 44 to 46 are plots similar to Figures 42 to 44 except that the section is a 12.9% Clark Y.

Figures 41 to 46 reveal the complex manner in which $\bar{C}_{pb}$ varies across the spoiler span, as the various parameters are changed. Plots of $\bar{\bar{C}}_{pb}$ against non dimensional spoiler span b_s/h reveal a considerable simplification. Figures 47 49 show plots of $\bar{\bar{C}}_{pb}$ against b_s/h. These figures show that at each chordwise location the value of $\bar{\bar{C}}_{pb}$ remains nearly constant for each airfoil, regardless of aspect ratio and spoiler length. The implications of this are discussed in Section 2.6.1

5. CONCLUSIONS

The use of the modified linear lifting line theory is shown to give good predictions of lift and rolling moment for finite wings fitted with part span spoilers. The prediction of pitching moment is not as good as for lift. This is due to the fact that the Brown theory for for spoilered airfoil sections gives predictions of pitching moment which are less accurate than for lift.

A required input to the theory is the base pressure coefficient behind the finite span spoilers. At the present time, the base pressure coefficient cannot be predicted theoretically. Experiments conducted in support of this thesis show that the base pressure coefficient varies in a complex manner with airfoil and spoiler geometry. However it is found that the base pressure coefficient averaged over span and incidence, $\bar{\bar{C}}_{pb}$ on any given airfoil section, is independent of spoiler length, and its use as an input to the theory gives good results. A method of predicting $\bar{\bar{C}}_{pb}$, which greatly reduces the amount of experimental measurements is presented.

The necessity for a base pressure input based on experimental measurements remains a weakness of the theory. Measurements must still be made for each spoiler height and inclination and airfoil section. In addition, if the wing is flapped, the flap angle and slot size will affect the base pressure. Since the experimental part of this thesis deals only with 10% spoilers mounted on unflapped wings, no attempt can be made to develop empirically based formulas for the prediction of base pressure, as changes are made to spoiler height and inclination,

flap angle and slot size. Further experiments will have to be made before this can be attempted.

Experiments on base vented spoilers show that base vents of about 10% of spoiler height or less give sectional characteristics which are little different from those of the corresponding unvented spoilers. Thus for the purposes of preliminary design, the unvented spoiler characteristics may be used, provided that the spoilers have base vents of about 10% or less.

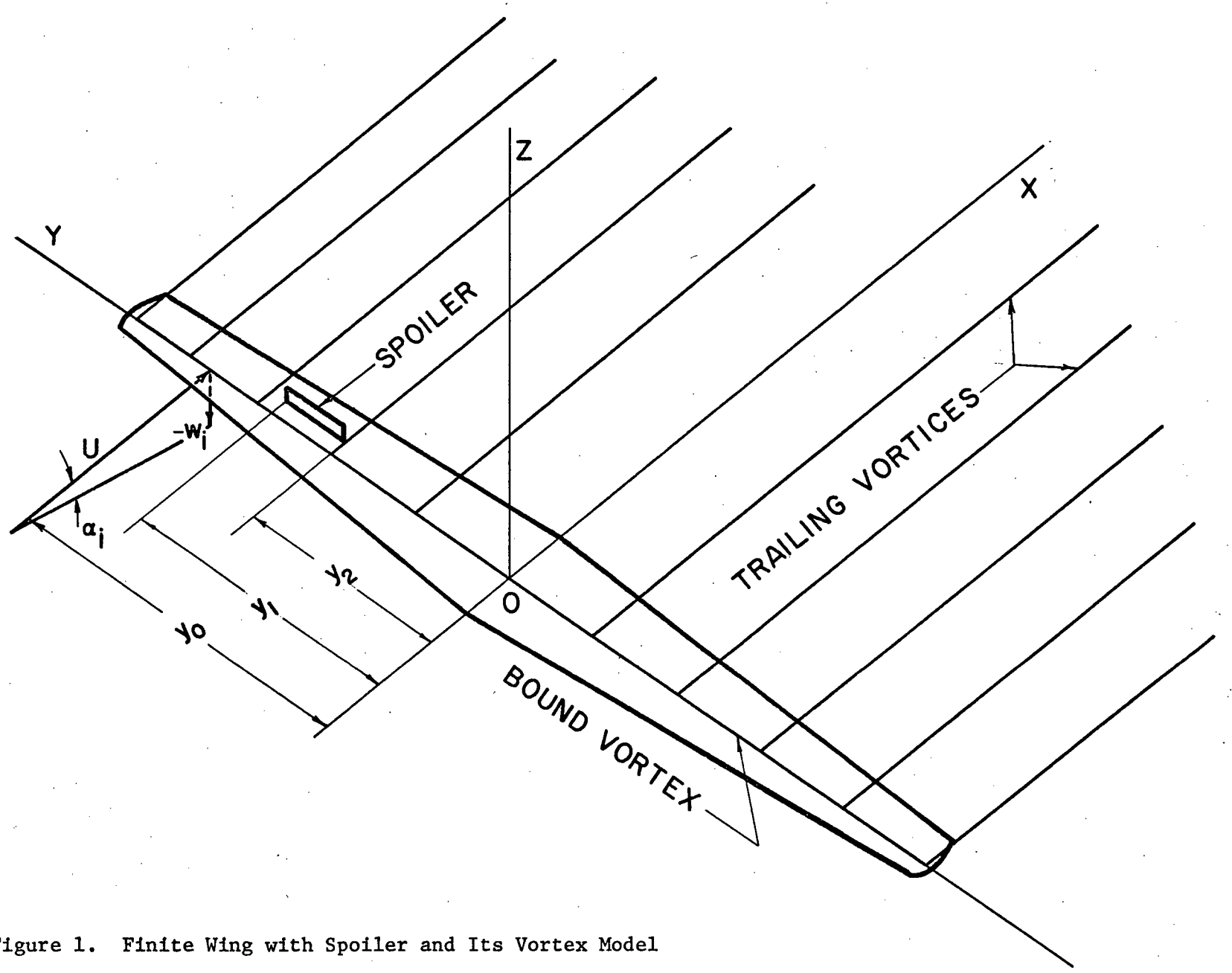

Figure 1. Finite Wing with Spoiler and Its Vortex Model

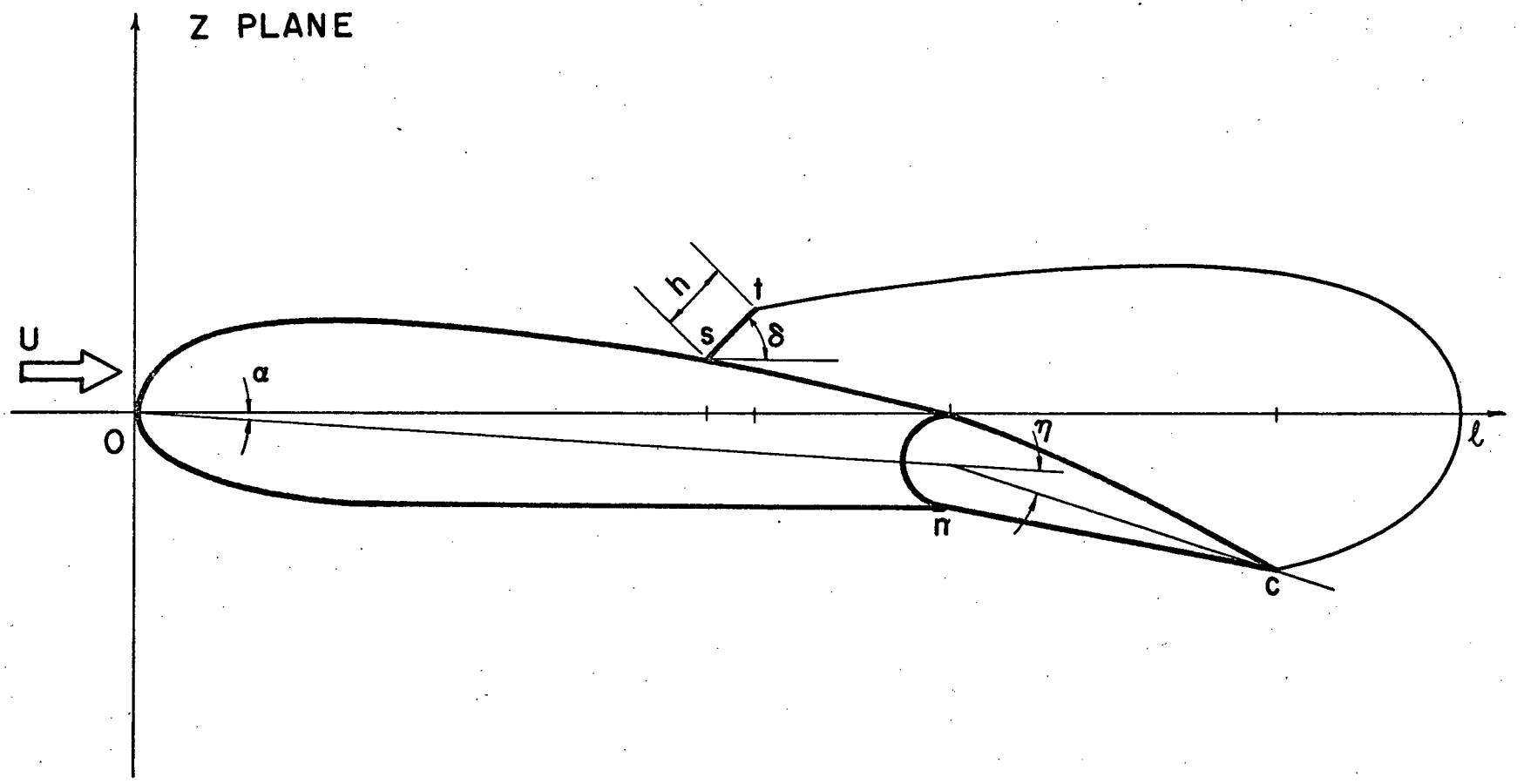

Figure 2. Airfoil in the Physical Plane

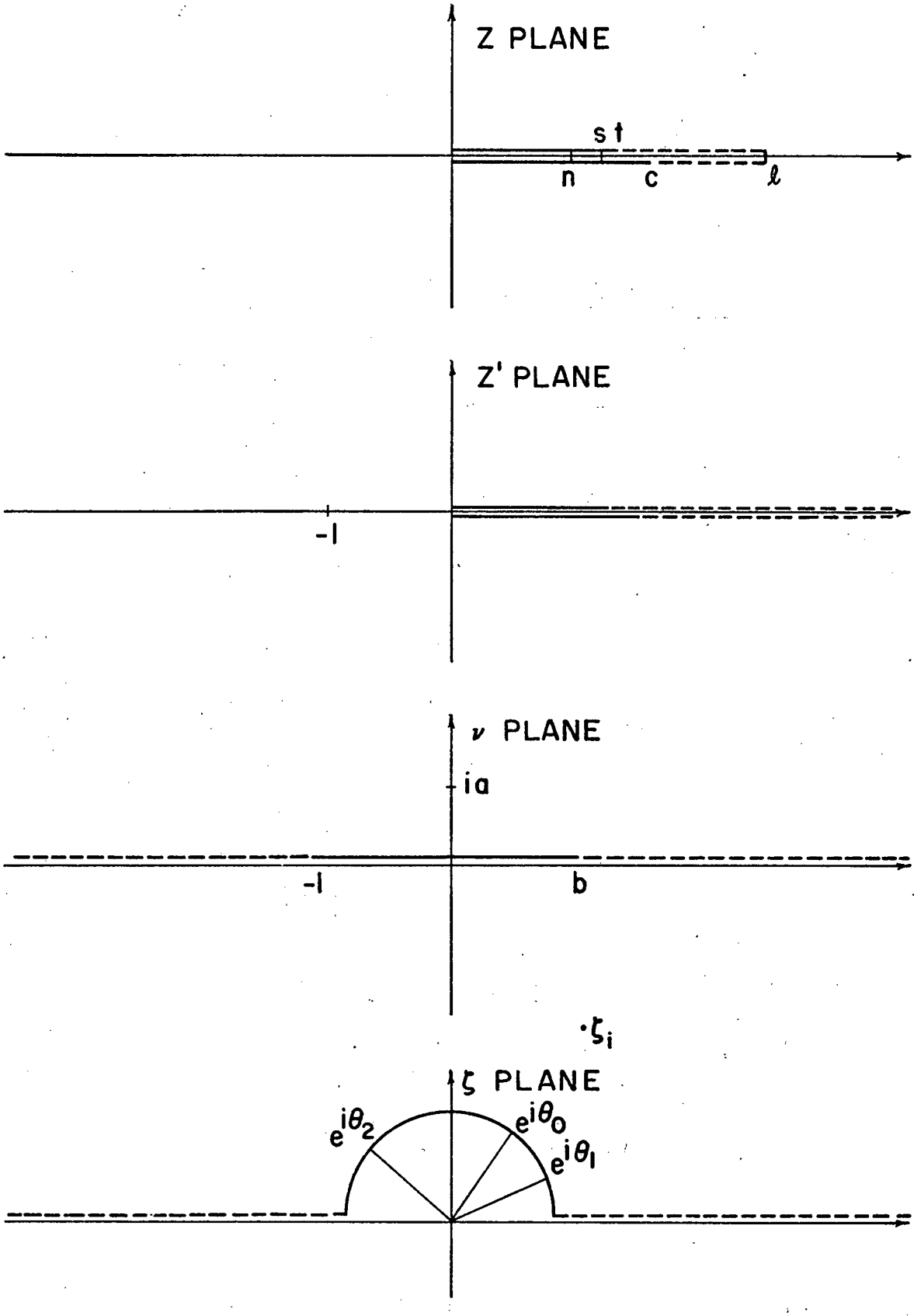

Figure 3. Complex Transform Planes

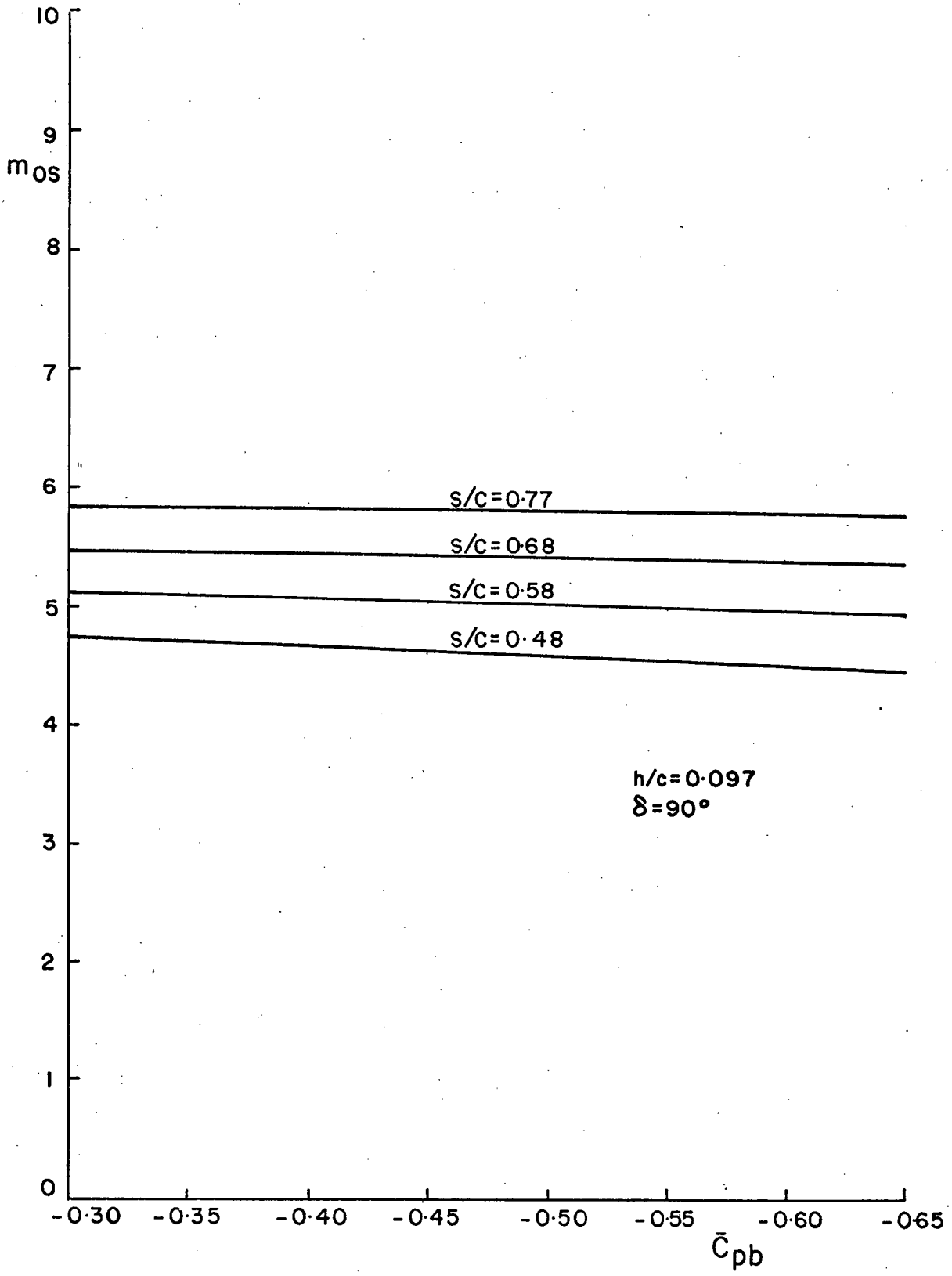

Figure 4 Variation of m_{os} with $\bar{C}_{pb}$ for NACA 0015 Airfoil Section with Normal Unvented Spoiler

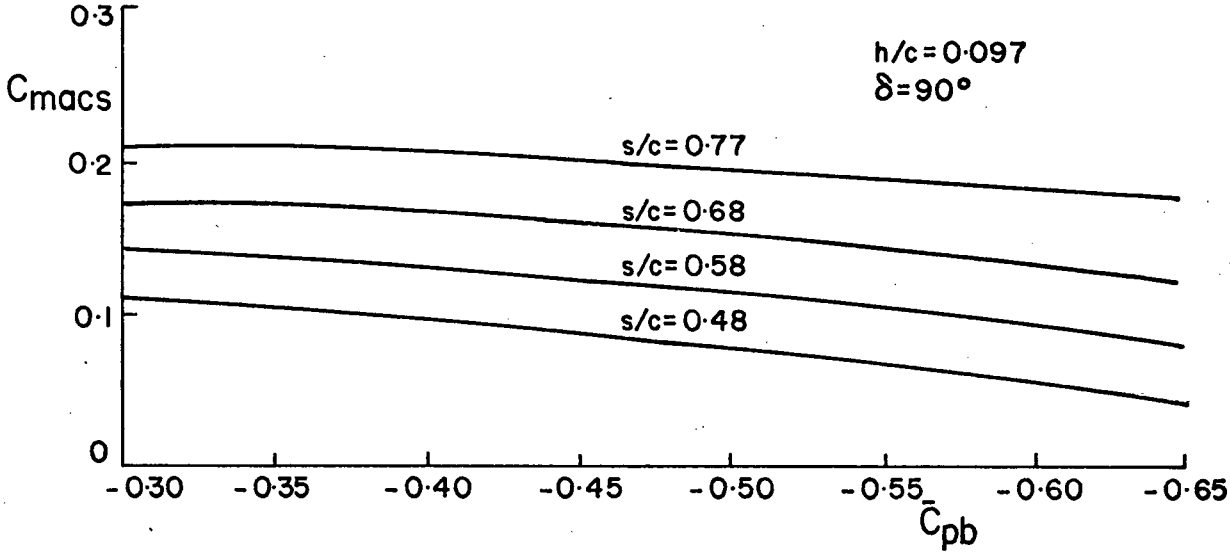

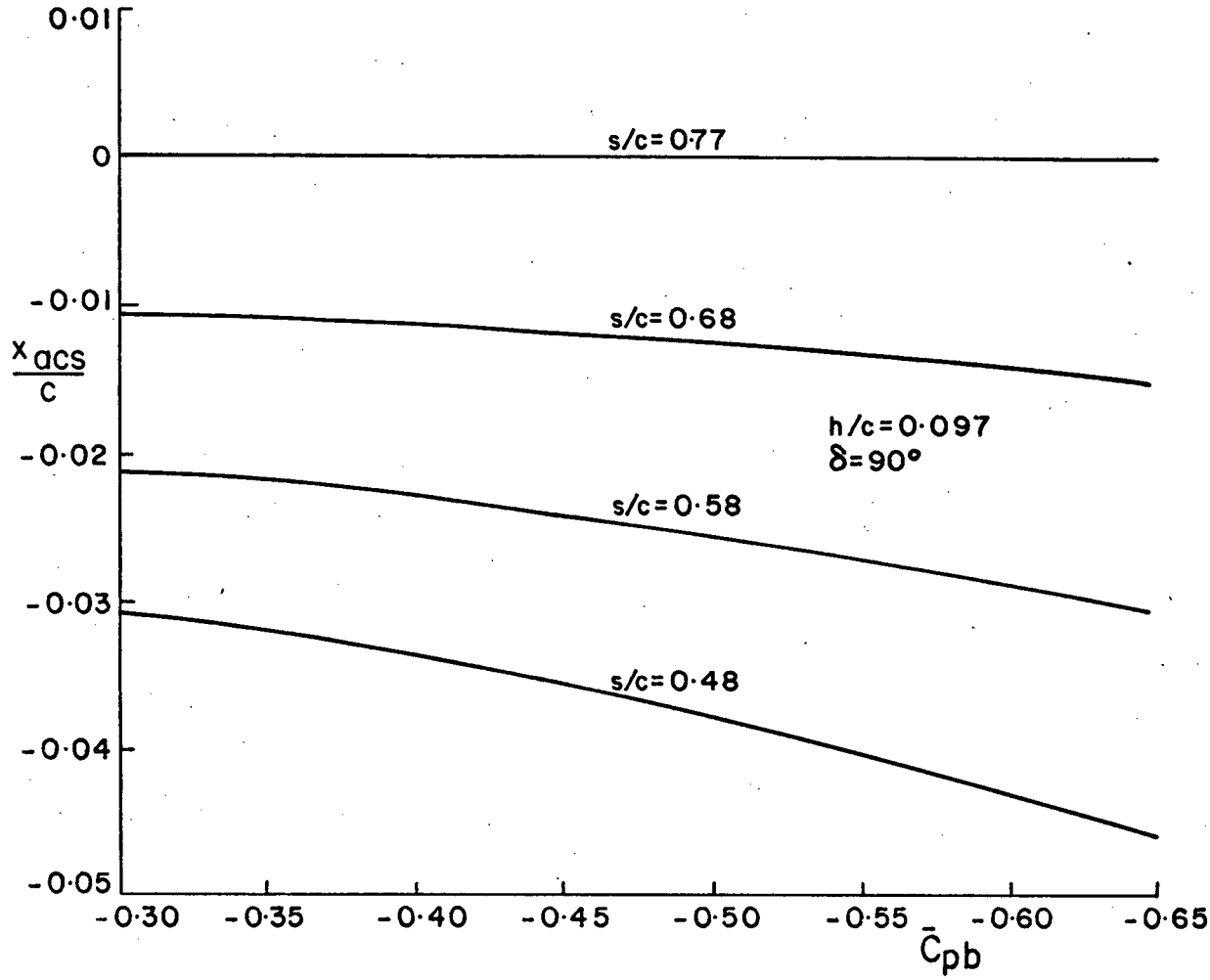

Figure 5 Variation of C_{macs} & x_{acs}/c with $\bar{C}_{pb}$ for NACA 0015 Airfoil Section with Normal Unvented Spoiler

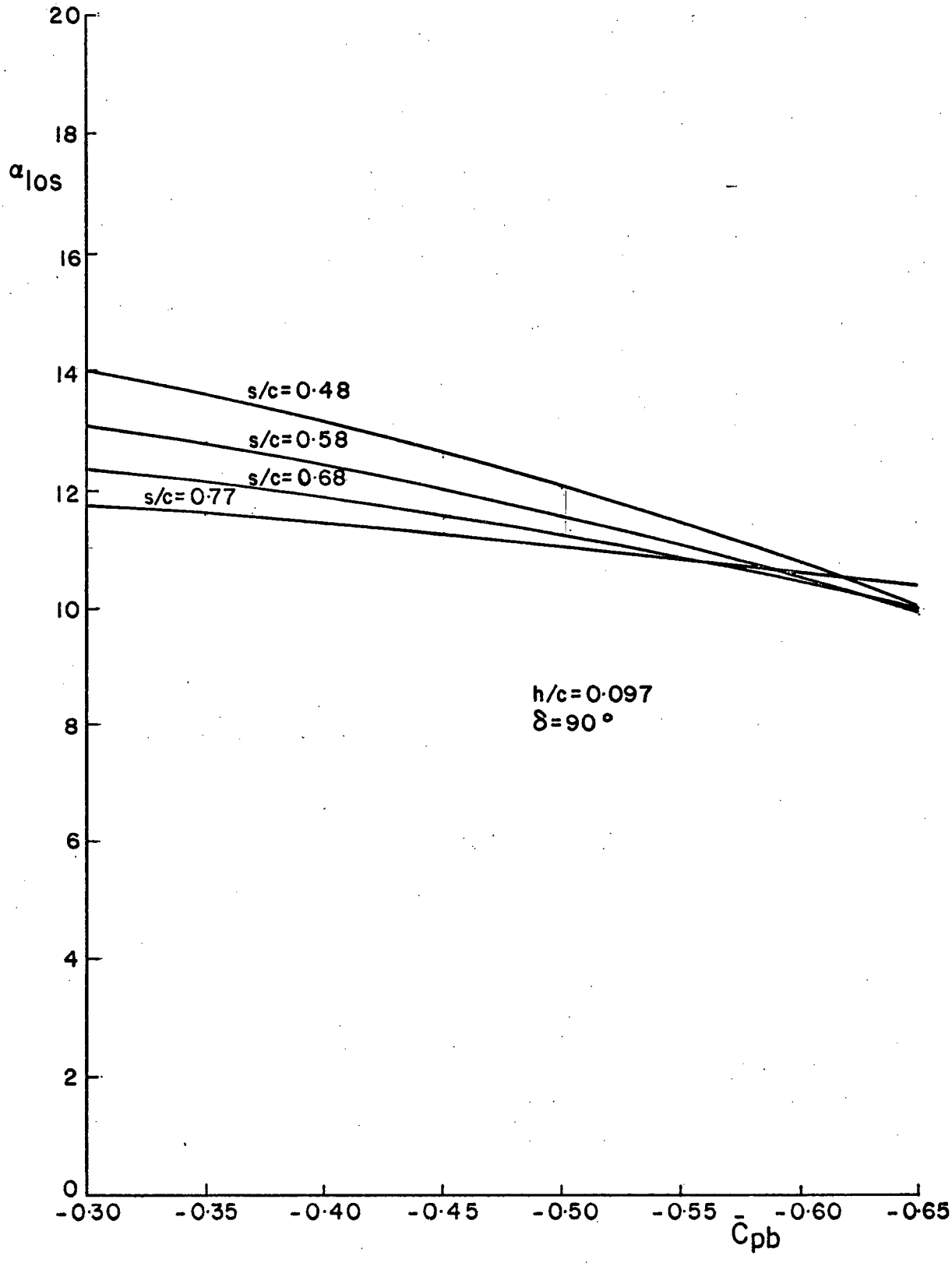

Figure 6 Variation of α_{los} with $\bar{C}_{pb}$ for NACA 0015 Airfoil Section with Normal Unvented Spoiler

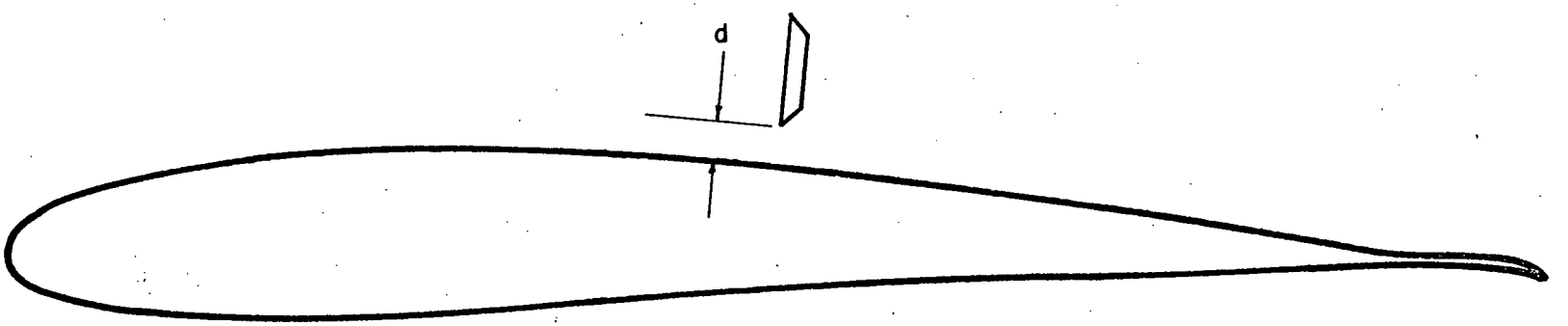

Figure 7 Modified Joukowsky Airfoil Section of 11% Thickness & 2.4% Camber with Base Vented Normal Spoiler

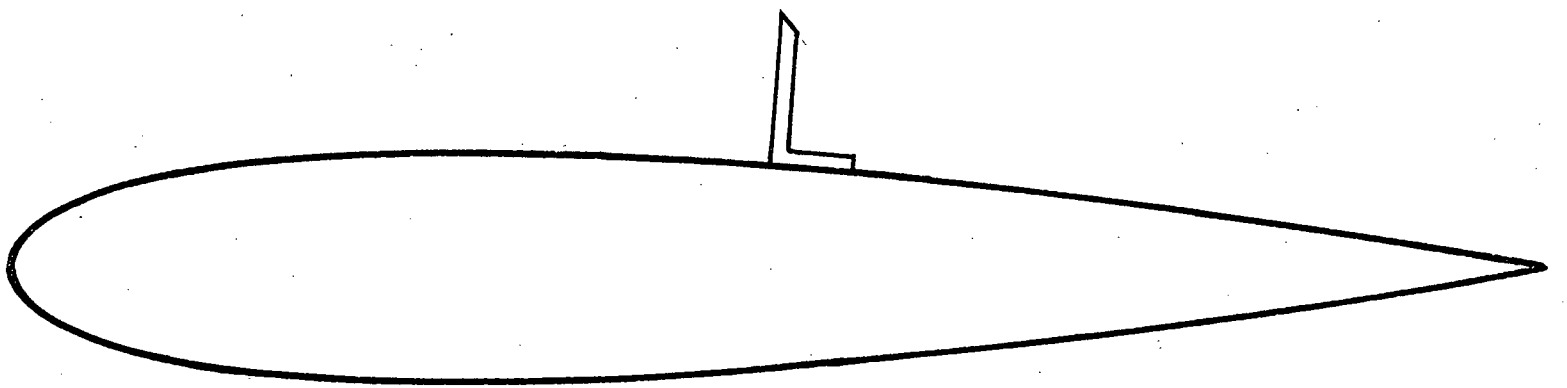

Figure 8 NACA 0015 Airfoil Section, with 9.7% Unvented Normal Spoiler

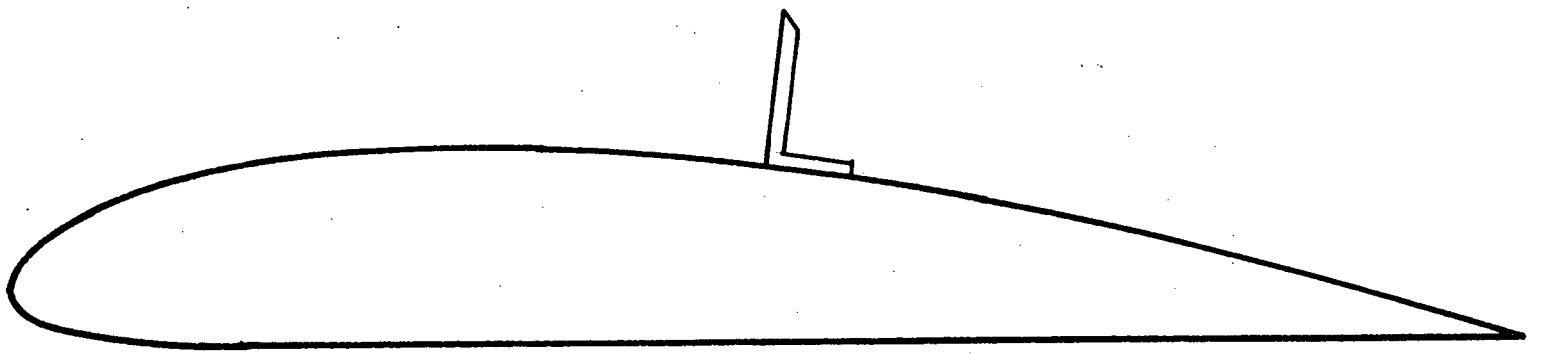

Figure 9 12.9% Thick Clark Y Airfoil Section with 10% Unvented Normal Spoiler

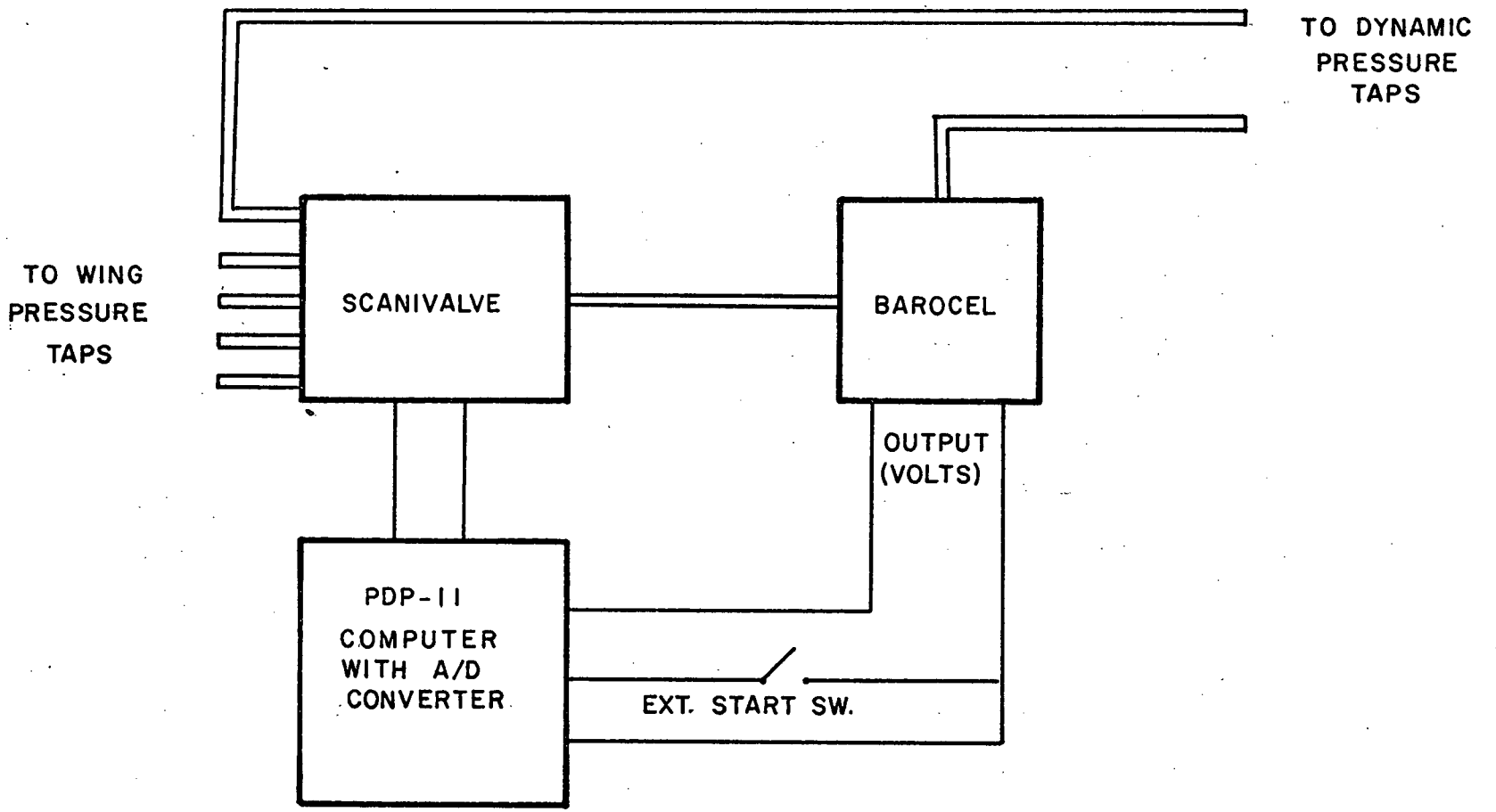

Figure 10 Base Pressure Measurement System

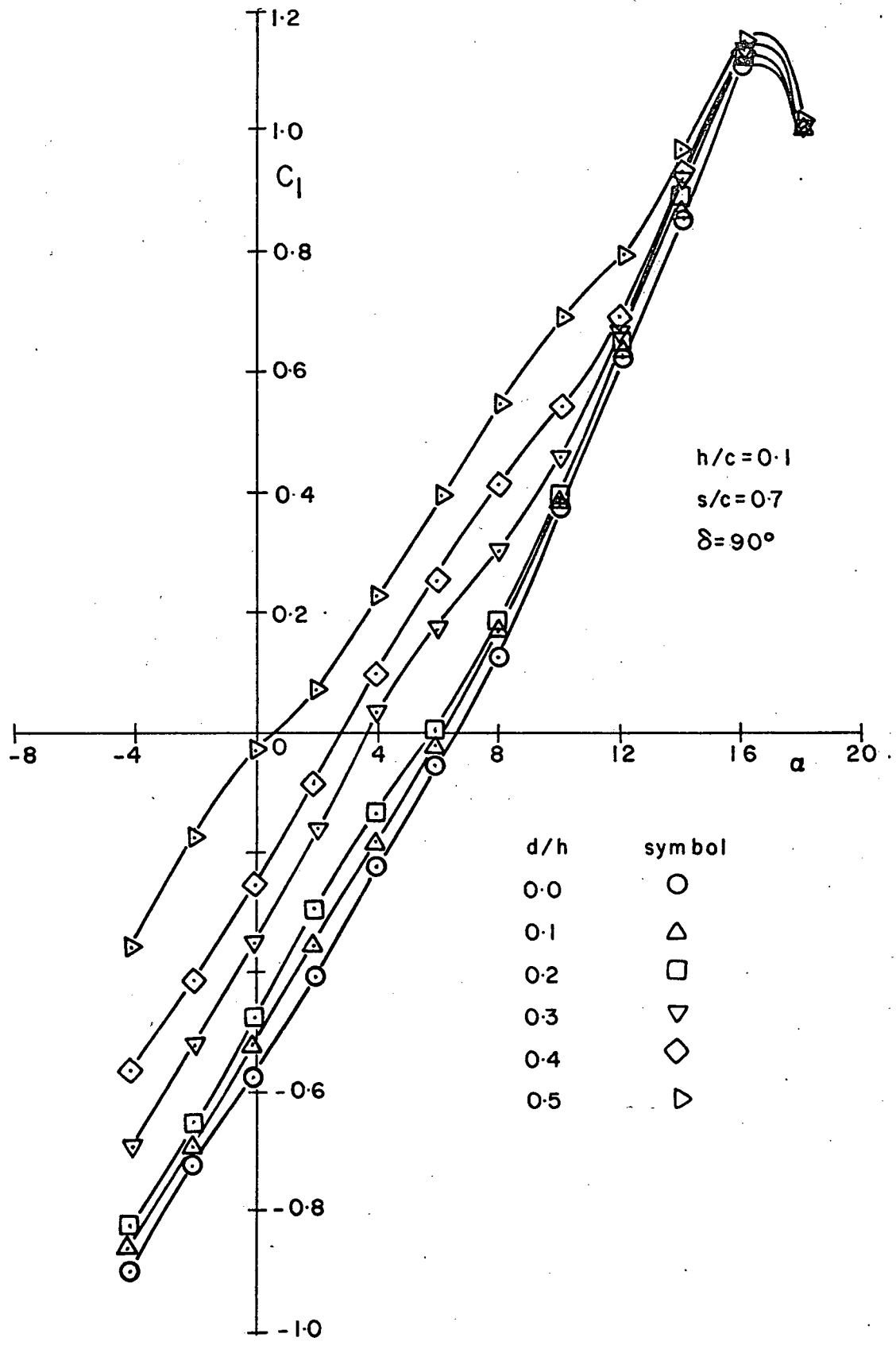

Figure 11. Lift Coefficient for Joukowsky Airfoil Section with Base Vented Normal Spoilers

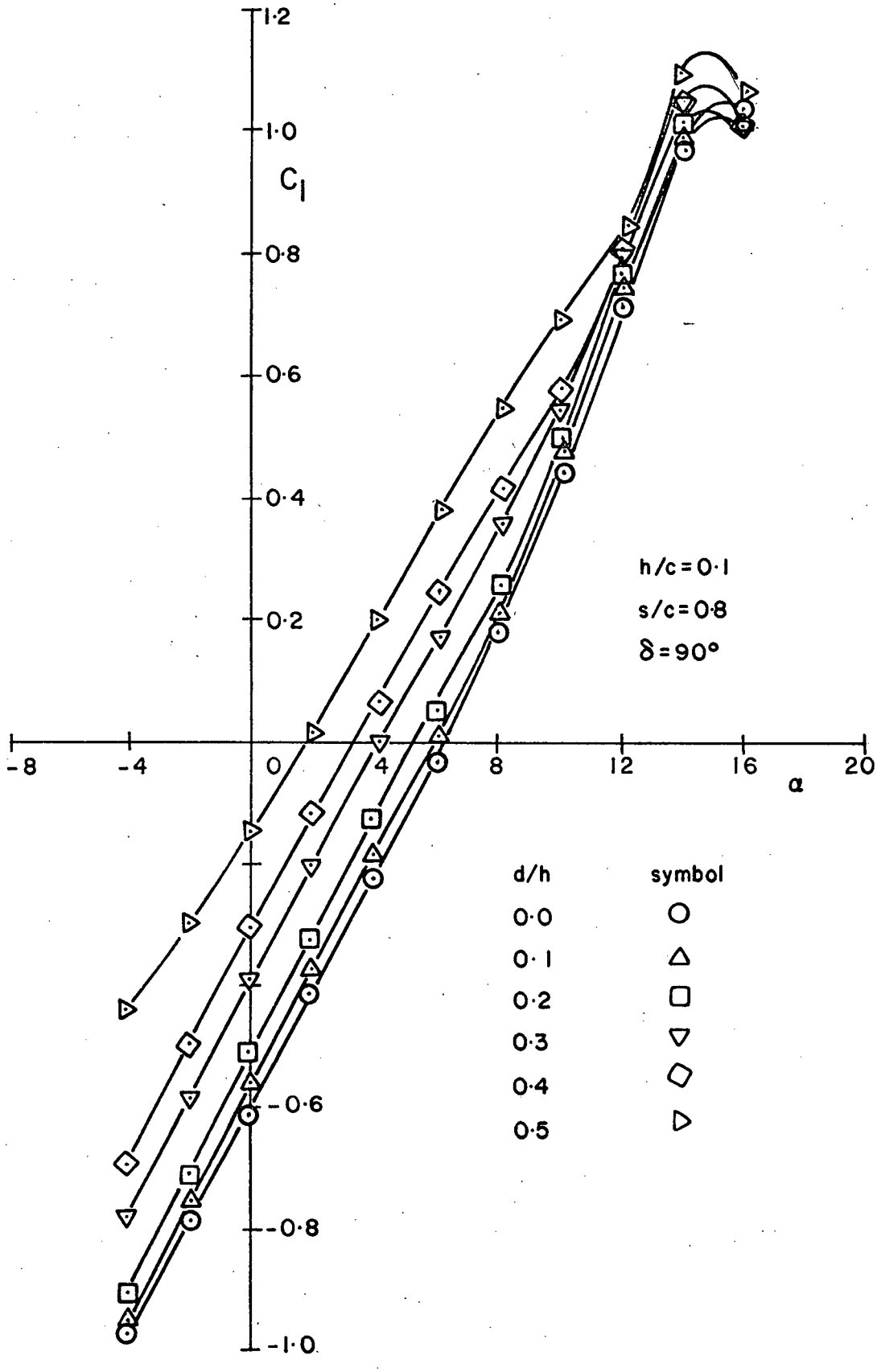

Figure 12 Lift Coefficient for Joukowsky Airfoil Section with Base Vented Normal Spoilers

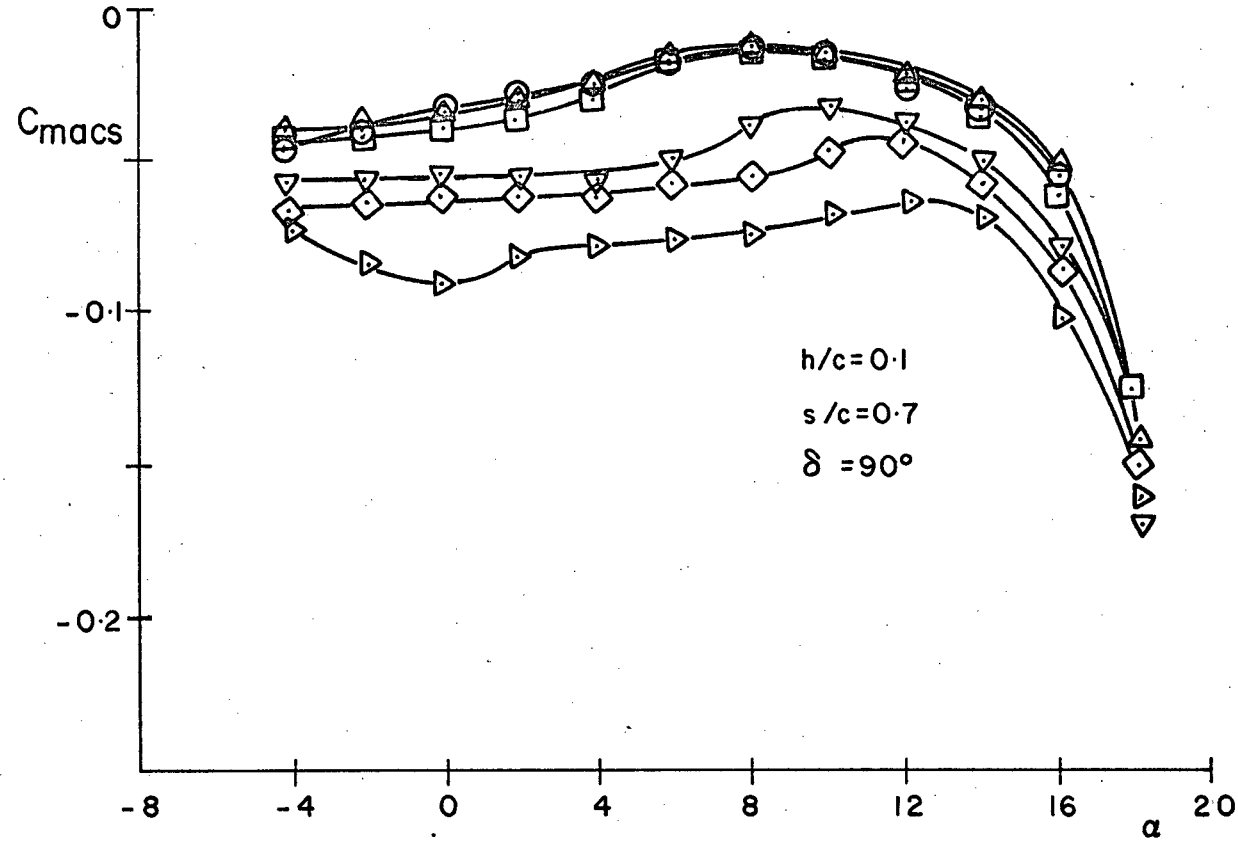

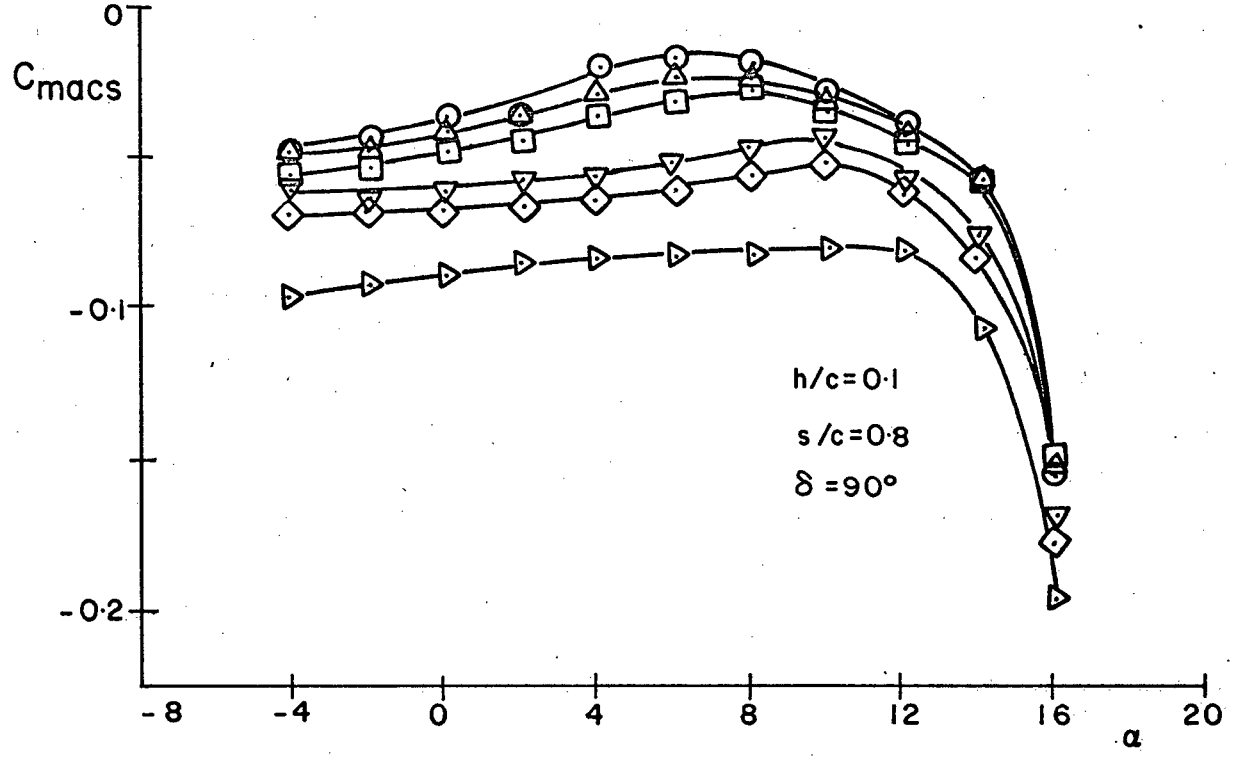

Figure 13 Pitching Moment Coefficient for Joukowsky Airfoil Section with Base Vented Normal Spoilers

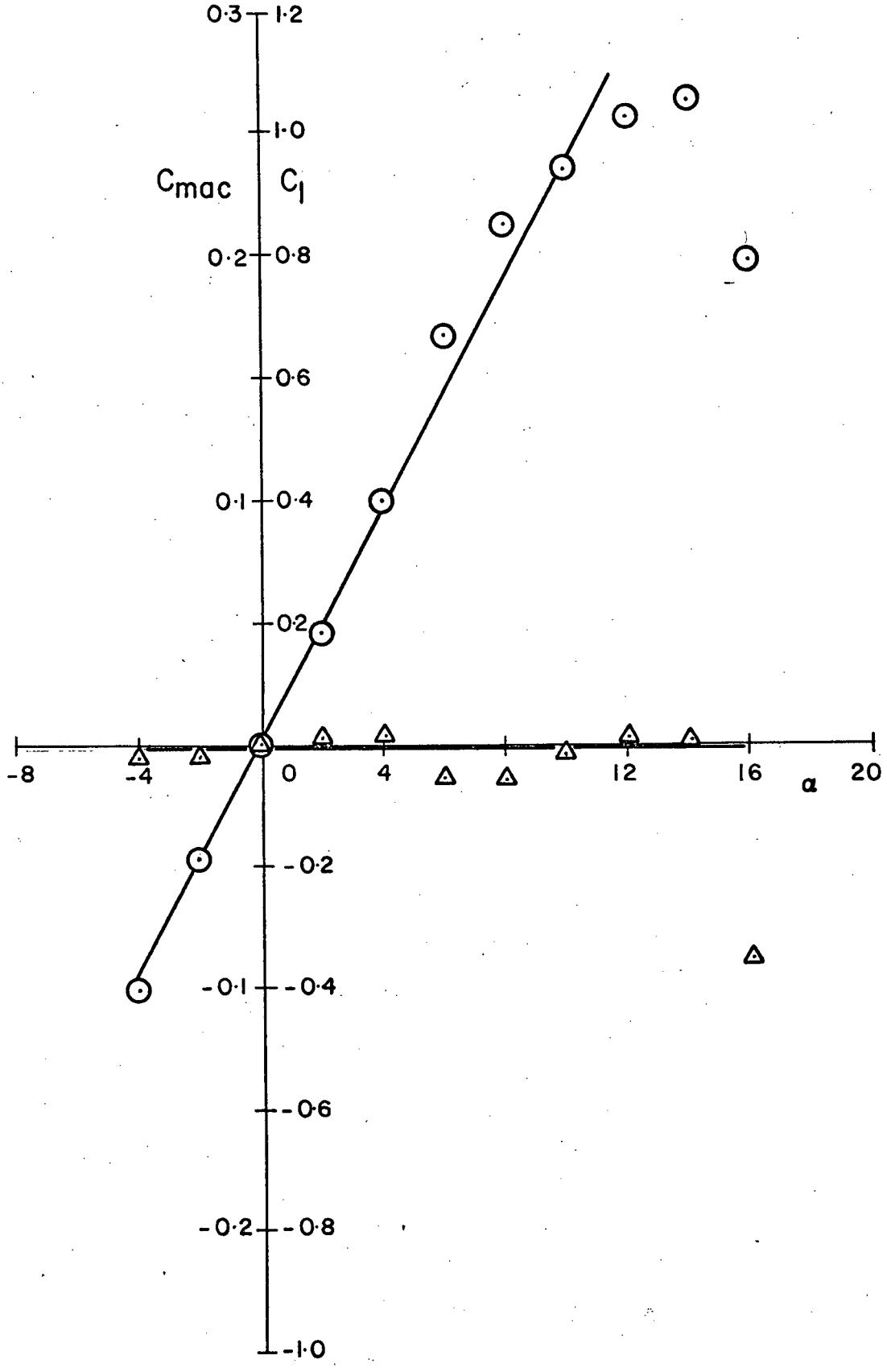

Figure 14. Lift & Pitching Moment Coefficients for a NACA 0015 Section;
—— linearisation; o experimental C_l; Δ experimental C_{mac}

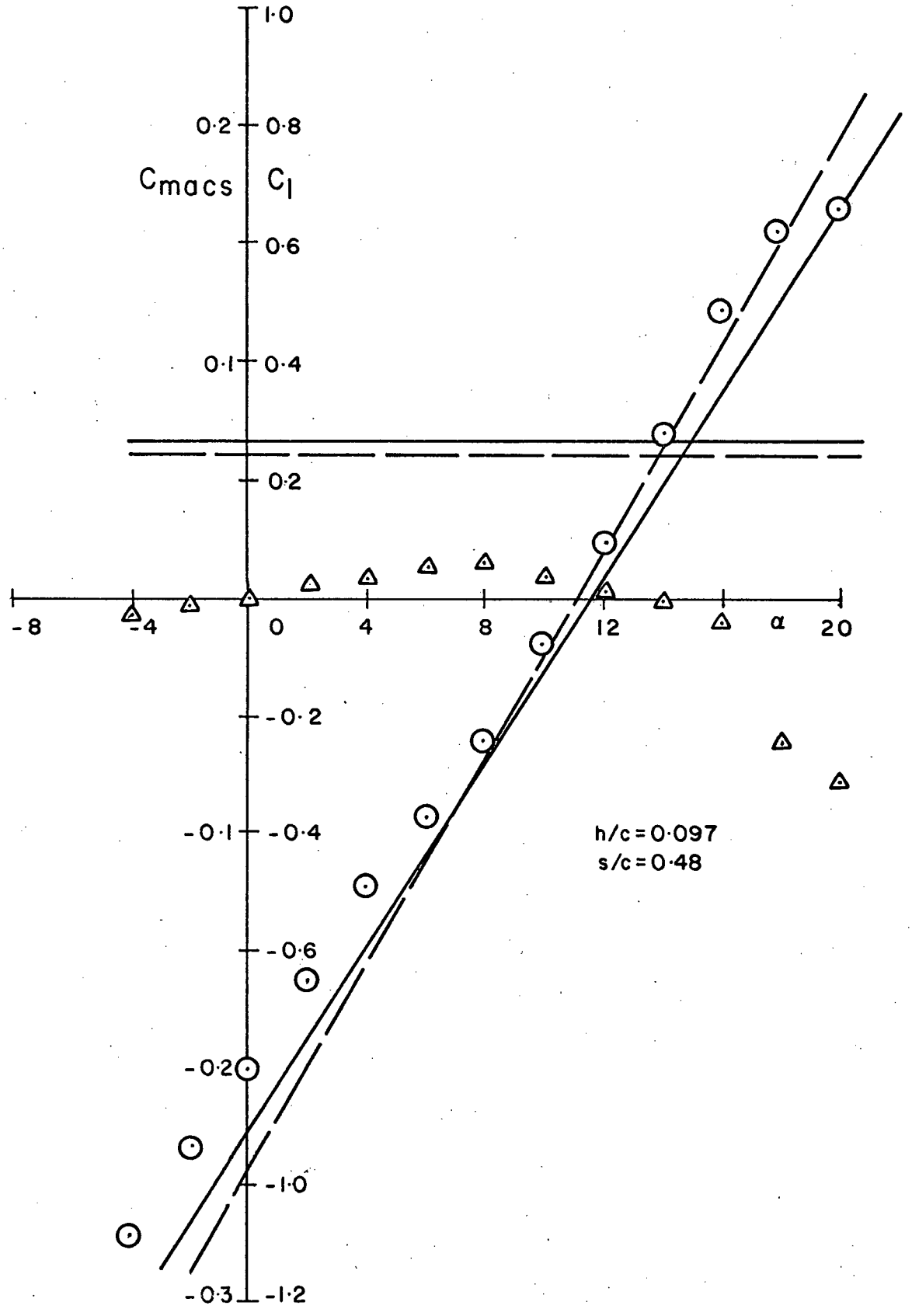

Figure 15 Lift & Pitching Moment Coefficients for NACA 0015 Airfoil Section with Normal Unvented Spoiler. —— theory ($\bar{C}_{pb}$ input); – – – theory (linearised C_{pb} input). o C_l experimental; Δ C_{macs} experimental

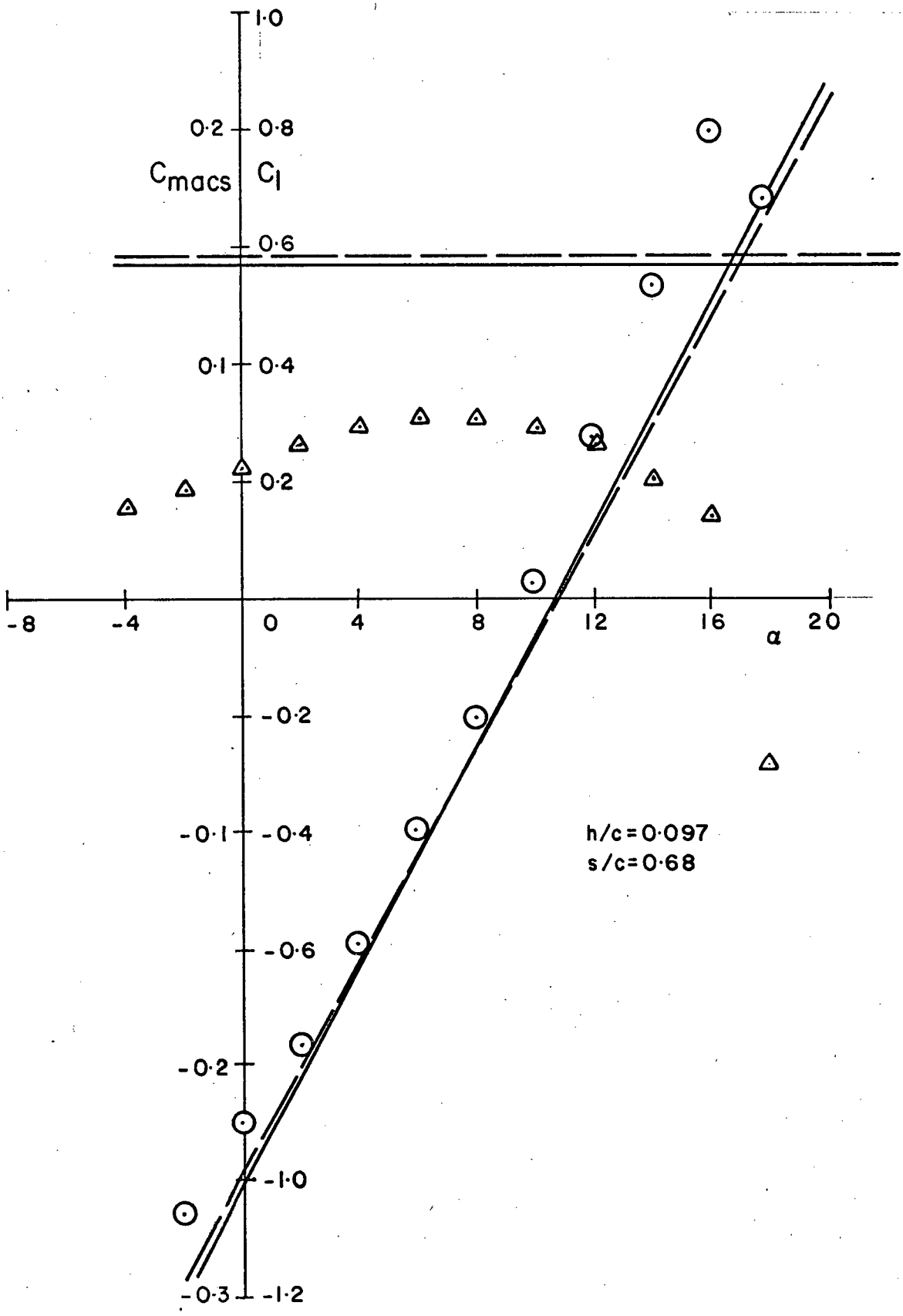

Figure 16 Lift & Pitching Moment Coeffieients for NACA 0015 Airfoil Section with Normal Unvented Spoiler. —— theory ($\bar{C}_{pb}$ input); — — — theory (linearised C_{pb} input); o C_l experimental; Δ C_{macs} experimental

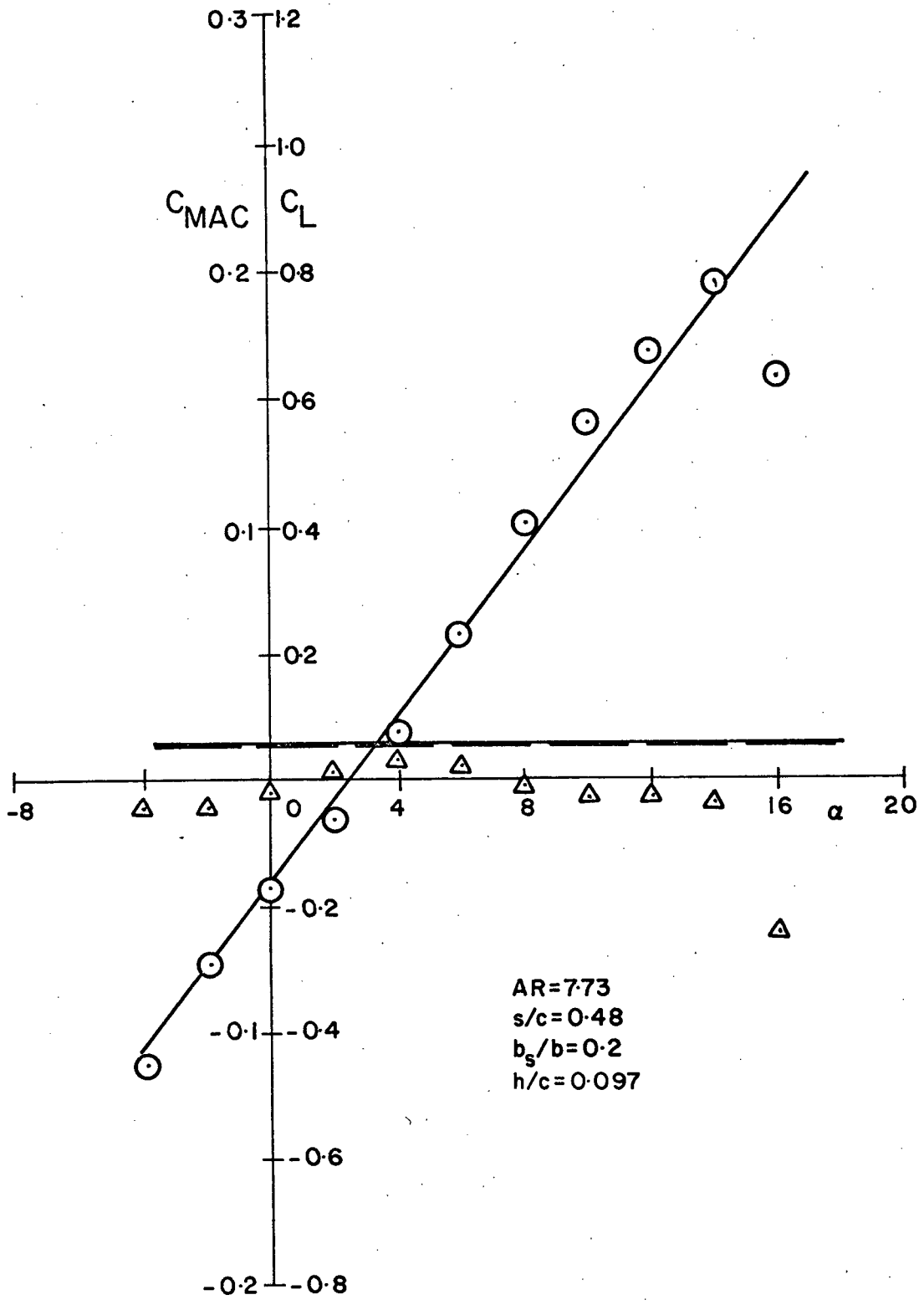

Figure 17 Lift & Pitching Moment Coefficients for Rectangular Half Wing of NACA 0015 Section with Normal Unvented Spoiler.—— theory ($\bar{\bar{C}}_{pb}$ input); — — — theory ($\bar{C}_{pb}$ input);o C_L experiment;Δ C_{MAC} experiment

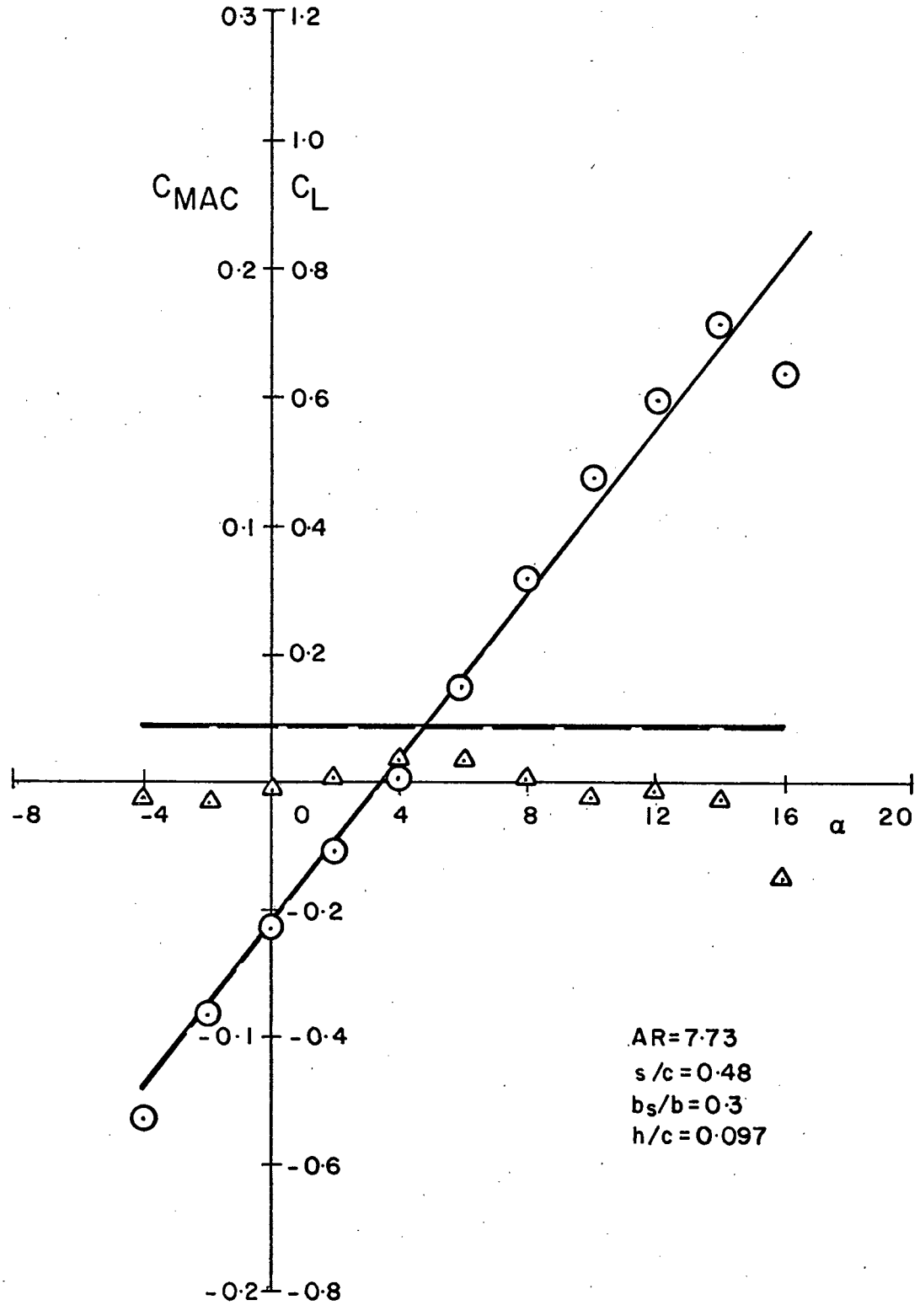

Figure 18 Lift & Pitching Moment Coefficients for Rectangular Half Wing of NACA 0015 Section with Normal Unvented Spoiler. —— theory ($\bar{\bar{C}}_{pb}$ input), – – – ($\bar{C}_{pb}$ input);o C_L experiment; Δ C_{MAC} experiment

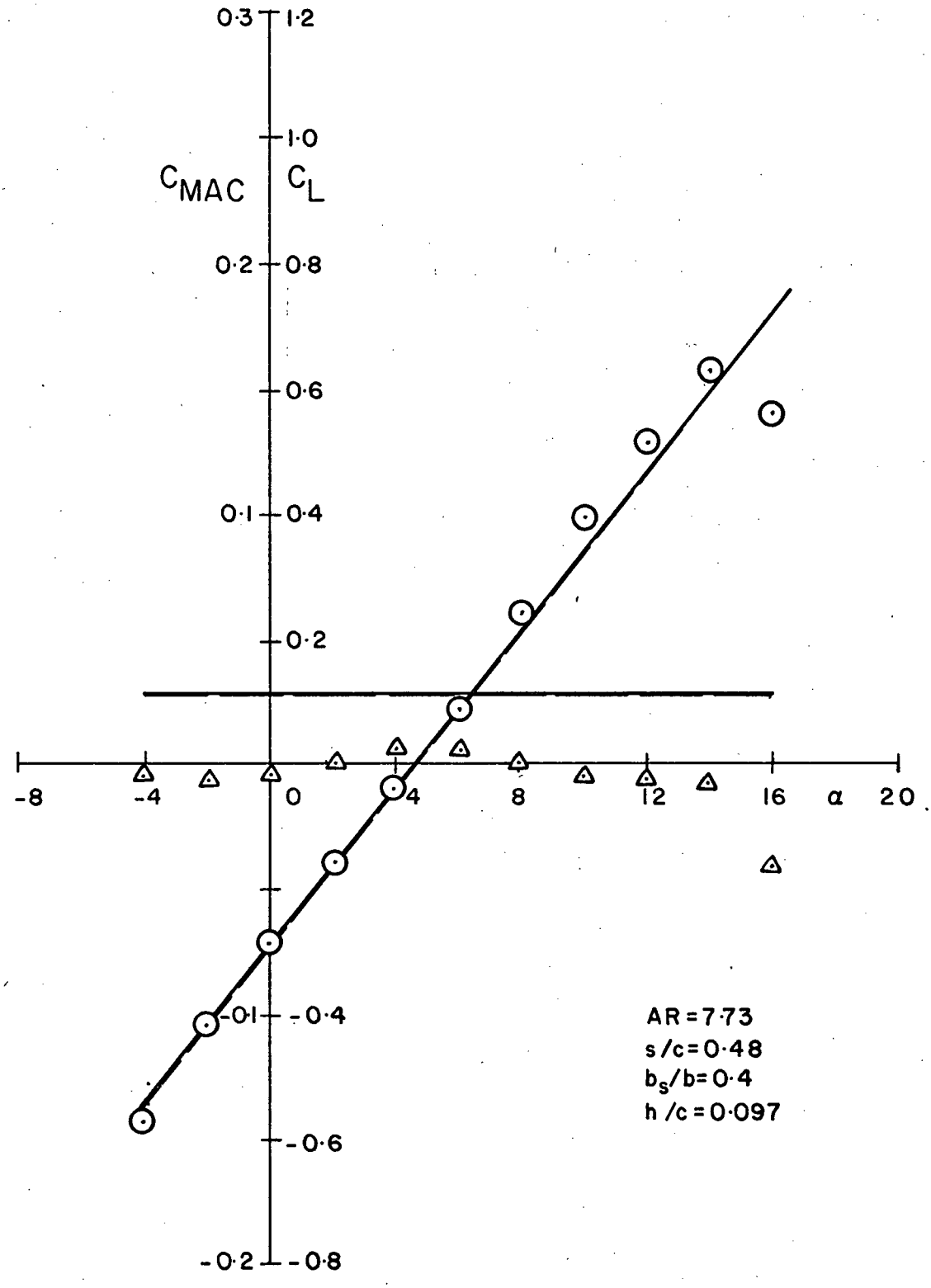

Figure 19 Lift & Pitching Moment Coefficients for Rectangular Half Wing of NACA 0015 Section with Normal Unvented Spoiler. —— theory ($\bar{\bar{C}}_{pb}$ input), – – – theory ($\bar{C}_{pb}$ input); o C_L experiment; Δ C_{MAC} experiment

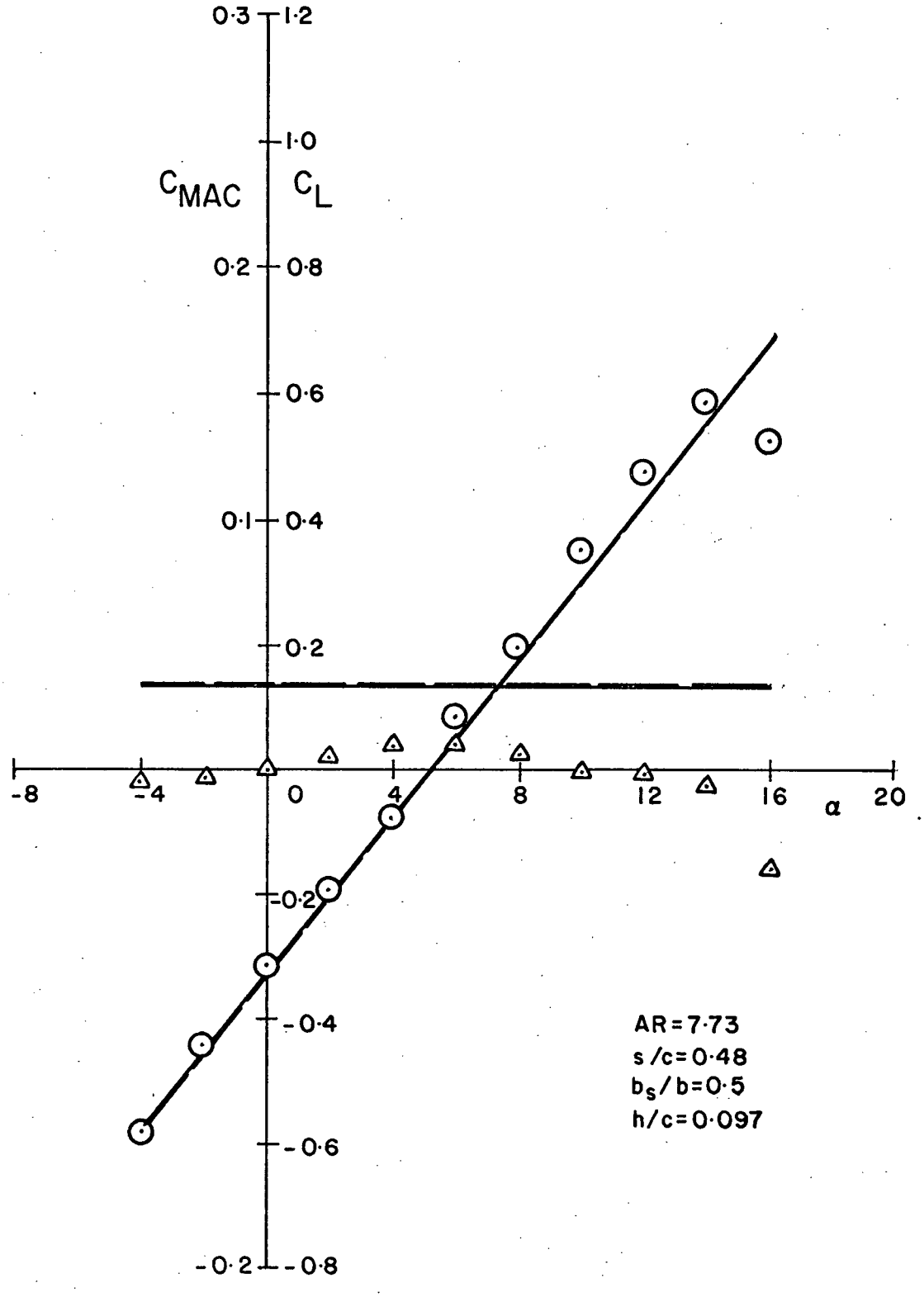

Figure 20 Lift & Pitching Moment Coefficients for Rectangular Half Wing of NACA 0015 Section with Normal Unvented Spoiler. —— theory ($\bar{\bar{C}}_{pb}$ input; – – – theory ($\bar{C}_{pb}$ input);o C_L experiment;Δ C_{MAC} experiment

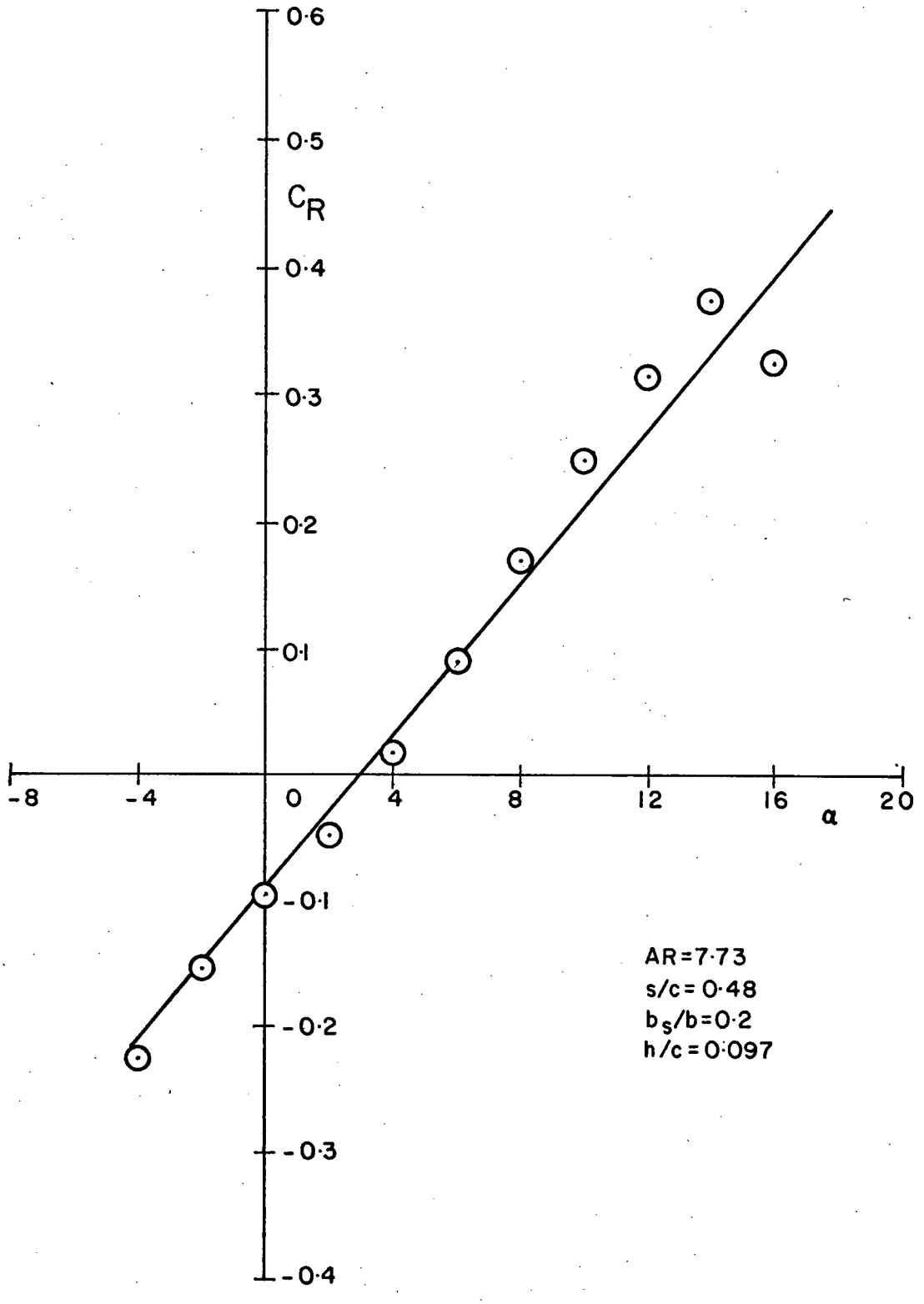

Figure 21 Rolling Moment Coefficient for Rectangular Half Wing of NACA 0015 Section with Normal Unvented Spoiler. ——— theory ($\bar{\bar{C}}_{pb}$ input); — — — theory ($\bar{C}_{pb}$ input); o experiment

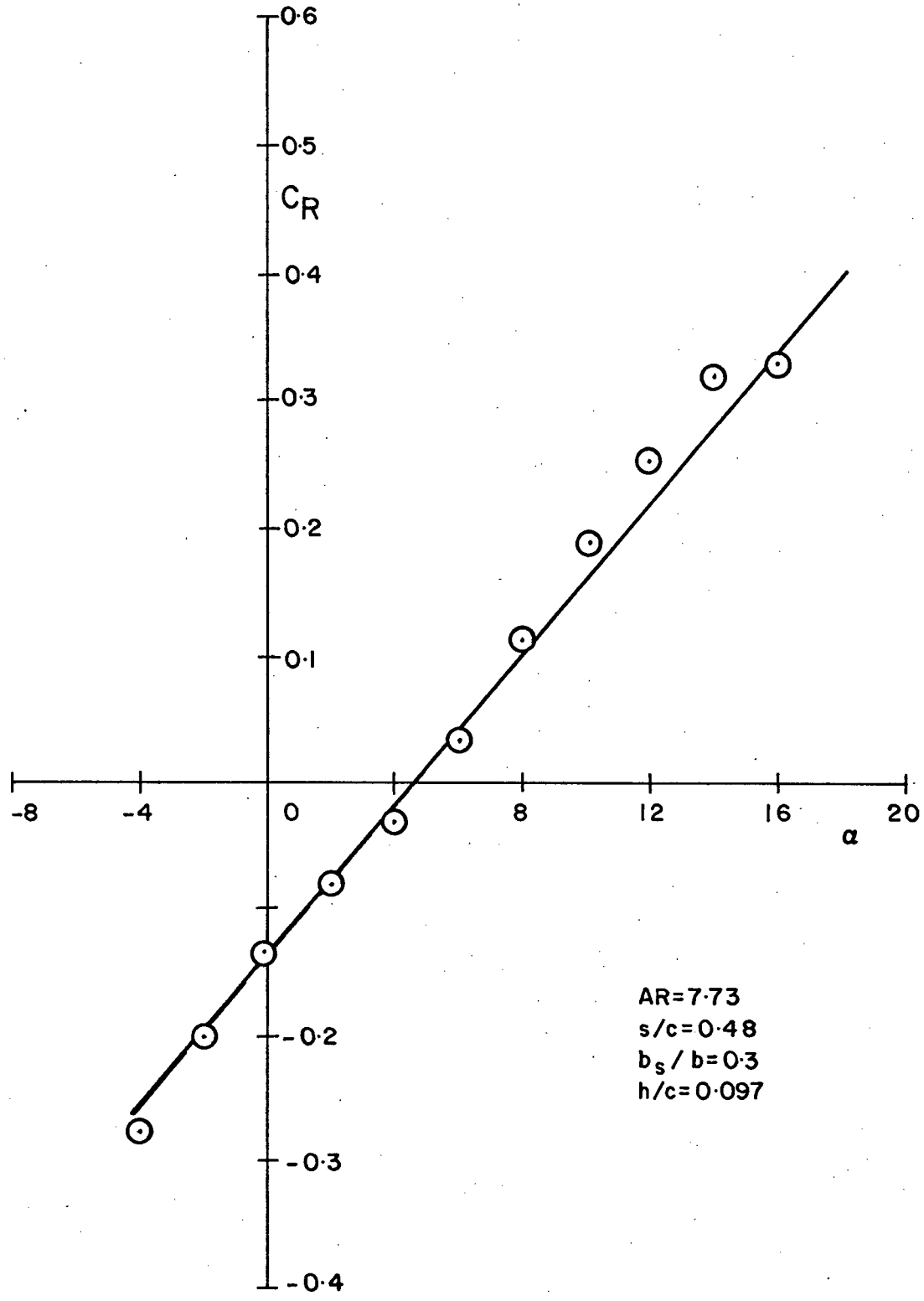

Figure 22 Rolling Moment Coefficient for Rectangular Half Wing of NACA 0015 Section with Normal Unvented Spoiler. —— theory ($\bar{\bar{C}}_{pb}$ input); — — — theory ($\bar{C}_{pb}$ input); o experiment

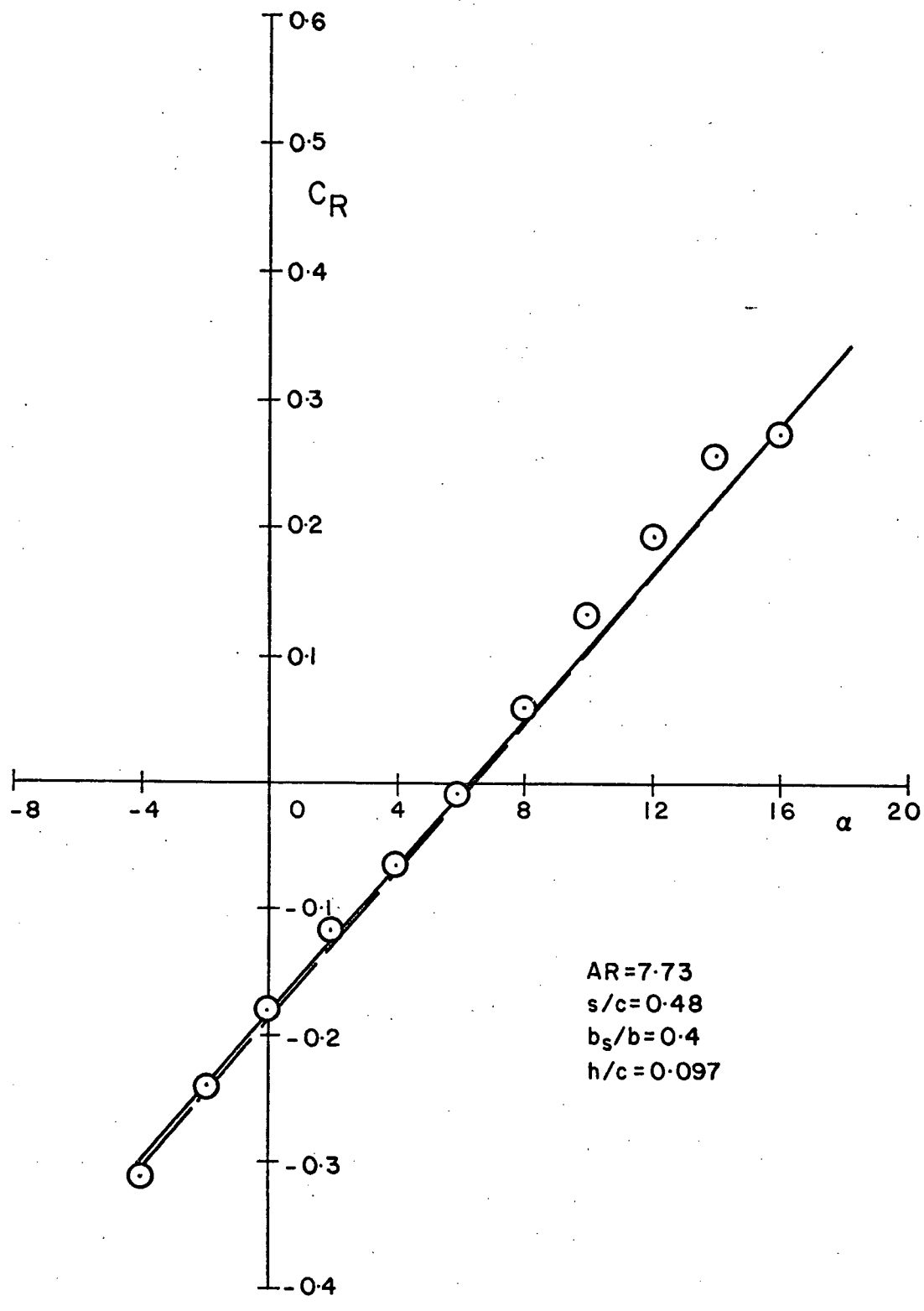

Figure 23 Rolling Moment Coefficient for Rectangular Half Wing of NACA 0015 Section with Normal Unvented Spoiler. —— theory ($\bar{\bar{C}}_{pb}$ input); — — — theory ($\bar{C}_{pb}$ input); o experiment

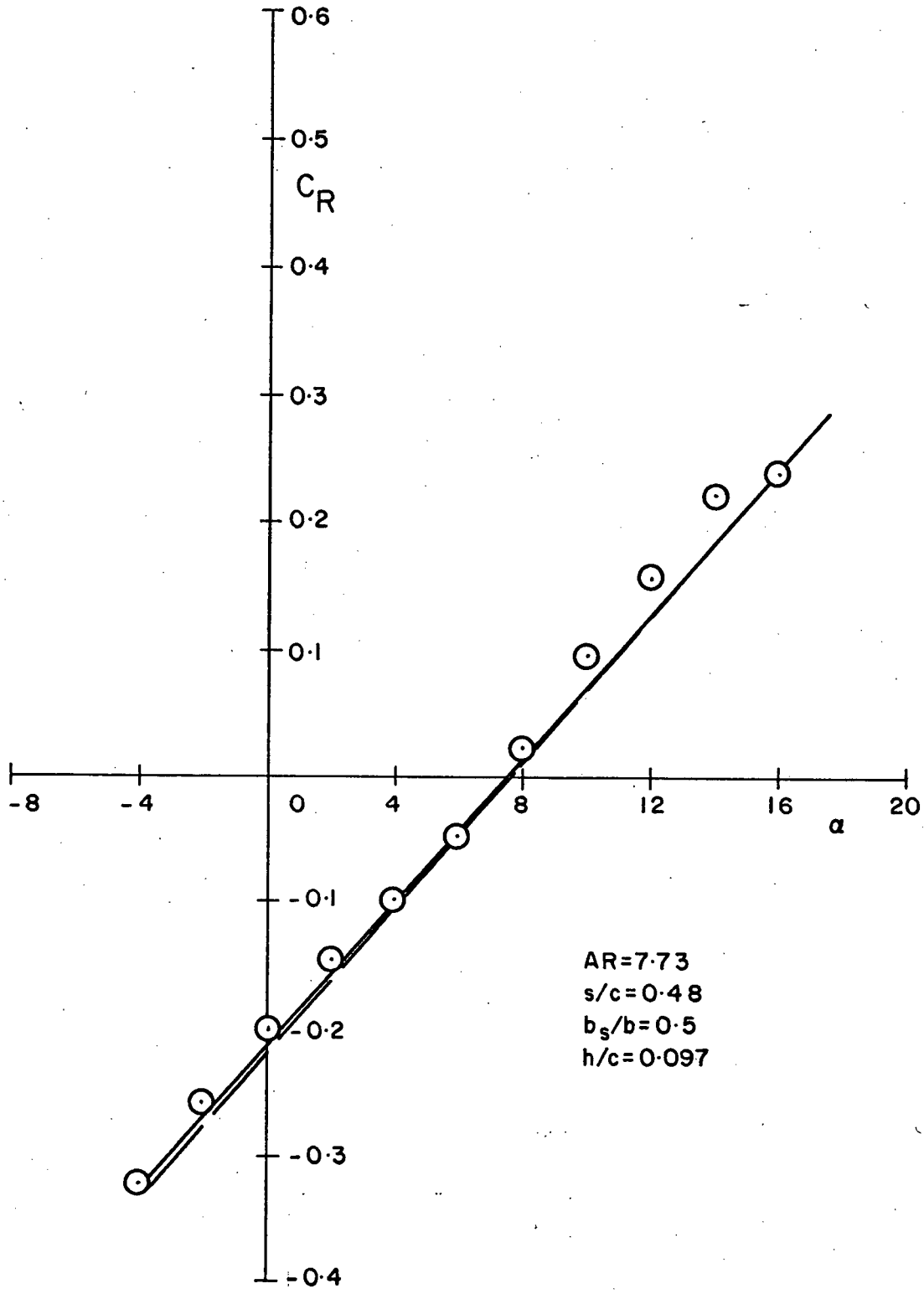

Figure 24 Rolling Moment Coefficient for Rectangular Half Wing of NACA 0015 Section with Normal Unvented Spoiler. ——— theory ($\bar{\bar{C}}_{pb}$ input); – – – theory ($\bar{C}_{pb}$ input); o experiment

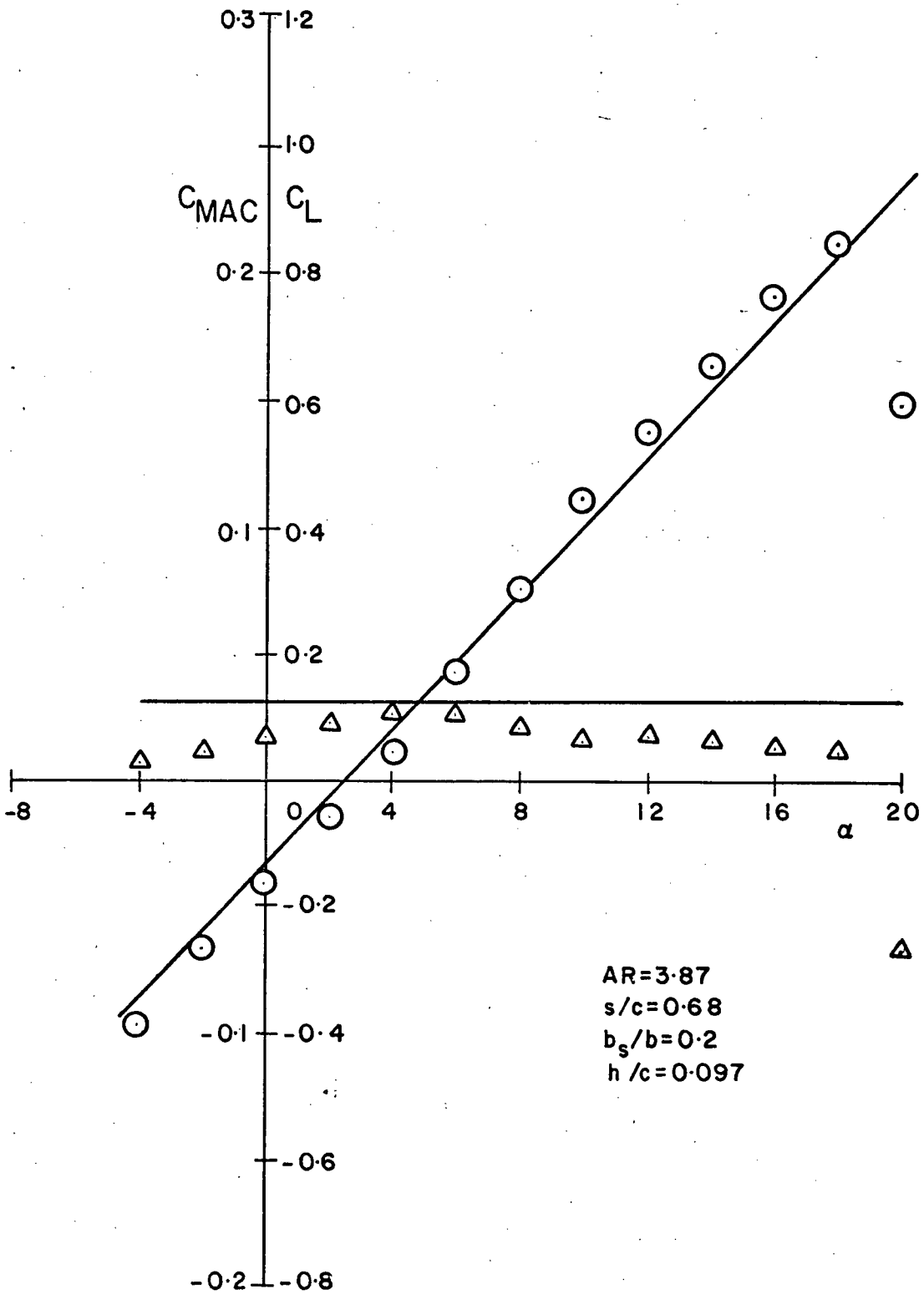

Figure 25 Lift & Pitching Moment Coefficients for Rectangular Half Wing of NACA 0015 Section with Normal Unvented Spoiler. ——— theory; o C_L experiment; Δ C_{MAC} experiment

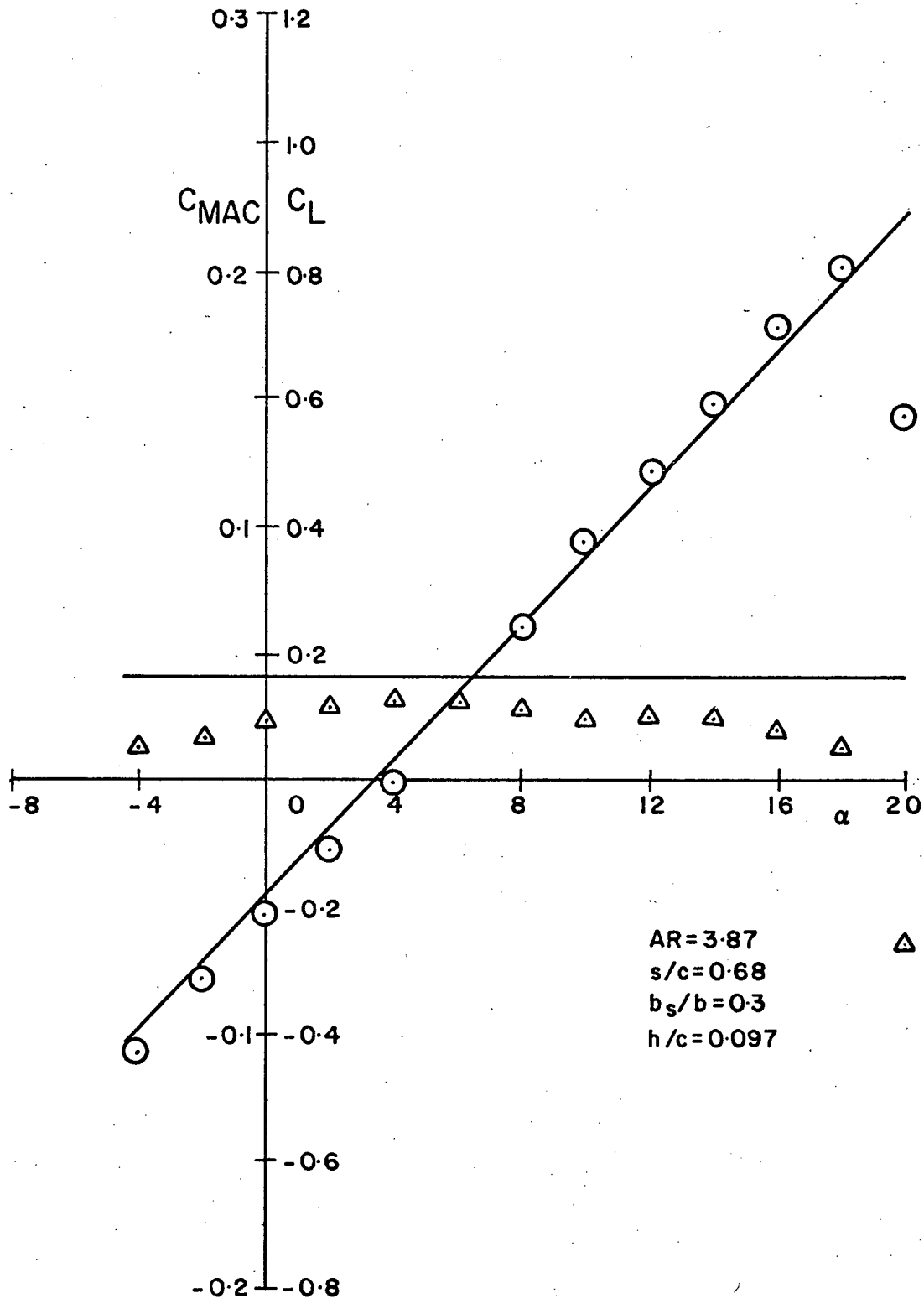

Figure 26 Lift & Pitching Moment Coefficients for Rectangular Wing of NACA 0015 Section with Normal Unvented Spoiler. ——— theory; o C_L experiment; Δ C_{MAC} experiment

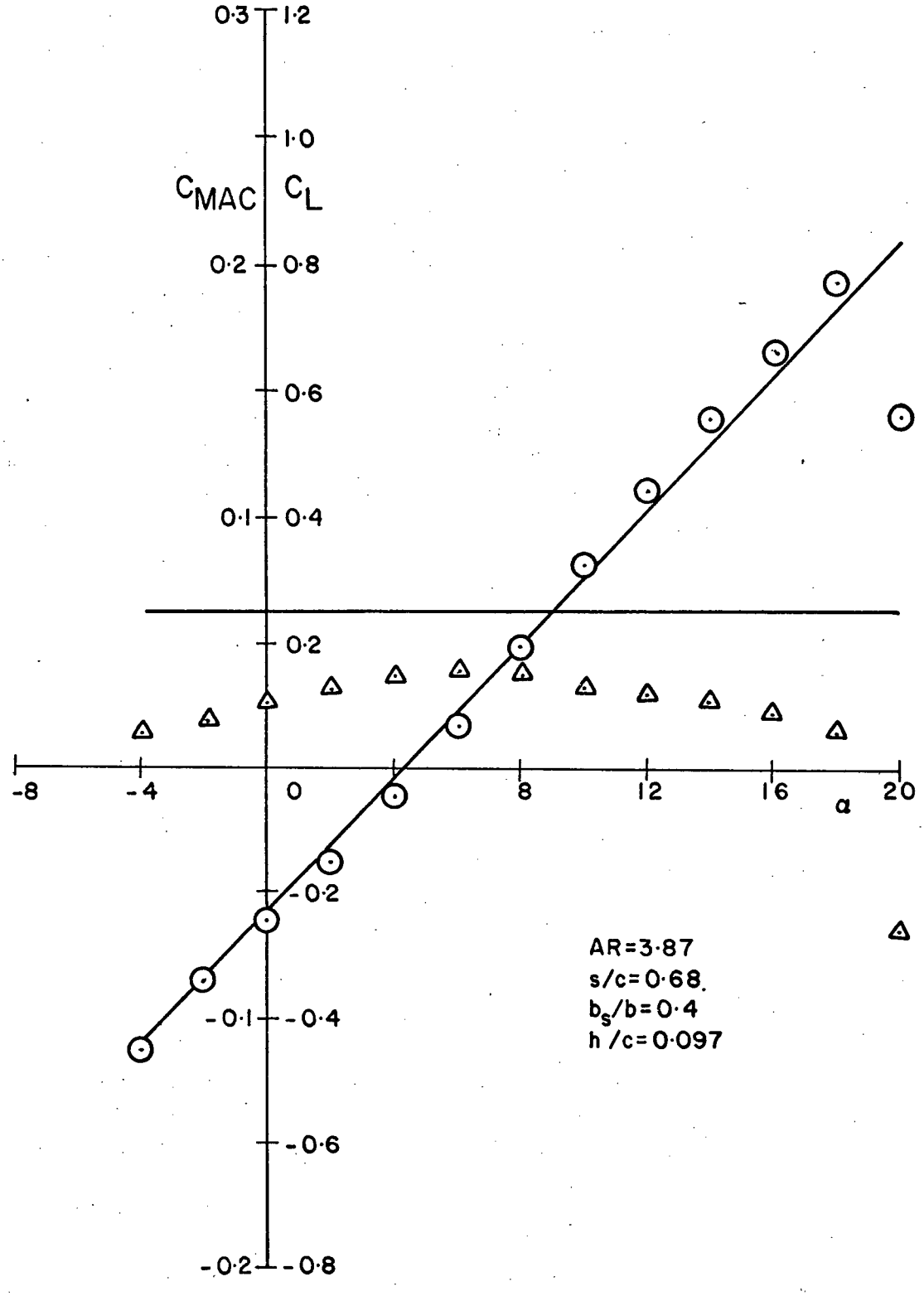

Figure 27 Lift & Pitching Moment Coefficients for Rectangular Half Wing of NACA 0015 Section with Normal Unvented Spoiler. —— theory; o C_L experiment; Δ C_{MAC} experiment

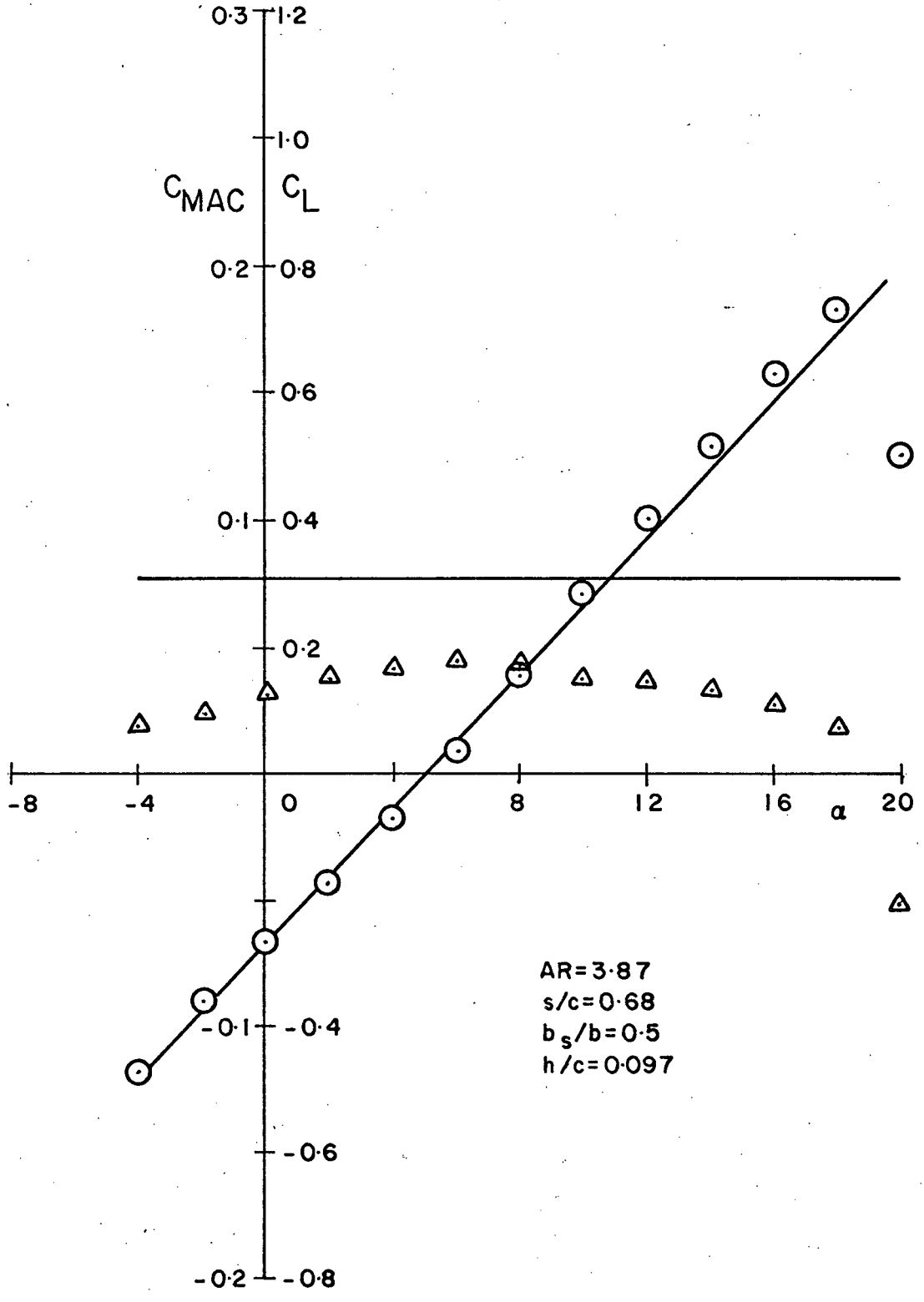

Figure 28 Lift & Pitching Moment Coefficients for Rectangular Half Wing of NACA 0015 Section with Normal Unvented Spoiler. —— Theory; o C_L experiment; Δ C_{MAC} experiment

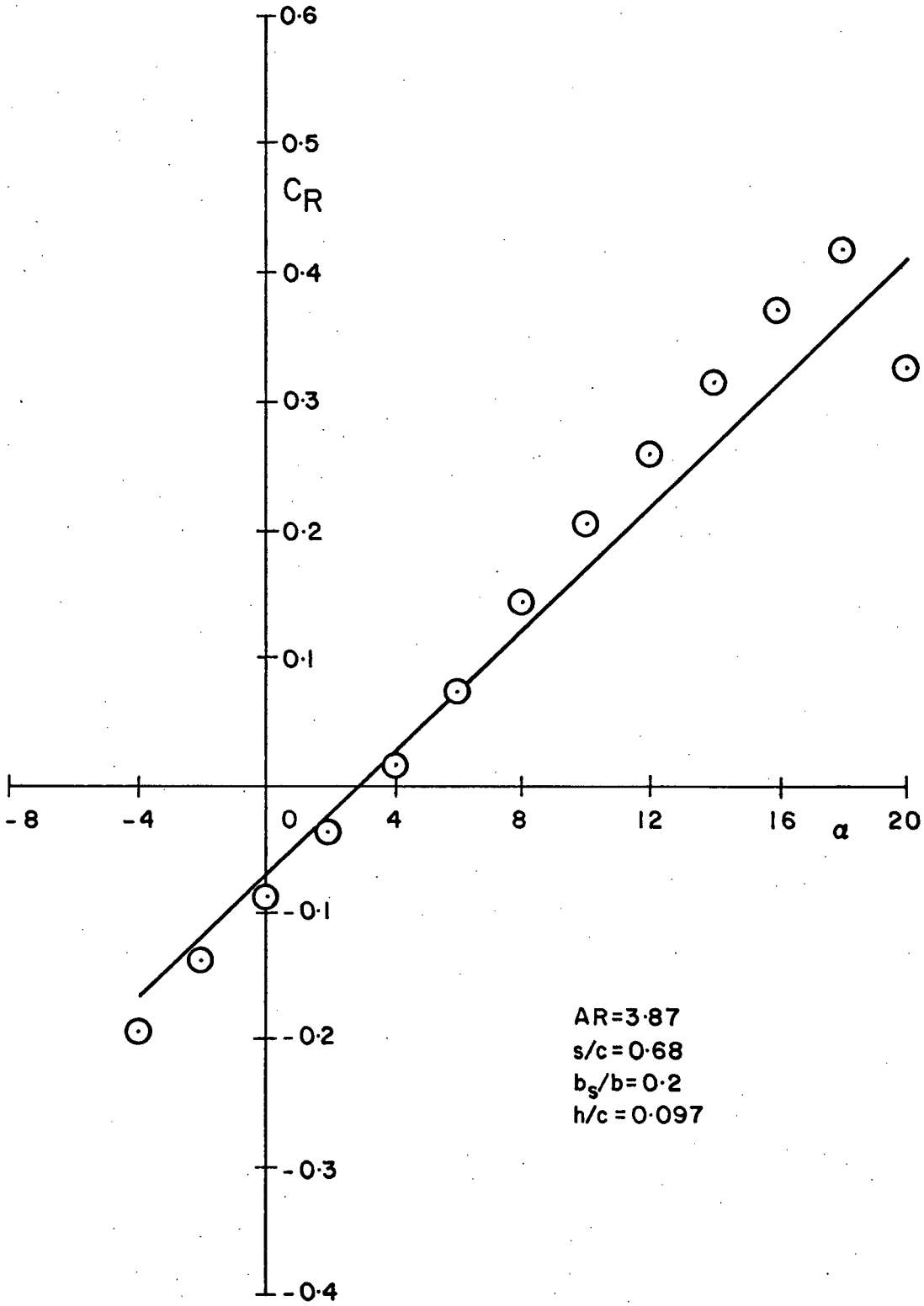

Figure 29 Rolling Moment Coefficient for Rectangular Half Wing of NACA 0015 Section with Normal Unvented Spoiler. —— theory; o C_R experiment;

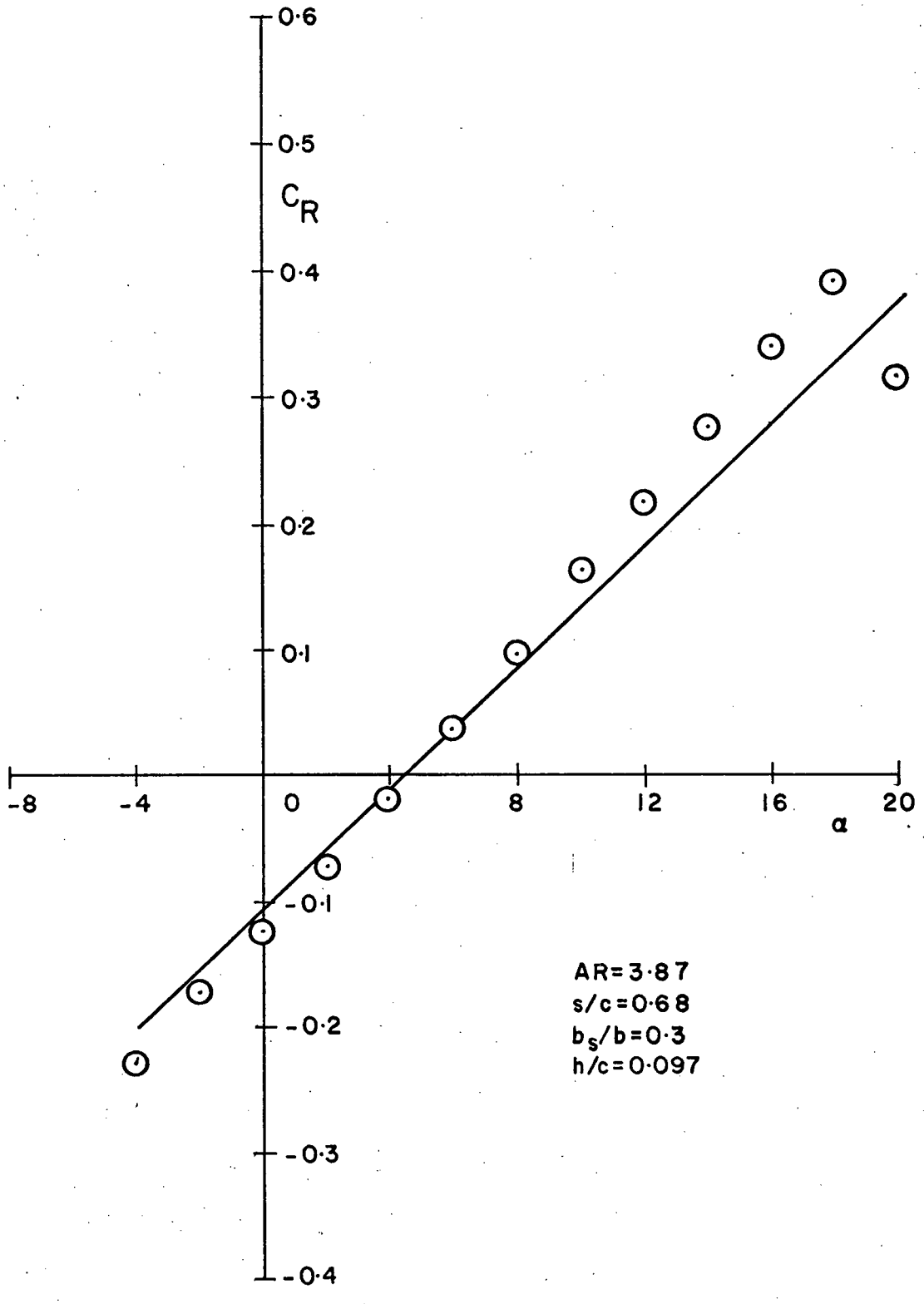

Figure 30 Rolling Moment Coefficient for Rectangular Half Wing of NACA 0015 Section with Normal Unvented Spoiler. —— theory; o C_R experiment

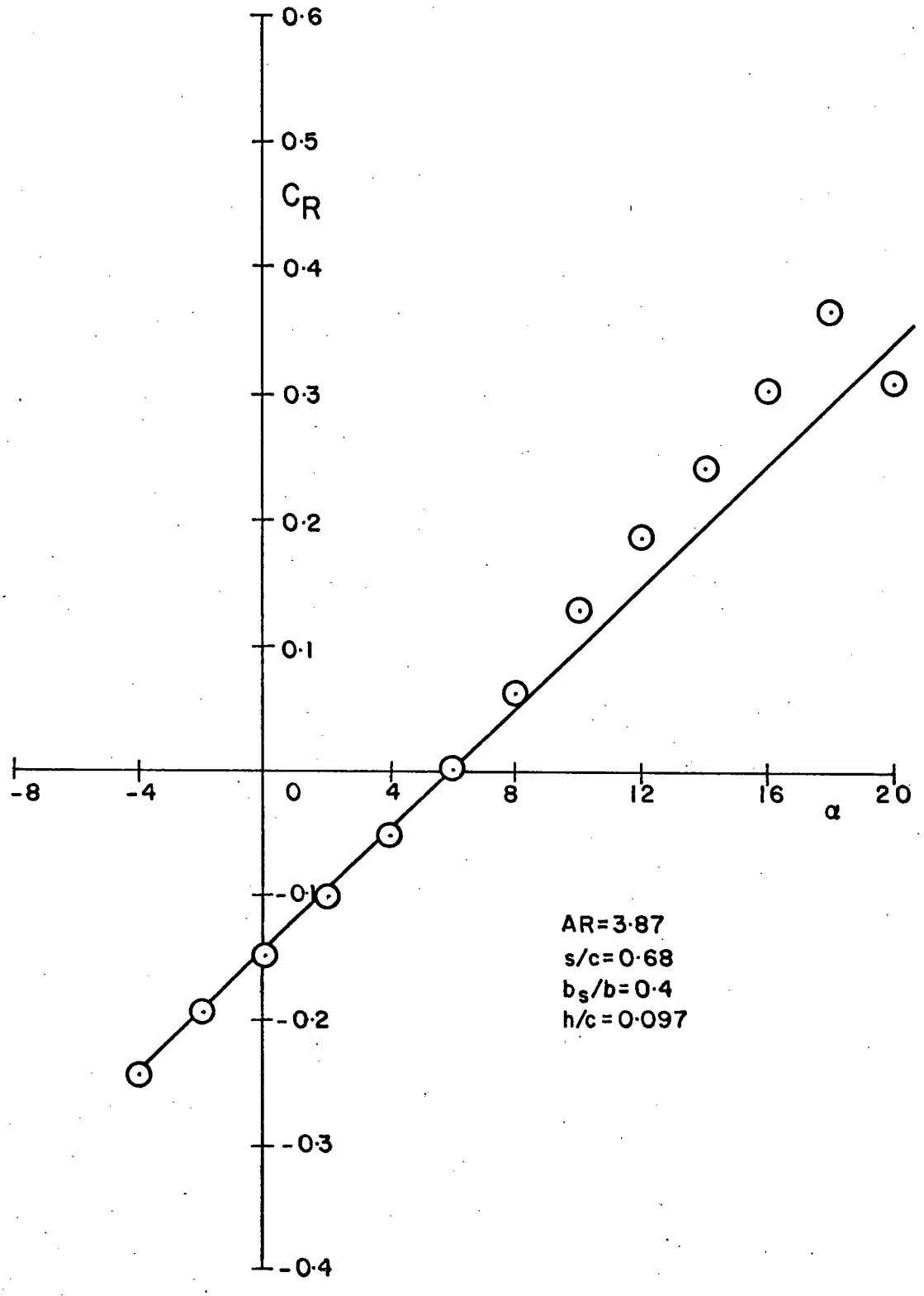

Figure 31 Rolling Moment Coefficient for Rectangular Half Wing of NACA 0015 Section with Normal Unvented Spoiler. —— theory; o experiment

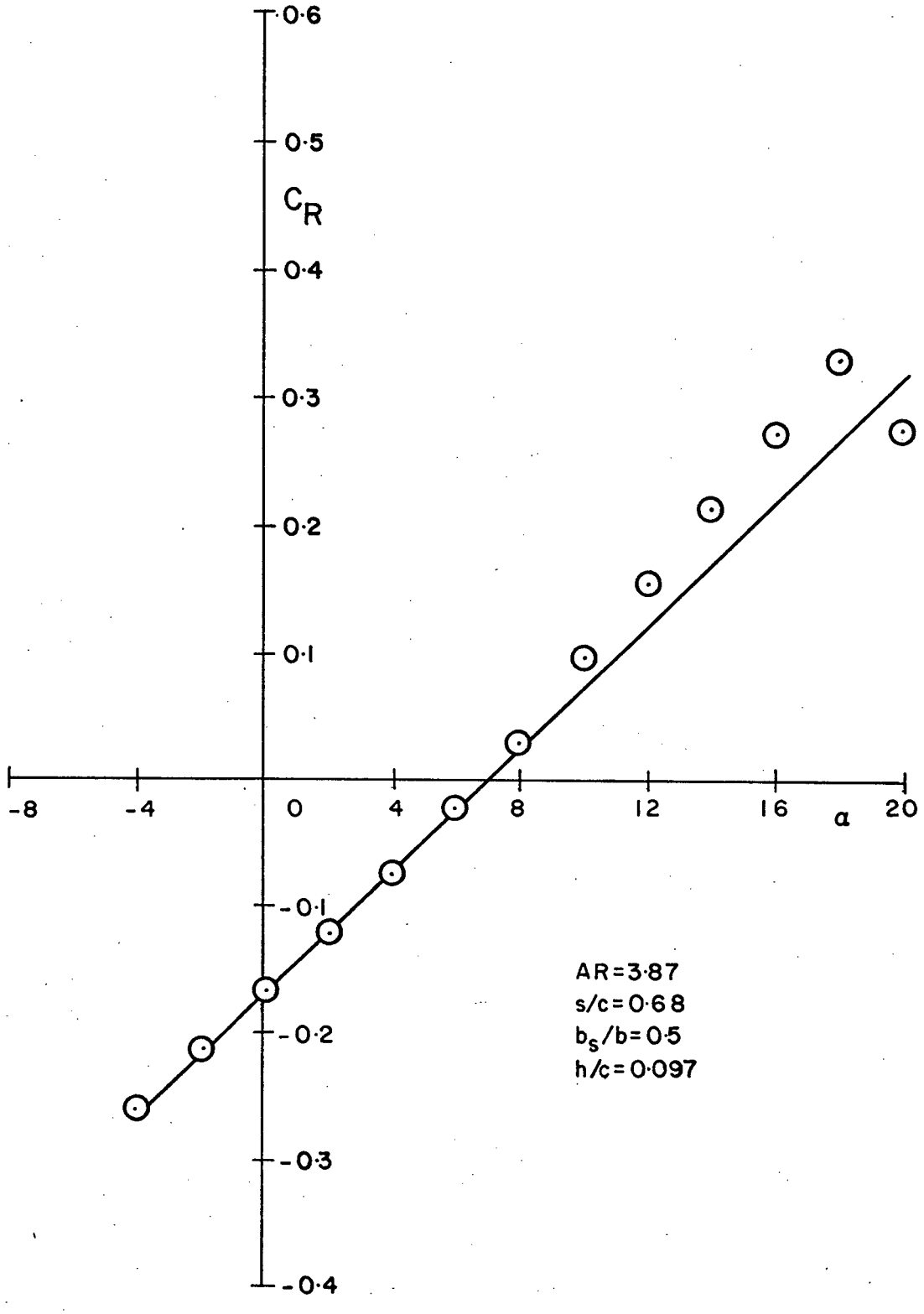

Figure 32 Rolling Moment Coefficient for Rectangular Half Wing of NACA 0015 Section with Normal Unvented Spoiler. ——— theory; o experiment

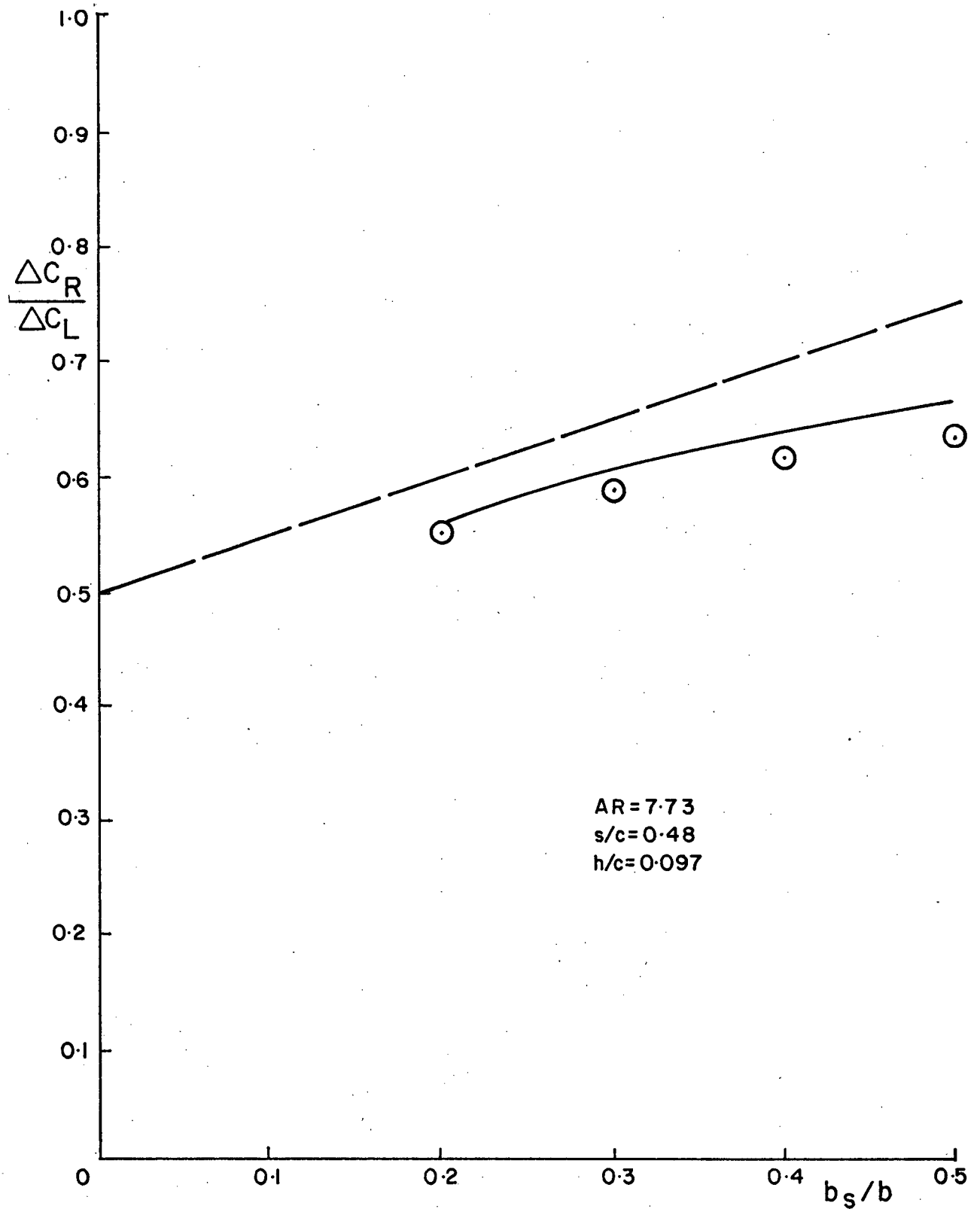

Figure 33 Effective Moment Arm of Incremental Lift Due to Normal Unvented Spoiler on Rectangular Wing of NACA 0015 Section. —— Theory; o experiment; — — — ΔC_L acting at midspan of spoiler

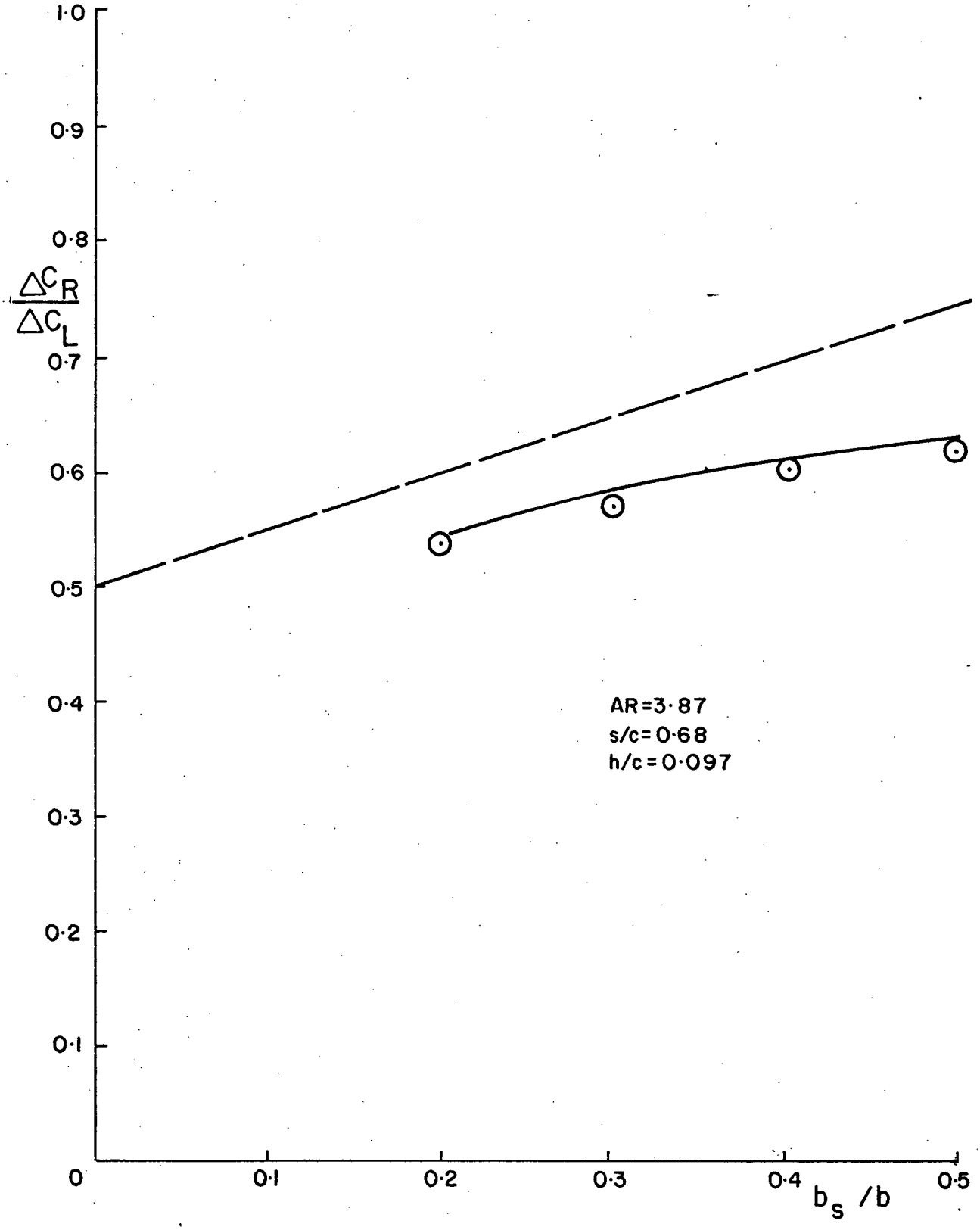

Figure 34 Effective Moment Arm of Incremental Lift Due to Normal Unvented Spoilers on Rectangular Wings of NACA 0015 Section. —— theory; o experiment; — — — ΔC_L acting at midspan of spoiler

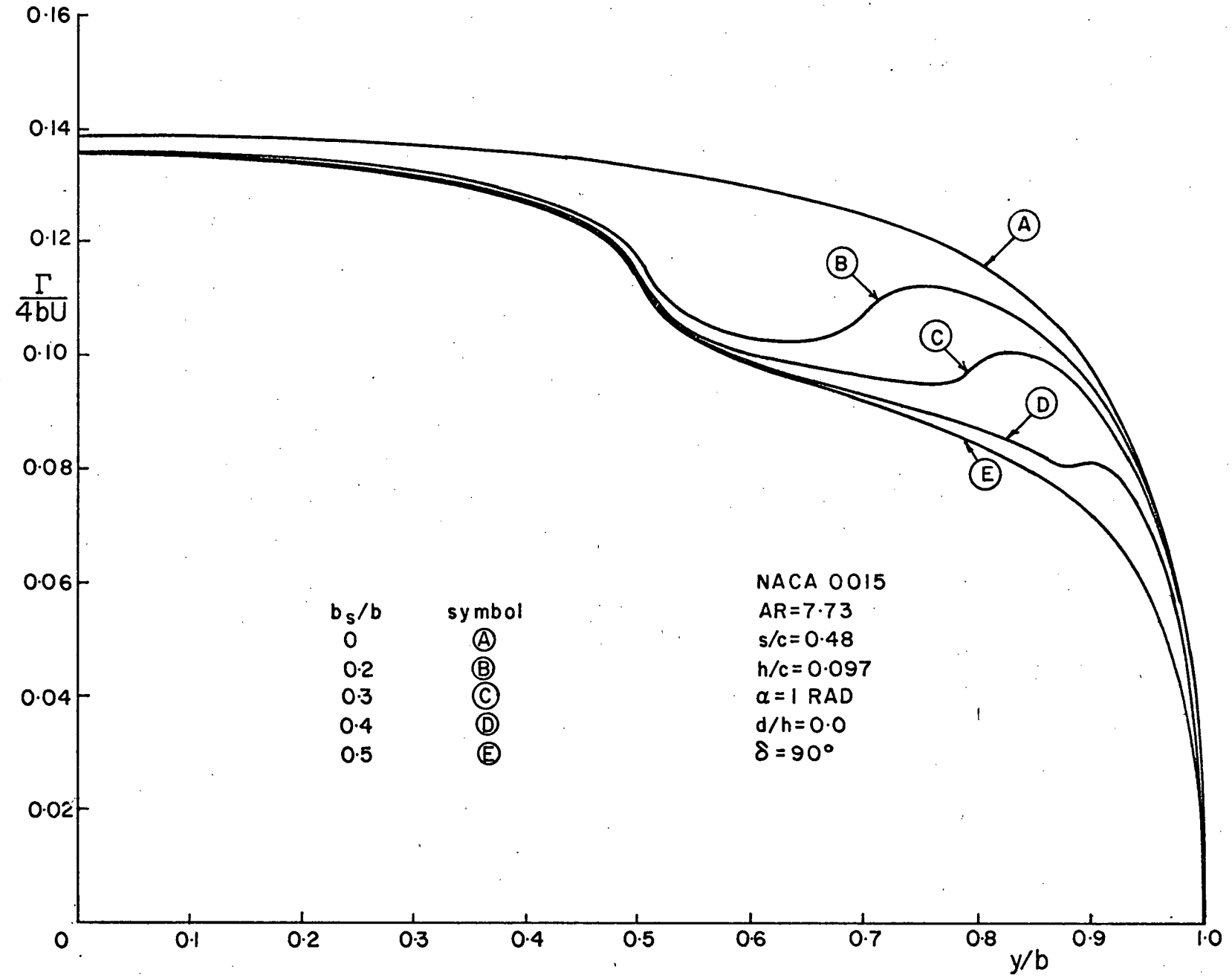

Figure 35 Spanwise Lift Distribution for Rectangular Wings with Symmetrically Deployed Spoilers

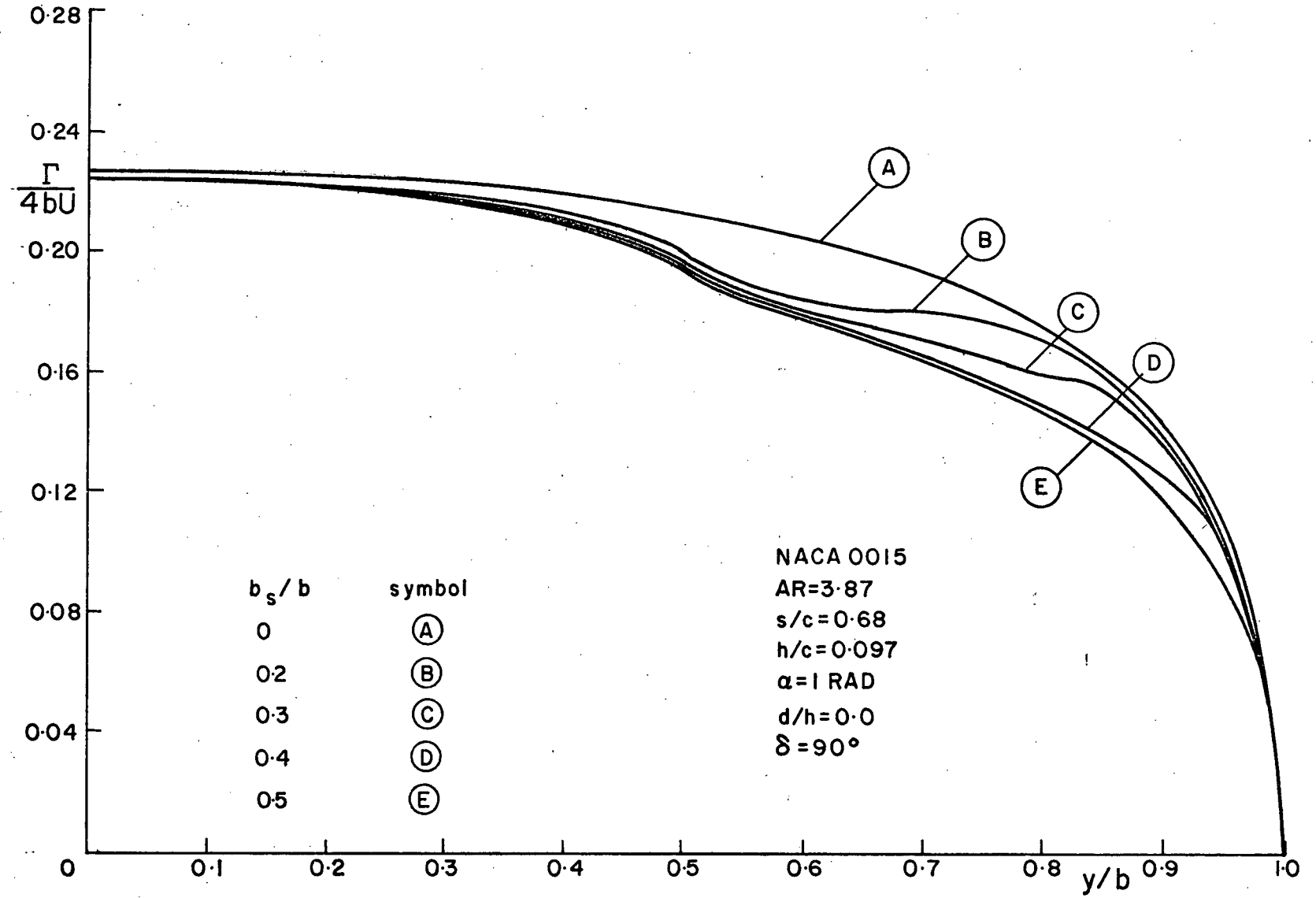

Figure 36. Spanwise Lift Distribution for Rectangular Wings with Symmetrically Deployed Spoilers

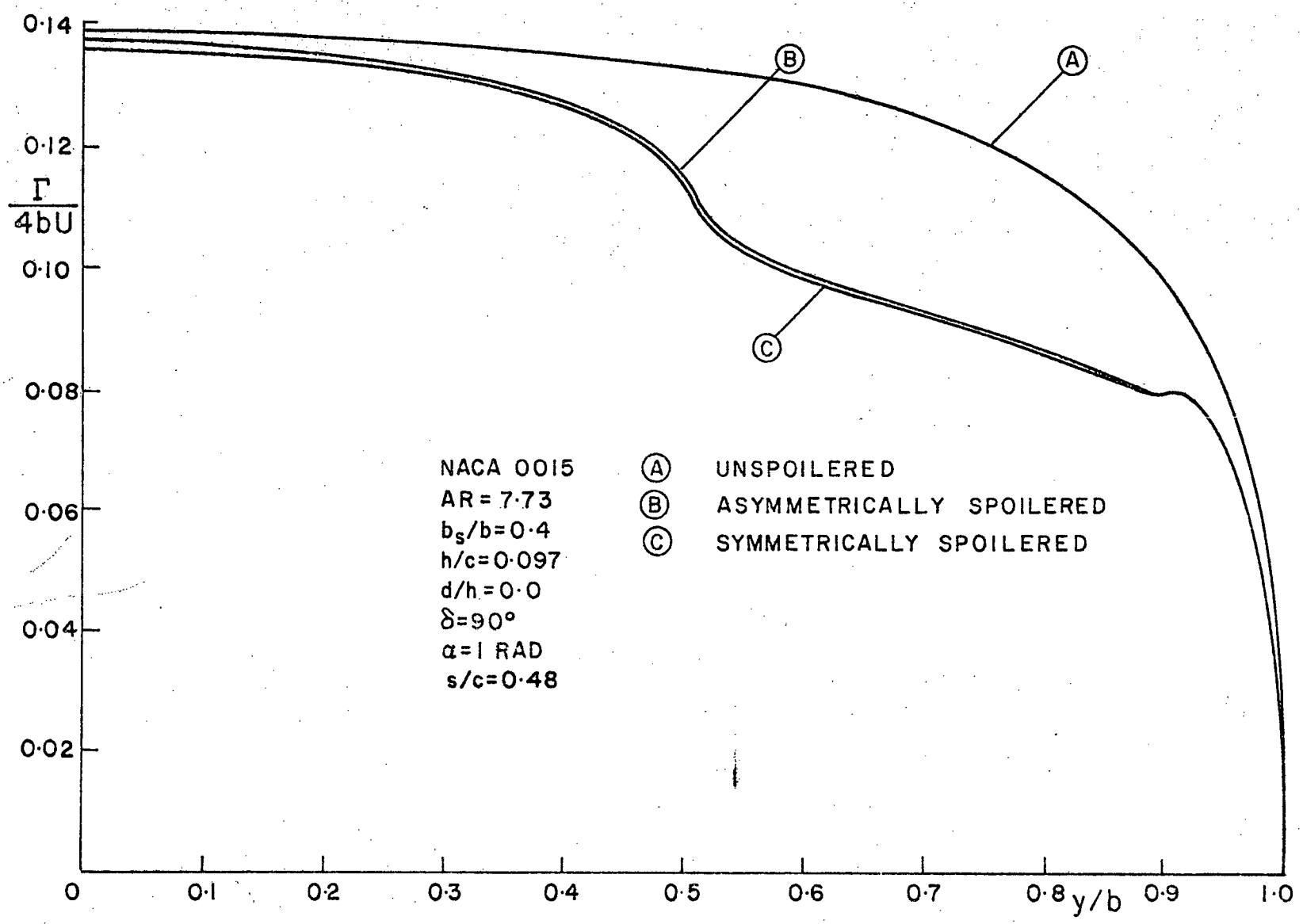

Figure 37 Spanwise Lift Distribution for Rectangular Wings of NACA 0015 Section

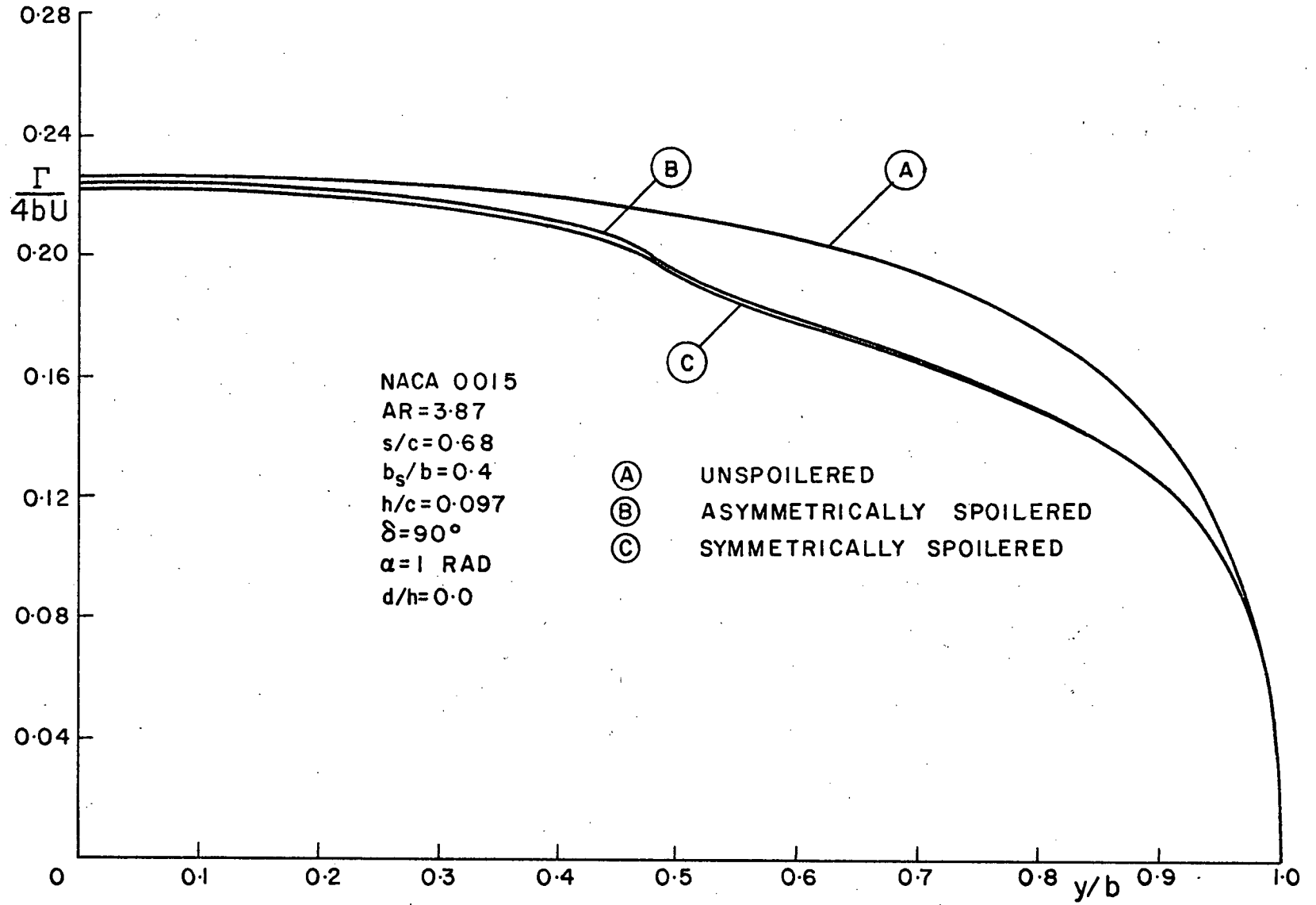

Figure 38 Spanwise Lift Distribution for Rectangular Wing of NACA 0015 Section

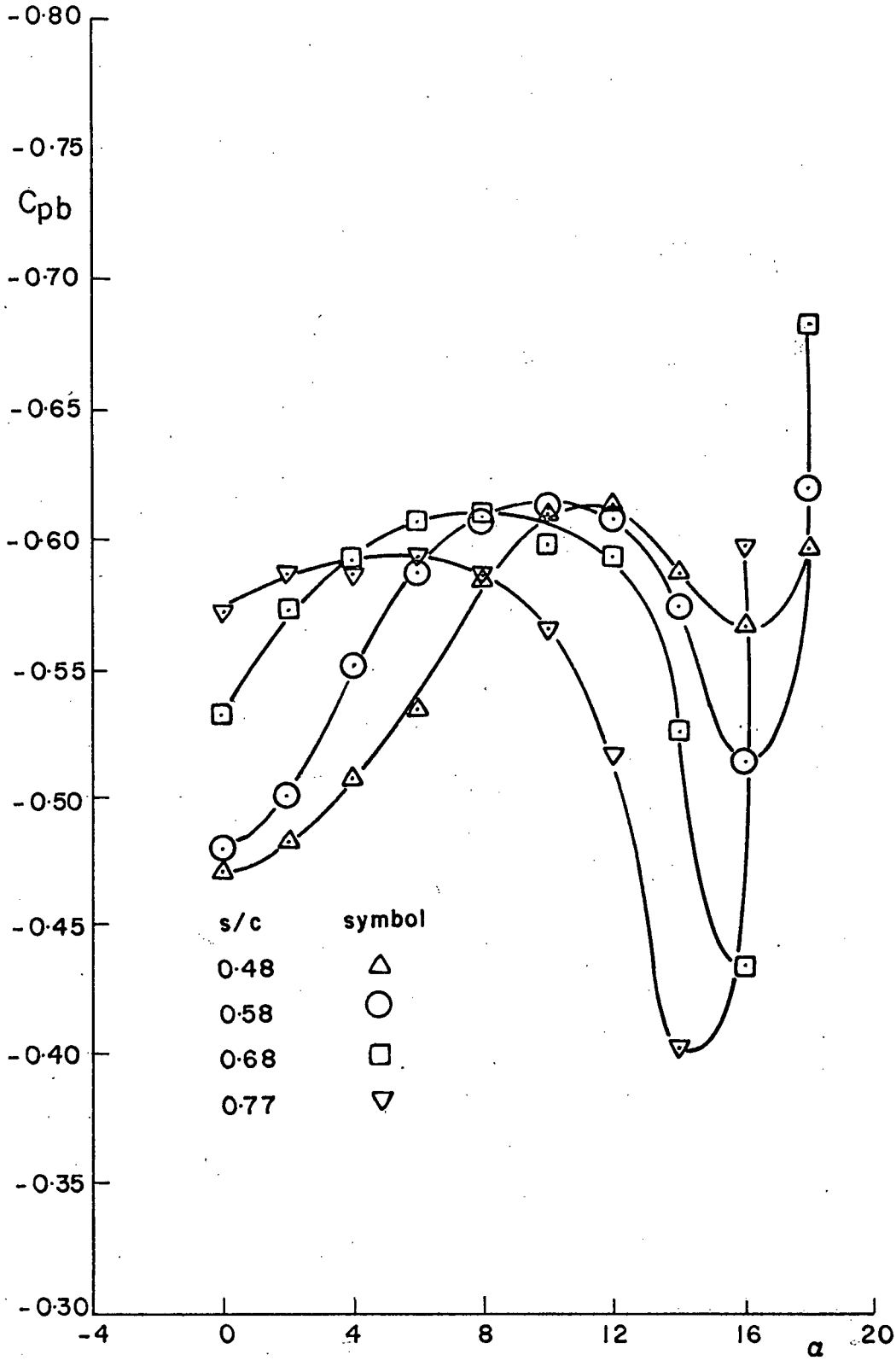

Figure 39 C_{pb} Distribution for NACA 0015 Section with 9.7% Normal Unvented Spoiler

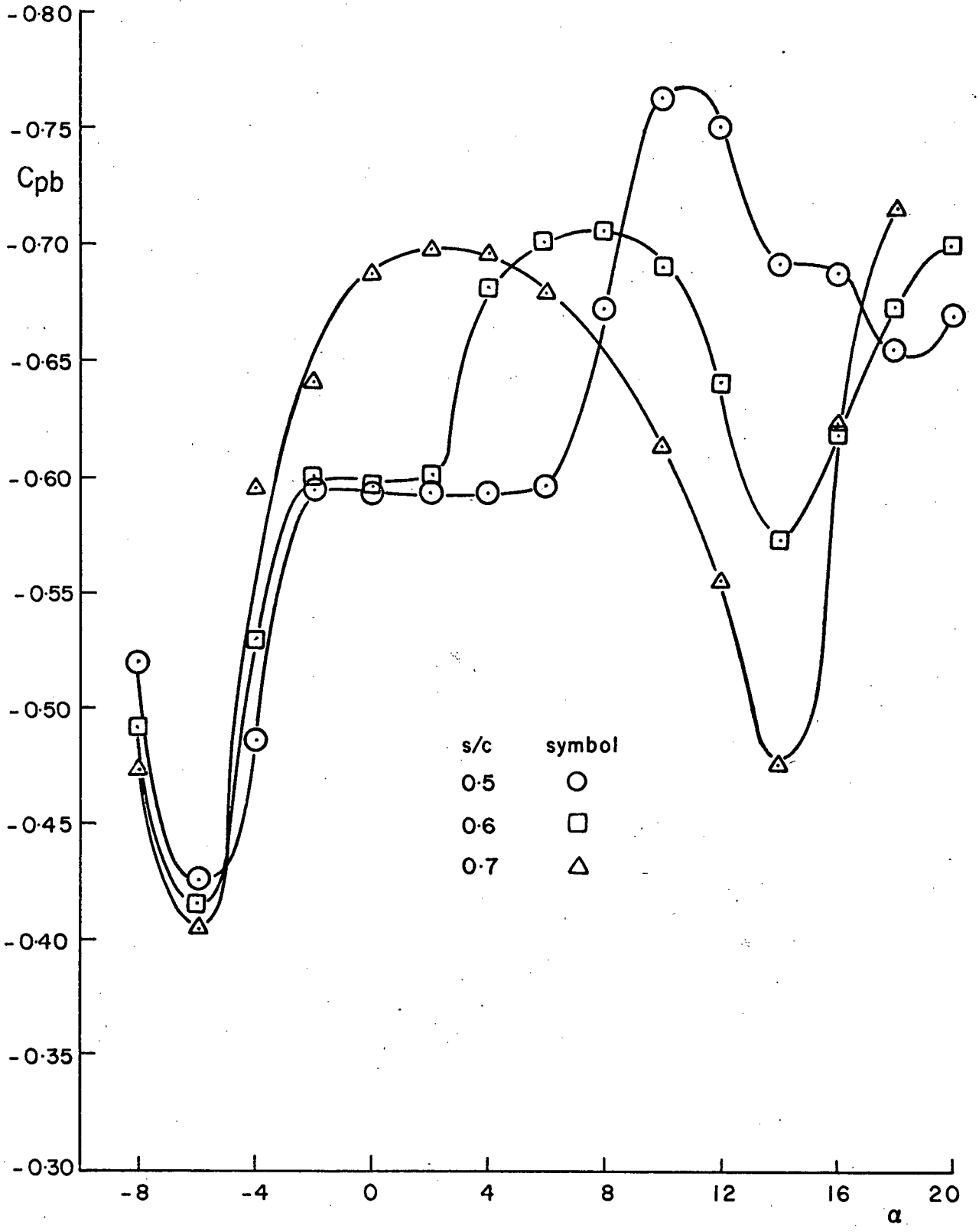

Figure 40 C_{pb} Distribution for a 12.9% Thick Clark Y Section with 10% Normal Unvented Spoiler

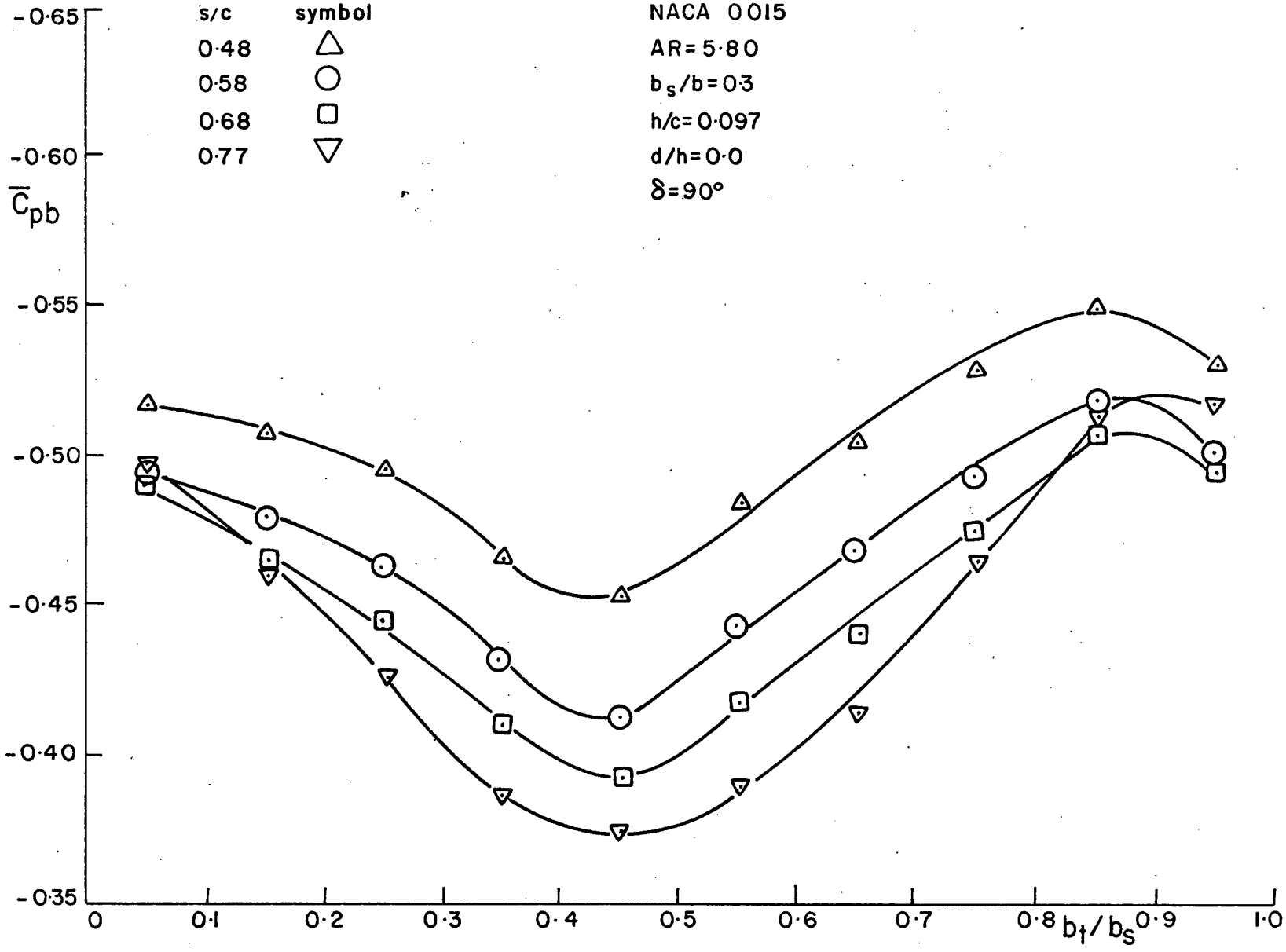

Figure 41 Variation of $\bar{C}_{pb}$ with Spoiler Position Along Chord for Rectangular Wings with Spoilers

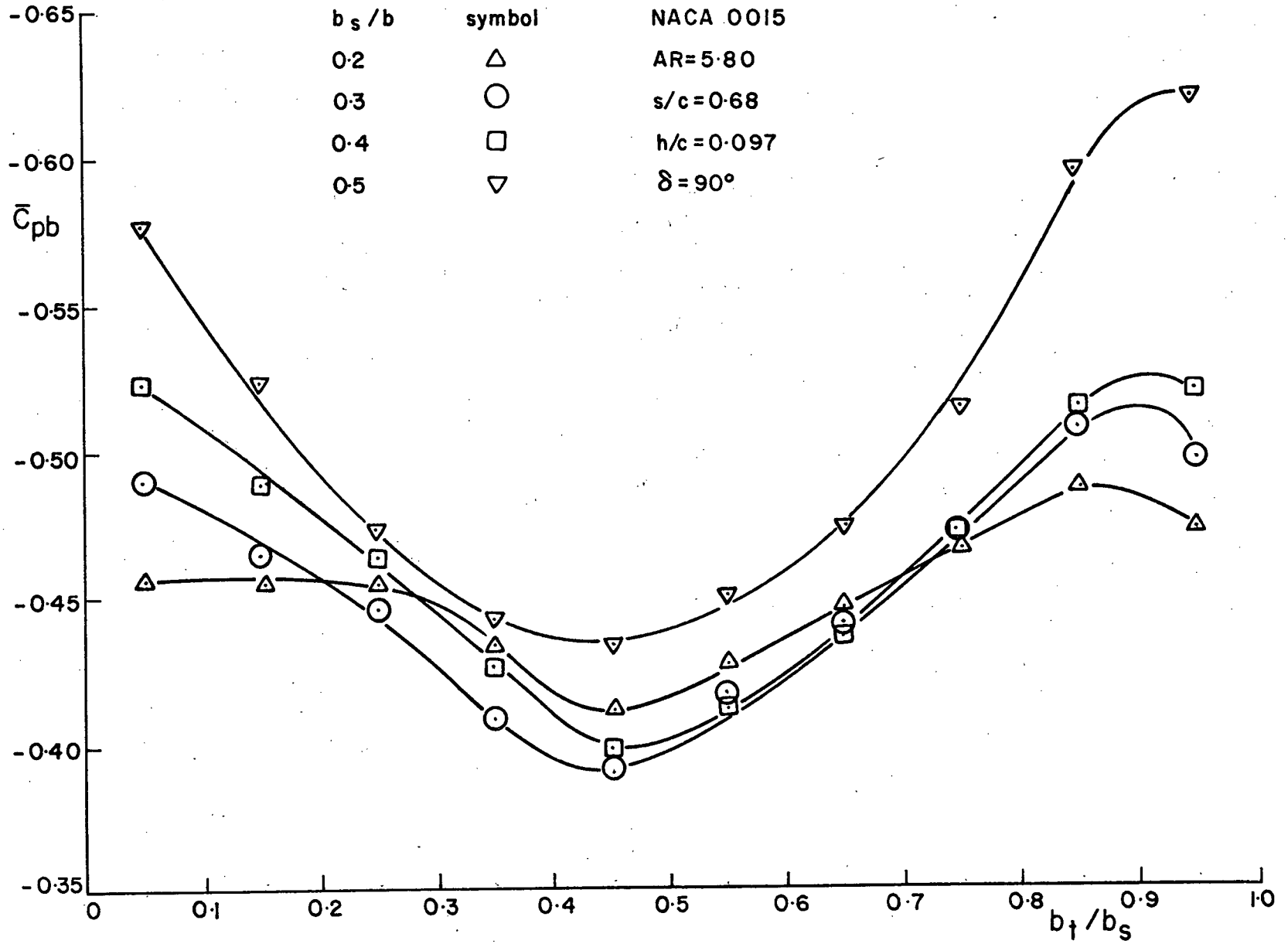

Figure 42 Variation of $\bar{C}_{pb}$ with Spoiler Span for Rectangular Wing with Spoilers

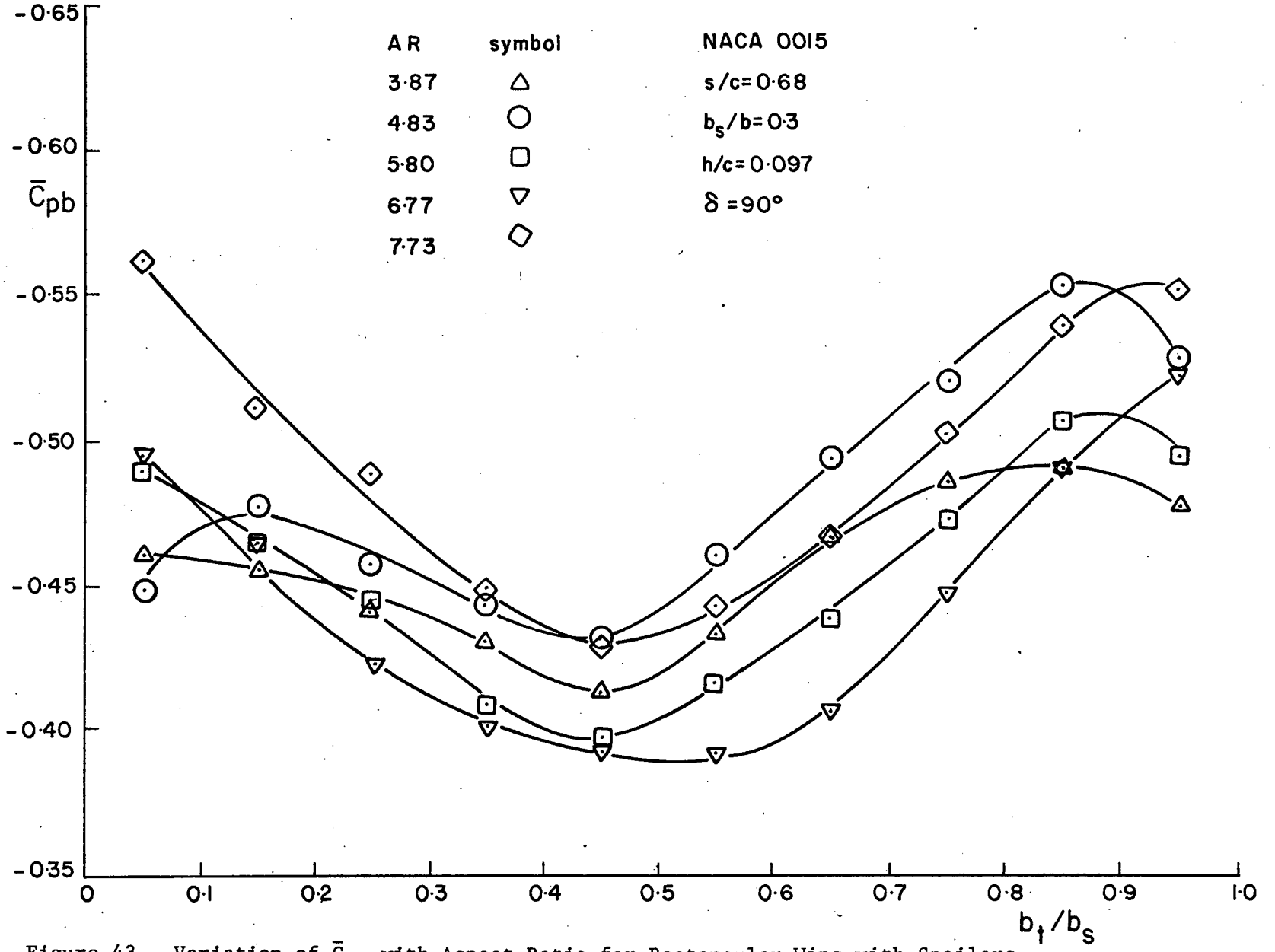

Figure 43 Variation of $\bar{C}_{pb}$ with Aspect Ratio for Rectangular Wing with Spoilers

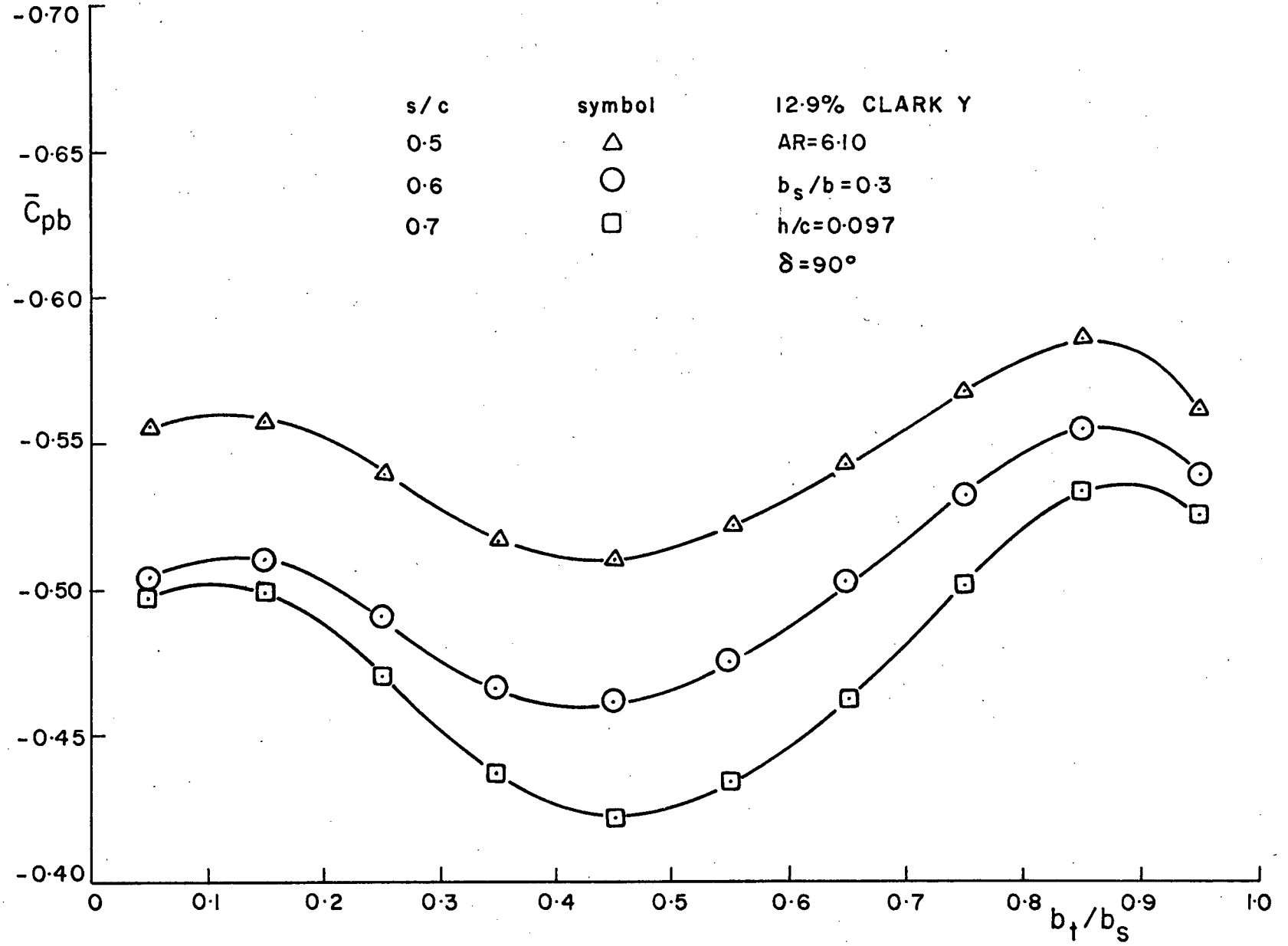

Figure 44 Variation of $\bar{C}_{pb}$ with Spoiler Position Along Chord for Rectangular Wings with Spoilers

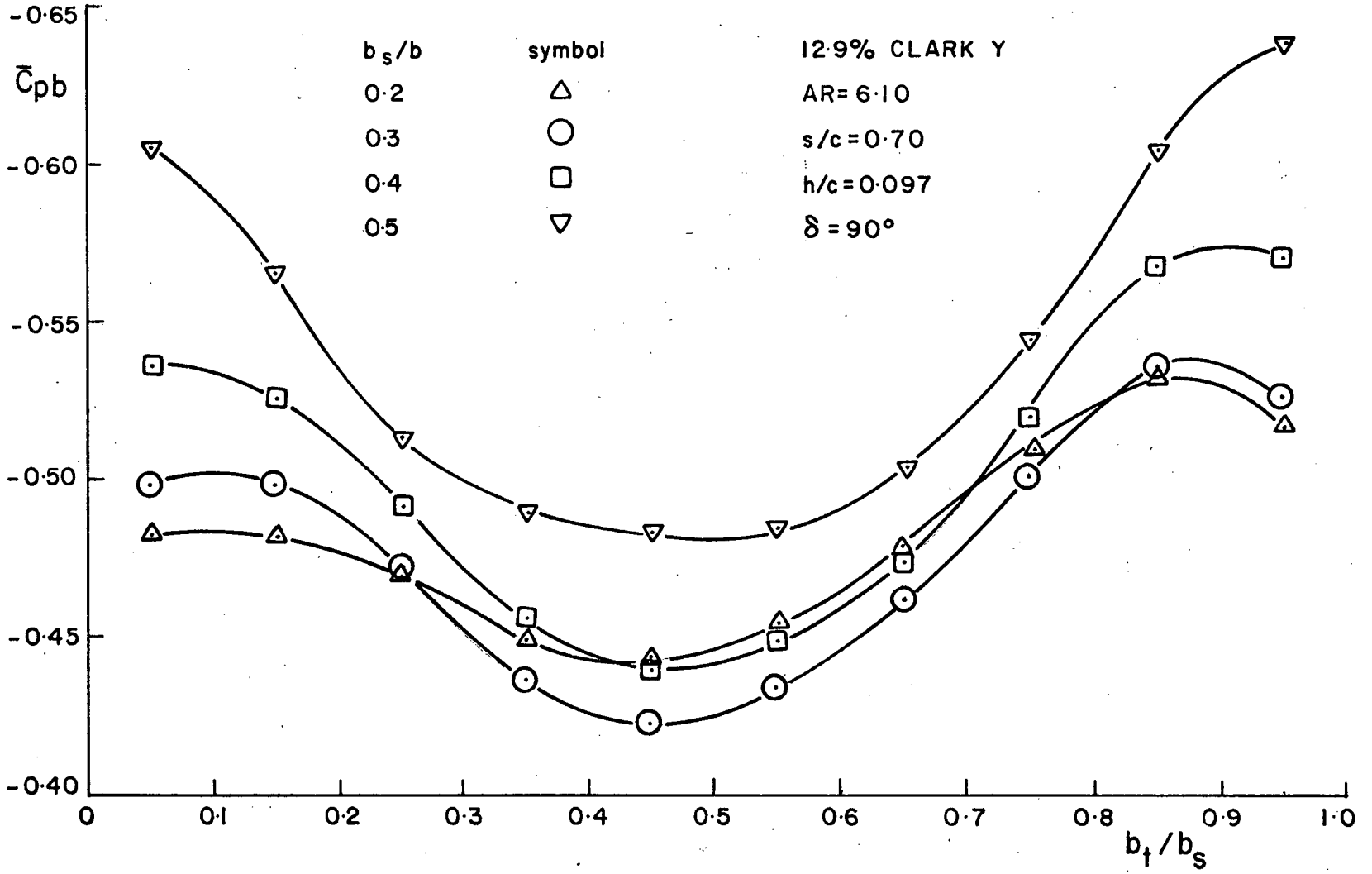

Figure 45 Variation of $\bar{C}_{pb}$ with Spoiler Span for Rectangular Wing with Spoiler

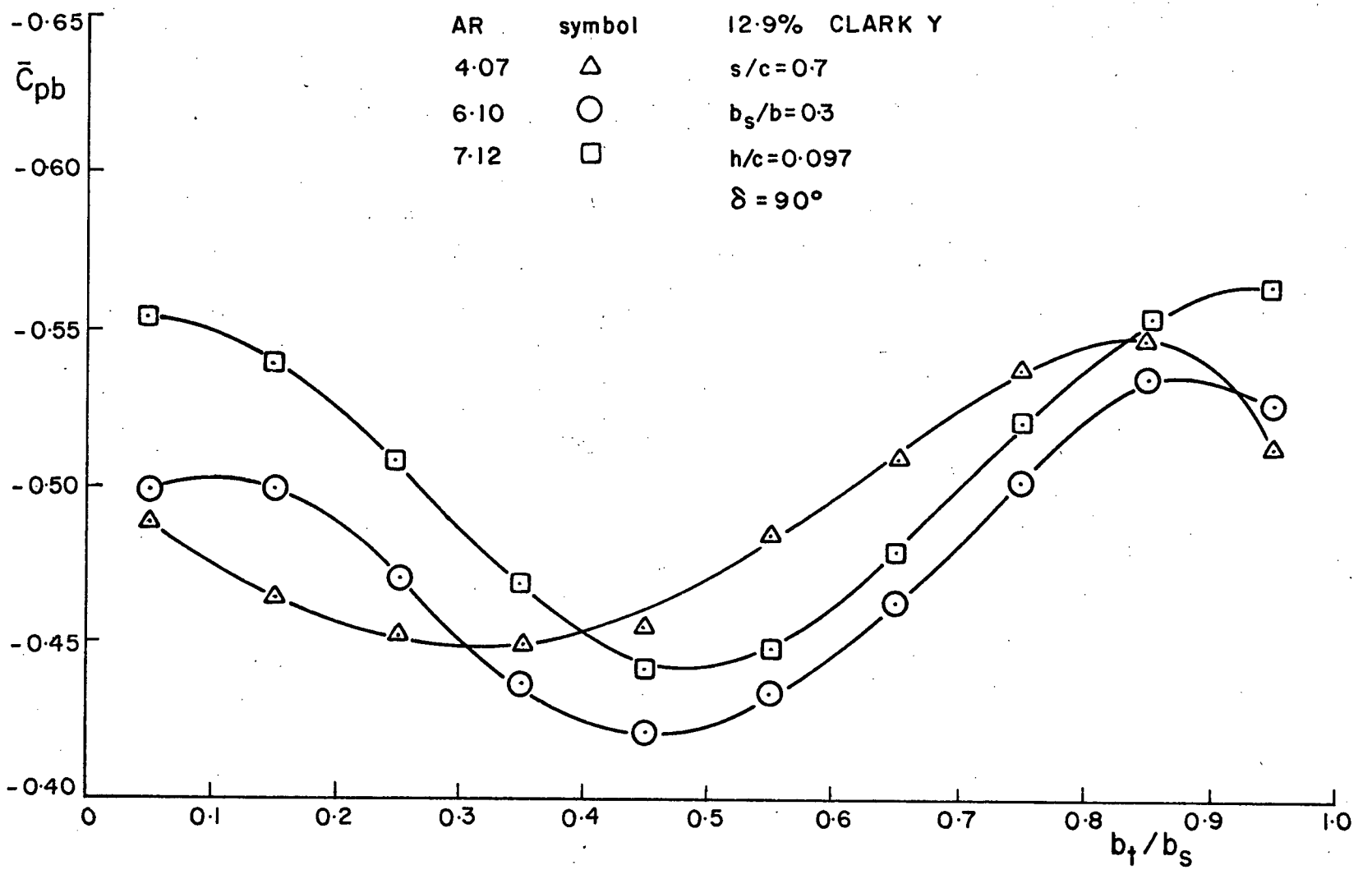

Figure 46 Variation of $\bar{C}_{pb}$ with Aspect Ratio for Rectangular Wings with Spoilers

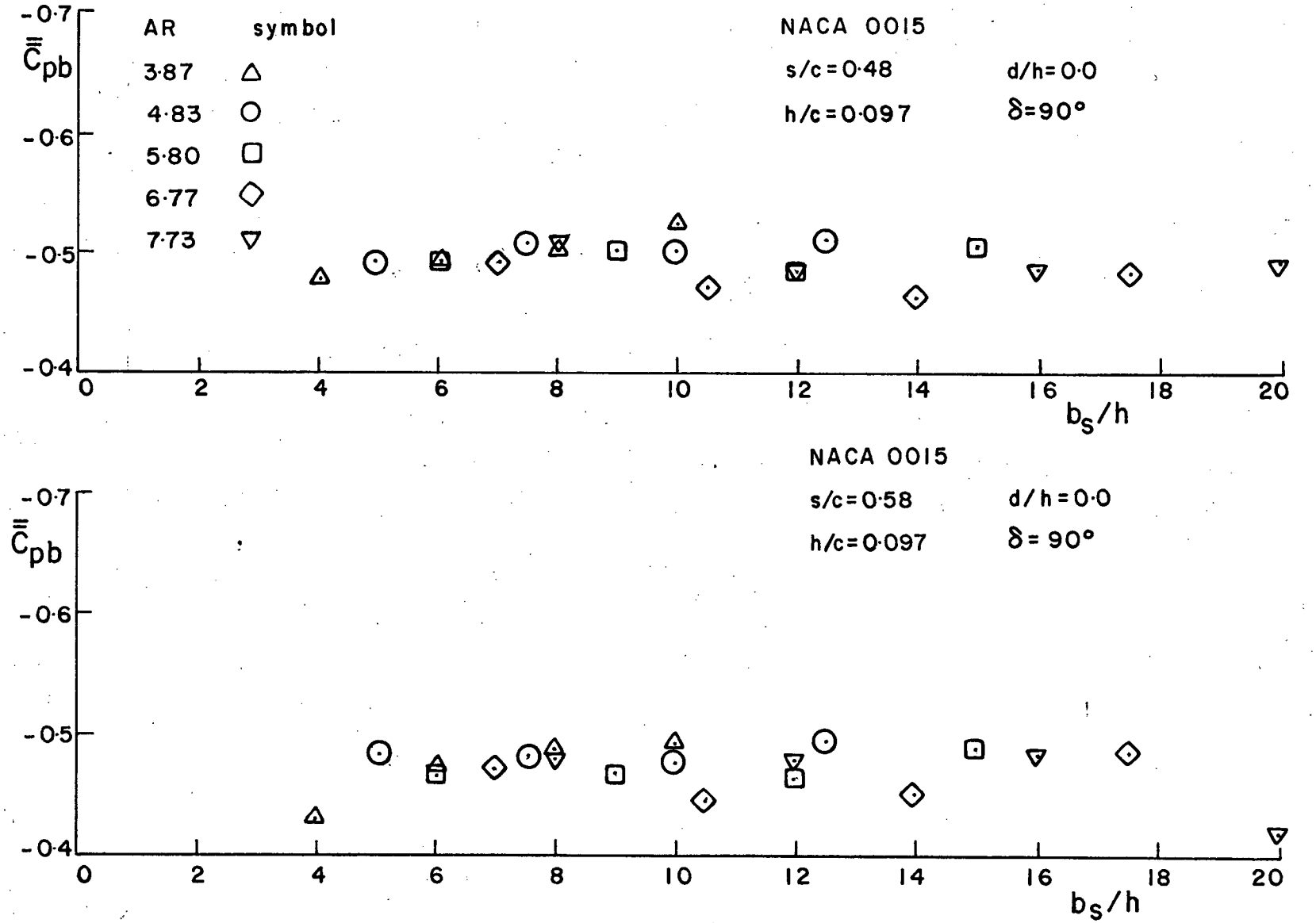

Figure 47 Variation of $\bar{\bar{C}}_{pb}$ with Spoiler Span for Rectangular Wing with Normal Unvented Spoiler

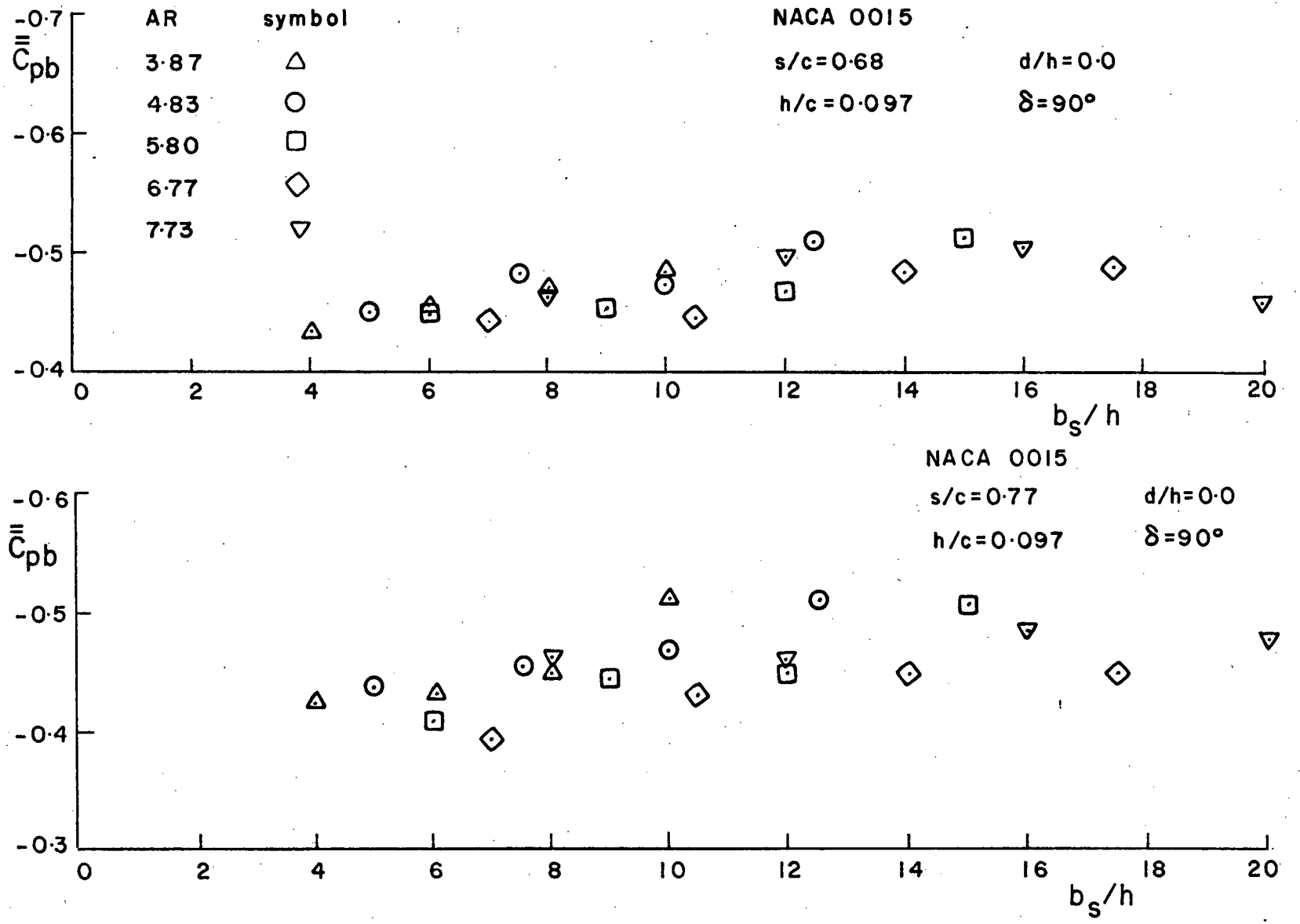

Figure 48 Variation of $\bar{\bar{C}}_{pb}$ with Spoiler Span for Rectangular Wings with Normal Unvented Spoilers

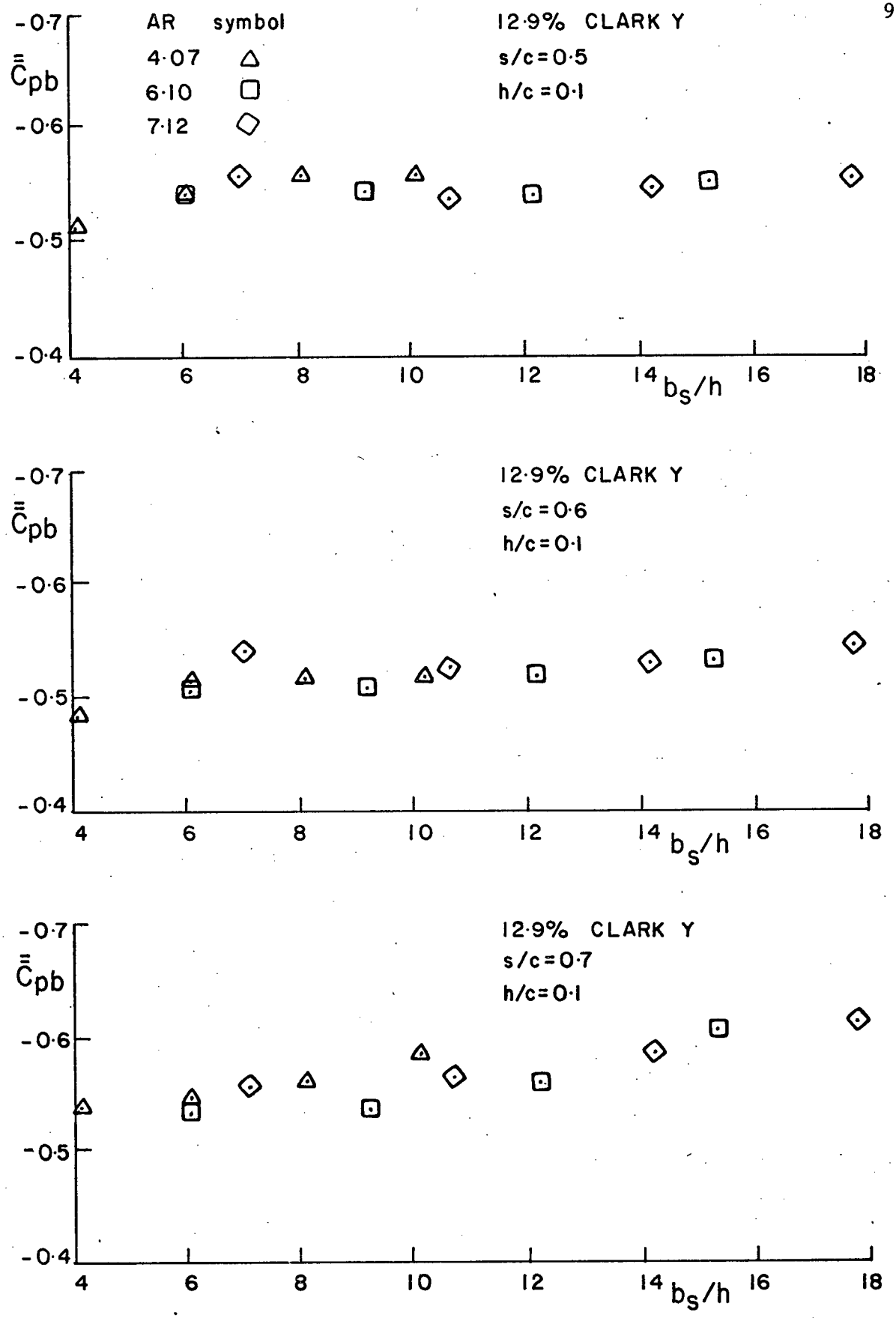

Figure 49 Variation of $\bar{\bar{C}}_{pb}$ with Spoiler Span for Rectangular Wings with Normal Unvented Spoilers

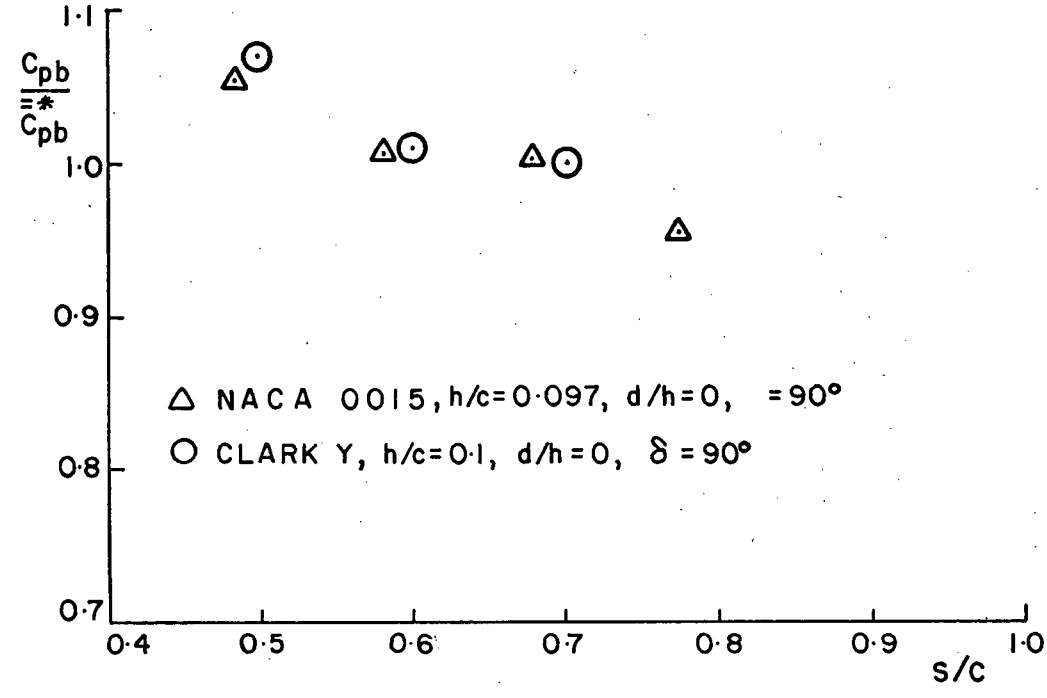

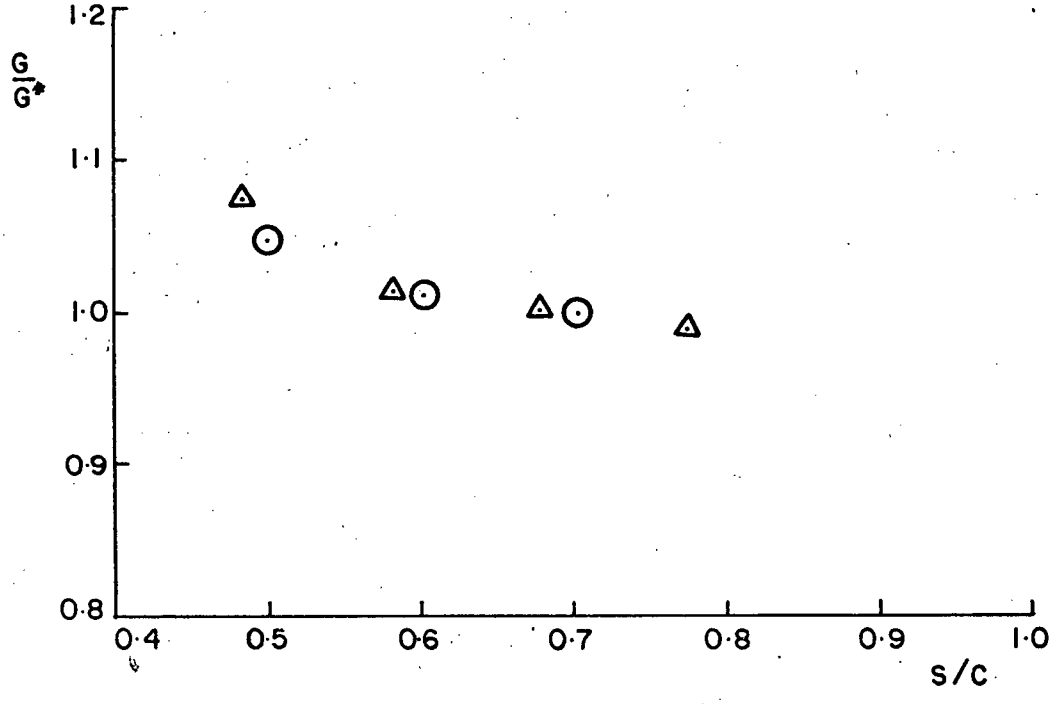

Figure 50 Variation of $\bar{\bar{C}}_{pb}$ / $\bar{\bar{C}}^{*}_{pb}$ and G/G* with s/c

REFERENCES

1. Woods, L.C., "The Theory of Subsonic Plane Flow", Cambridge University Press, 1961.

2. Barnes, C.S., "A Developed Theory of Spoilers on Airfoils, A.R.C. R & M, CP 887, July 1965.

3. Jandali, T., "A Potential Flow Theory for Airfoil Spoilers", Ph.D. Thesis, University of British Columbia, 1971.

4. Brown, G.P., "Steady and Non-Steady Potential Flow Methods for Airfoils with Spoilers", Ph.D. Thesis, University of British Columbia, 1971.

5. Prandtl, L., "Applications of Modern Hydrodynamics to Aeronautics", NACA Report No. 116, 1921.

6. Jones, R.T., "Correction of the Lifting Line Theory for the Effect of the Chord", NACA Technical Note No. 817, 1941.

7. Glauert, H., "Elements of Airfoil and Airscrew Theory", Cambridge University Press, 1927.

8. Wieselsberger, C., " Theoretical Investigations of the Effect of the Ailerons on the Wing of an Aeroplane", NACA TM 510, 1928.

9. Bernier, R., "Steady & Transient Aerodynamics of Spoilers on Airfoils", M.A.Sc. Thesis, University of British Columbia, 1977.

10. Parkin, B.R., "Linearised Theory of Cavity Flows in Two Dimensions", RAND Report, P-1745, 1959.

11. Biot, M.A., "Some Simplified Methods in Airfoil Theory", Journal of the Aeronautical Sciences, 9, 1942, p185.

12. Hoerner, S.F., "Fluid Dynamic Drag", Published by Author, 1965.

13. Pope, A. & Harper, J.J., "Low Speed Wind Tunnel Testing", Wiley, 1966

APPENDIX

$$K = 2R1\left[\ell a_1\left(i(1+\frac{1}{a_o^2})\left[\frac{R1\lambda_1\ [\ ImE - (\alpha - \tfrac{1}{2}M_o)\ ] - Im\lambda_1 R1E}{R1\lambda_1 Im\lambda_2 - Im\lambda_1 Re\lambda_2}\right] - \right.\right.$$

$$i\left[\frac{e^{i\theta_0}}{(a_o e^{i\theta_0}-1)^2} + \frac{e^{-i\theta_0}}{(a_o e^{-i\theta_0}-1)^2}\right]\left[\frac{R1\lambda_2[ImE-(\alpha-\tfrac{1}{2}M_o)]-Im\lambda_2 R1E}{R1\lambda_2 Im\lambda_1 - Im\lambda_2 R1\lambda_1}\right.$$

$$\left.+\frac{\theta_1 Sin\delta}{\pi} + \frac{\theta_2-\pi}{\pi}\eta\right] + \frac{Sin\delta}{\pi}\left[\frac{1}{a_o-e^{i\theta_1}} - \frac{1}{a_o-e^{-i\theta_1}}\right]+$$

$$\frac{\eta}{\pi}\left[\frac{1}{a_o-e^{i\theta_2}} - \frac{1}{a_o-e^{-i\theta_2}}\right] + i\sum_{n=1}^{\infty}\frac{nM_n}{a_o^{n+1}} +$$

$$\left.\left.i\sum_{n=0}^{\infty} N_n \frac{\left[\frac{1-n}{a_o} - \frac{e^{i\theta_0}}{a_o e^{i\theta_0}-1} - \frac{e^{-i\theta_0}}{a_o e^{-i\theta_0}-1}\right]}{a_o^{n-1}(a_o e^{i\theta_0}-1)(a_o e^{-i\theta_0}-1)}\right)\right] \Big/$$

$$R1\left[\ell a_1\left(i\frac{Im\lambda_2}{R1\lambda_2 Im\lambda_1 - R1\lambda_1 Im\lambda_2}\left[\frac{e^{i\theta_0}}{(a_o e^{i\theta_0}-1)^2} + \frac{e^{-i\theta_0}}{(a_o e^{-i\theta_0}-1)^2}\right]-\right.\right.$$

$$\left.\left.i\frac{Im\lambda_1}{R1\lambda_1 Im\lambda_2 - Im\lambda_1 R1\lambda_2}\left(1+\frac{1}{a_o^2}\right)\right)\right] \qquad (29)$$

where

$$a_o = \frac{1-b}{1+b} + \frac{2ia}{1+b} + \left[\left\{ \frac{1-b}{1+b} + \frac{2ia}{1+b} \right\}^2 - 1 \right]^{\frac{1}{2}}$$

$$a_1 = \frac{ia}{1+b} \left[1 + \frac{\frac{1-b}{1+b} + \frac{2ia}{1+b}}{\left[\left\{ \frac{1-b}{1+b} + \frac{2ia}{1+b} \right\}^2 - 1 \right]^{\frac{1}{2}}} \right]$$

$$C_{ps} = -2 \left[C_o + \frac{\eta(\theta_2 - \pi)}{\pi} + \frac{\theta_1 \, \mathrm{Sin}\delta}{\pi} \right] \frac{\mathrm{Sin}\theta}{\mathrm{Cos}\theta_0 - \mathrm{Cos}\theta} + 4B_o \mathrm{Sin}\theta$$

$$- \frac{2\mathrm{Sin}\delta}{\pi} \ln \left[\frac{\mathrm{Sin}\frac{1}{2}|\theta - \theta_1|}{\mathrm{Sin}\frac{1}{2}(\theta + \theta_1)} \right] - \frac{2\eta}{\pi} \ln \left[\frac{\mathrm{Sin}\frac{1}{2}|\theta - \theta_2|}{\mathrm{Sin}\frac{1}{2}(\theta + \theta_2)} \right] +$$

$$2\sum_{n=1}^{\infty} M_n \, \mathrm{Sin}\, n\theta + \frac{\sum_{n=1}^{\infty} N_n \, \mathrm{Sin}\, n\theta}{\mathrm{Cos}\theta_0 - \mathrm{Cos}\,\theta} - K \qquad (30)$$

$$C_{ls} = \frac{4\pi}{c} \, \mathrm{Im} \left(iB_o \ell a_1 \left(1 + \frac{1}{a_o^2}\right) - i \left[C_o + \frac{\theta_1 \mathrm{Sin}\delta}{\pi} + \frac{(\theta_2 - \pi)\eta}{\pi} \right] \right.$$

$$\ell a_1 \left[\frac{e^{i\theta_0}}{(a_o e^{i\theta_0} - 1)^2} + \frac{e^{-i\theta_0}}{(a_o e^{-i\theta_0} - 1)^2} \right] + \frac{\mathrm{Sin}\delta}{\pi} \ell a_1 \left[\frac{1}{a_o - e^{i\theta_1}} \right.$$

$$\left. - \frac{1}{a_o - e^{-i\theta_1}} \right] + \frac{\eta}{\pi} a_1 \left[\frac{1}{a_o - e^{i\theta_2}} - \frac{1}{a_o - e^{-i\theta_2}} \right] + i\ell a_1 \sum_{n=1}^{\infty} \frac{nM_n}{a_o^{n+1}}$$

$$\left. + i\ell a_1 \sum_{n=0}^{\infty} N_n \, \frac{\left[\frac{1-n}{a_o} - \frac{e^{i\theta_0}}{a_o e^{i\theta_0} - 1} - \frac{e^{-i\theta_0}}{a_o e^{-i\theta_0} - 1} \right]}{a_o^{n-1} (a_o e^{i\theta_0} - 1)(a_o e^{-i\theta_0} - 1)} \right) \qquad (31)$$

$$C_{mos} = -\frac{4\pi}{c^2}\,\mathrm{Im}\left[iC_o \ell^2 a_2 \left(\frac{\zeta_o}{(a_o\zeta_o-1)^2} \left[\frac{a_1^2\zeta_o}{(a_o\zeta_o-1)a_2} - 1 \right] + \right.\right.$$

$$\left.\left. \frac{\bar{\zeta}_o}{(a_o\bar{\zeta}_o-1)^2} \left[\frac{a_1^2\bar{\zeta}_o}{(a_o\bar{\zeta}_o-1)a_2} - 1 \right] \right) + iB_o \ell^2 a_2 \left[1 - \frac{1}{a_o^2} \frac{a_1^2}{a_o a_2} - 1 \right] \right.$$

$$- i\ell^2 a_2 \sum_{n=1}^{\infty} M_n \frac{n}{a_o^{n+1}} \left[\frac{a_1^2}{a_o a_2} \left(\frac{n+1}{2}\right) - 1 \right] +$$

$$i\ell^2 a_2 \sum_{n=0}^{\infty} N_n \left(\frac{1}{a_o-\bar{\zeta}_o} \frac{1}{a_o-\zeta_o} \left[\frac{n-1}{a_o^n} \frac{a_1^2}{a_o a_2} - 1 + \frac{(n-1)(n-2)}{2!\, a_o^{n+1}} \frac{a_1^2}{a_2} \right] \right.$$

$$+ \frac{a_1^2(n-1)}{a_2(a_o-\bar{\zeta}_o)a_o^n(a_o-\zeta_o)^2} + \frac{1}{a_o-\bar{\zeta}_o} \frac{1}{a_o^{n-1}(a_o-\zeta_o)^2} \left[\right.$$

$$\left. \frac{a_1^2}{(a_o-\zeta_o)a_2} - 1 \right] + \frac{a_1^2(n-1)}{a_2(a_o-\zeta_o)a_o^n(a_o-\bar{\zeta}_o)} +$$

$$+ \frac{1}{a_2(a_o-\zeta_o)^2(a_o-\bar{\zeta}_o)^2 a_o^{n-1}} + \frac{1}{a_o^{n-2}(a_o-\zeta_o)(a_o-\bar{\zeta}_o)^2} \left[\right.$$

$$\left. \left. \frac{a_1^2}{(a_o-\bar{\zeta}_o)a_2} - 1 \right] \right) + \ell^2 a_2 \left[i\theta_1 \frac{\mathrm{Sin}\delta}{\pi} + i(\theta_2-\pi) \frac{\eta}{\pi} \right] \left(\right.$$

$$\left. \frac{\zeta_o}{(a_o\zeta_o-1)^2} \left[\frac{a_1^2\zeta_o}{(a_o\zeta_o-1)a_2} - 1 \right] + \frac{\bar{\zeta}_o}{(a_o\bar{\zeta}_o-1)^2} \left[\frac{a_1^2\bar{\zeta}_o}{(a_o\bar{\zeta}_o-1)a_2} - 1 \right] \right)$$

$$+\frac{\sin\delta}{\pi}\,\ell^2 a_2\left[\frac{1}{(a_o-\zeta_1)}-\frac{1}{(a_o-\bar{\zeta}_1)}-\frac{a_1^2}{2(a_o-\zeta_1)^2 a_2}+\right.$$

$$\left.\frac{a_1^2}{2(a_o-\bar{\zeta}_1)^2 a_2}\right]+\frac{\eta}{\pi}\,\ell^2 a_2\left[\frac{1}{(a_o-\zeta_2)}-\frac{1}{(a_o-\bar{\zeta}_2)}-\right.$$

$$\left.\left.\frac{a_1^2}{2(a_o-\zeta_2)^2 a_2}+\frac{a_1^2}{(a_o-\bar{\zeta}_2)^2 a_2}\right]\right] \qquad (32)$$

where a_o and a_1 are the same as in equation (29) and

$$a_2=\frac{ia}{1+b}\left(\frac{3}{4}+\frac{\frac{2ia}{1+b}+\frac{3}{4}\,\frac{1-b}{1+b}}{\left[\frac{2ia}{1+b}+\frac{1-b}{1+b}\right]^2-1}-\frac{\frac{ia}{1+b}\left[\frac{2ia}{1+b}+\frac{1-b}{1+b}\right]^2}{2\left[\left\{\frac{2ia}{1+b}+\frac{1-b}{1+b}\right\}^2-1\right]^{3/2}}\right)$$